ChemPhysChem

Supporting Information

Induced Protic Behaviour in Aprotonic Ionic Liquids by Anion Basicity for Efficient Carbon Dioxide Capture

Darius J. Yeadon,* Johan Jacquemin,* Natalia V. Plechkova, Manuel Maréchal, and Kenneth R. Seddon[+]

Experimental

Materials

Tetrabutylphosphonium hydroxide, $[P_{4444}][OH]$, ~40 wt.% in water was purchased from TCI, with ethanoic (≥99 %), propanoic (≥99 %), and octanoic (≥99 %) acids obtained from Sigma-Aldrich, along with tetrabutylphosphonium chloride, $[P_{4444}]Cl$. Triple distilled deionised water was used for the preparation of ionic liquid-water binary mixtures.

Synthesis of $[P_{4444}][C_nCOO]$ Ionic Liquids

Tetrabutylphosphonium carboxylate ionic liquids, $[P_{4444}][C_nCOO]$ (n = 1, 2 and 7), were prepared and characterised as previously reported.[1]

Preparation of $[P_{4444}][C_nCOO]$-Water Mixtures

The binary ionic liquid-water mixtures were prepared in air-tight glass vials (4 cm^3) on a mass balance (Explorer EX225D/AD Ohaus balance, ±0.01 mg), inside a dry dinitrogen filled AtmosBag glove bag. A range of ionic liquid-water mixtures, in terms of water mole fraction (x_w), were prepared by adding specific amounts of water to the dry $[P_{4444}][C_nCOO]$ (n = 1,2 and 7) ionic liquids. Samples were gently heated to ensure homogeneity.

Nuclear Magnetic Resonance Spectroscopy

Nuclear Magnetic Resonance (NMR) spectra were obtained with a Bruker Avance III spectrometer, 400 MHz: ^{1}H-NMR spectra were recorded at 399.90 MHz (16 scans), ^{13}C-NMR spectra at 100.56 MHz (1024 scans) and ^{31}P-NMR spectra at 161.87 MHz (64 scans). Locking was performed using an internal capillary containing d_6-dimethylsulfoxide (d_6-dmso, as an external lock). Dry samples were loaded into NMR tubes inside the glovebox and water containing samples inside an AtmosBag glove bag filled with dry dinitrogen. The NMR tubes were capped using the standard cap and sealed with parafilm. Chemical shifts were determined relative to tetramethylsilane. ^{31}P-NMR spectra were recorded using two capillary systems of d_6-dmso as locking solvent, and trimethylphosphate as reference. The standard operating temperature of the spectrometer was 300 K, with measurements having been performed at different temperatures, depending on their melting points.

Infrared Spectroscopy

Infrared (IR) spectra were recorded on a PerkinElmer Spectrum 100, in a range of 4000-550 cm^{-1}, equipped with a Universal ATR (attenuated total reflectance) sampling accessory utilising a DiComp™ diamond-coated zinc (II) selenide crystal with a resolution of 4 cm^{-1}. A small droplet of sample was placed on top of the diamond crystal and pressure applied with the gauge to ensure good contact and to minimise contact with air.

Small- and Wide-Angle X-ray Scattering (SWAXS)

Small- and Wide- Angle X-ray scattering measurements were performed using a Xenocs setup equipped with a Mo GENIX anode over a large q-range from 0.3 to 28 nm^{-1}. The K_α radiation (λ = 0.071 nm) is selected using multilayered curved mirrors focusing the beam toward infinity. The size of the beam at the sample position (0.8 x 0.8 mm^2) is defined by two sets of scatterless FORVIS slits. The scattered beam was recorded using a large online scanner detector (345 mm in diameter from MAR Research) located at 748 mm from the sample. Sample and empty cell transmissions are determined using an offline pin diode that can be inserted downstream from the sample. Quartz capillaries (2 mm in diameter with a wall thickness of 0.01 mm) from Hilgenberg were used as sample containers. FIT2D was used to perform the treatment of the data. The usual corrections for background (empty cell and detector noise) subtractions and intensity normalization using Lupolen™ as standard were applied. The scattered intensities are expressed as a function of q, the scattering vector, and $q = (4\pi/\lambda)\sin(\theta/2)$, where λ is the wavelength of the incident beam, and θ the scattering angle. The standard silver behenate was used for the q-range calibration. The experimental resolution is $\Delta q/q$ = 0.05.

CO_2 Gas Absorption by Gravimetric Saturation

Dry gravimetric CO_2 absorption measurements were performed in glass vials (4 cm^3) containing known mass of ionic liquid (approximately 1 g) and sealed with a rubber septum. The ionic liquids were handled inside a dry dinitrogen filled glovebox with the weight of the samples recorded on a mass balance with an accuracy of ±0.1 mg. Prior to measurements the ionic liquids were dried on a freeze-dryer after multiple melting/freezing cycles to remove any remaining trapped gas. Sample vials were heated to 338 K in a sand bath and bubbled with CO_2 at a rate of one to two bubbles a second, whilst under constant agitation with a magnetic stirrer. The mass of the sample vials was recorded at timed intervals to monitor the CO_2 absorption. The quantity of CO_2 absorbed was calculate from the increased mass of the sample vials. The absorption of CO_2 was recorded as a mole ratio between CO_2 and ionic liquid, $n_{CO_2} : n_{IL}$, as well as weight percent, wt.%, of CO_2.

For the equimolar mixtures with water, the ionic liquid was prepared as for the dry ionic liquids and handled inside a dry dinitrogen filled glovebox. The appropriate amount of water was added to the ionic liquid inside an AtmosBag glove bag filled with dry N_2. Prior to addition water was degassed with multiple melting/freezing cycles whilst under vacuum. The CO_2 was bubbled through the ionic liquid-water mixture at a rate of one to two bubbles a second at room temperature (295 K). The mass of the samples was recorded at timed intervals to monitor the CO_2 uptake, with the calculated quantity of stored CO_2 .

Results

1. NMR Spectroscopy

Table S1.1 – ^{1}H-NMR chemical shifts, δ, of the dry $[P_{4\,4\,4\,4}][C_1COO]$ and low water content mixtures at 353 K.

	$[P_{4\,4\,4\,4}]^+$				$[C_1COO]^-$	
	α	β	γ	δ	CH_3	Water
x_w	δ / ppm				δ / ppm	δ / ppm
0	2.21	1.19	1.07	0.53	1.19	
0.1312	2.18	1.17	1.06	0.52	1.20	4.75
0.2201	2.16	1.16	1.06	0.51	1.20	4.32
0.2606	2.15	1.16	1.06	0.52	1.21	4.14

Table S1.2 – ^{1}H-NMR chemical shifts, δ, of $[P_{4\,4\,4\,4}][C_1COO]$-water mixtures at 300 K.

	$[P_{4\,4\,4\,4}]^+$				$[C_1COO]^-$	
	α	β	γ	δ	$-CH_3$	Water
x_w	δ / ppm				δ / ppm	δ / ppm
0.3014	2.16	1.14	1.04	0.50	1.21	4.53
0.3466	2.15	1.14	1.05	0.51	1.22	4.46
0.4447	2.09	1.11	1.04	0.49	1.21	4.33
0.5050	2.06	1.10	1.04	0.49	1.22	4.27
0.5970	2.01	1.07	1.05	0.48	1.23	4.18
0.6700	1.93	1.03	1.03	0.45	1.22	4.00
0.7143	1.91	1.04	1.03	0.46	1.24	4.05
0.7511	1.90	1.05	1.05	0.47	1.26	4.04
0.8001	1.85	1.04	1.03	0.46	1.27	4.02
0.8383	1.81	1.03	1.03	0.46	1.29	4.02
0.8572	1.76	1.00	1.00	0.43	1.27	4.04
0.9010	1.72	1.00	0.99	0.44	1.30	4.07
0.9503	1.62	0.95	0.94	0.39	1.31	4.14
1						4.26

Table S1.3 – ^{1}H-NMR chemical shifts, δ, of the dry $[P_{4444}][C_2COO]$ and low water content mixtures at 333 K.

	$[P_{4444}]^+$				$[C_2COO]^-$		
	α	β	γ	δ	$-CH_3$	$-CH_2-$	Water
x_w	δ / ppm				δ / ppm		δ / ppm
0	2.21	1.15	1.06	0.52	1.44	0.54	
0.1220	2.19	1.14	1.04	0.50	1.43	0.50	3.93

Table S1.4 – ^{1}H-NMR chemical shifts, δ, of $[P_{4444}][C_2COO]$-water mixtures at 300 K.

	$[P_{4444}]^+$				$[C_2COO]^-$		
	α	β	γ	δ	$-CH_3$	$-CH_2-$	Water
x_w	δ / ppm				δ / ppm		δ / ppm
0.2174	2.12	1.11	1.04	0.49	0.49	1.47	4.72
0.3173	2.13	1.10	1.03	0.49	0.51	1.46	4.72
0.4060	2.12	1.11	1.05	0.50	0.51	1.48	4.59
0.5003	2.07	1.06	1.04	0.48	0.50	1.48	4.30
0.6052	1.99	1.04	1.03	0.47	0.50	1.49	4.28
0.6686	1.95	1.04	1.03	0.46	0.50	1.50	4.19
0.7010	1.93	1.04	1.04	0.46	0.50	1.51	4.11
0.7502	1.89	1.03	1.02	0.45	0.49	1.52	4.01
0.8024	1.83	1.01	1.01	0.44	0.49	1.53	4.03
0.8336	1.79	1.01	1.00	0.43	0.49	1.54	4.04
0.8573	1.76	1.00	1.00	0.42	0.48	1.54	4.04
0.9009	1.71	0.99	0.98	0.42	0.49	1.56	4.07
0.9502	1.63	0.95	0.94	0.40	0.48	1.58	4.17
1							4.26

Table S1.5 – ^{1}H-NMR chemical shifts, δ, of the dry $[P_{4444}][C_7COO]$ and water mixtures at 300 K.

	$[P_{4444}]^+$				$[C_7COO]^-$				
	α	β	γ	δ	$-CH_3$	$-(CH_2)_4-$	$-CH_2-$	$-CH_2-COO^-$	Water
x_w	δ / ppm				δ / ppm				δ / ppm
0	2.25	1.14	1.06	0.52	0.45	0.84	1.06	1.46	
0.1143	2.24	1.15	1.07	0.53	0.45	0.84	1.07	1.47	5.28
0.2055	2.21	1.14	1.06	0.52	0.45	0.84	1.06	1.48	4.84
0.2516	2.20	1.13	1.07	0.52	0.45	0.84	1.07	1.48	4.69
0.3404	2.18	1.13	1.07	0.52	0.44	0.84	1.07	1.49	4.55
0.4101	2.15	1.13	1.07	0.51	0.44	0.83	1.07	1.49	4.47
0.5029	2.11	1.08	1.07	0.51	0.44	0.83	1.07	1.49	4.19
0.5992	2.05	1.08	1.07	0.50	0.43	0.82	1.07	1.51	4.16
0.6734	1.99	1.08	1.07	0.50	0.42	0.82	1.07	1.54	4.10
0.6975	1.97	1.07	1.07	0.49	0.42	0.81	1.07	1.52	4.08
0.7524	1.92	1.06	1.06	0.48	0.41	0.80	1.06	1.53	4.04
0.7990	1.88	1.05	1.05	0.48	0.41	0.80	1.05	1.54	4.03
0.8348	1.84	1.05	1.05	0.47	0.40	0.79	1.05	1.55	4.04
0.8569	1.82	1.04	1.04	0.47	0.40	0.79	1.04	1.56	4.05
0.9003	1.76	1.02	1.02	0.45	0.38	0.78	1.02	1.57	4.09
0.9503	1.68	1.00	0.99	0.43	0.36	0.76	0.99	1.58	4.18
1									4.26

Table S1.6 – ^{13}C-NMR chemical shifts, δ, of the dry [P_{4444}][C_1COO] and low water content mixtures at 353 K.

	$[P_{4444}]^+$							$[C_1COO]^-$	
	α		β		γ		δ	$-CH_3$	$-COO^-$
x_w	δ / ppm		δ / ppm		δ / ppm		δ / ppm	δ / ppm	
0	18.48	18.01	23.67	23.51	23.50	23.45	12.98	25.88	171.76
0.1312	18.38	17.91	23.61	23.46	23.43	23.38	12.94	25.82	171.85
0.2201	18.44	17.97	23.64	23.49	23.45	23.42	13.01	25.53	172.52
0.2606	18.36	17.89	23.52	23.37	23.35	23.31	12.87	25.49	172.20

Table S1.7 – ^{13}C-NMR chemical shifts, δ, of [P_{4444}][C_1COO]-water mixtures at 300 K.

	$[P_{4444}]^+$							$[C_1COO]^-$	
	α		β		γ		δ	$-CH_3$	$-COO^-$
x_w	δ / ppm		δ / ppm		δ / ppm		δ / ppm	δ / ppm	
0.3014	18.32	17.84	24.10	23.92	23.75	23.71	13.52	25.98	172.79
0.3466	18.31	17.94	24.08	24.02	23.74	23.80	13.51	25.92	172.91
0.4447	18.29	17.82	24.03	23.88	23.71	23.68	13.51	25.77	173.21
0.5050	18.27	17.80	23.99	23.84	23.69	23.65	13.50	25.62	173.53
0.5970	18.21	17.74	23.91	23.76	23.62	23.58	13.48	25.41	173.99
0.6700	18.13	17.66	23.80	23.65	23.52	23.48	13.43	25.20	174.73
0.7143	18.11	17.64	23.78	23.62	23.49	23.45	13.42	25.04	174.95
0.7511	18.10	17.71	23.74	23.68	23.44	23.49	13.40	24.91	175.39
0.8001	18.06	17.68	23.67	23.61	23.35	23.41	13.34	24.72	176.08
0.8383	18.04	17.70	23.63	23.61	23.30	23.39	13.32	24.58	176.45
0.8572	18.02	17.55	23.60	23.45	23.25	23.20	13.28	24.54	176.93
0.9010	18.01	17.53	23.54	23.39	23.15	23.11	13.20	24.34	177.85
0.9503	17.94	17.46	23.45	23.30	22.95	22.91	13.00	23.99	179.29

Table S1.8 – ^{13}C-NMR chemical shifts, δ, of the dry [P_{4444}][C_2COO] and low water content mixtures at 333 K.

	$[P_{4444}]^+$							$[C_2COO]^-$		
	α		β		γ		δ	$-CH_3$	$-CH_2-$	$-COO^-$
x_w	δ / ppm		δ / ppm		δ / ppm		δ / ppm	δ / ppm		
0	18.53	18.06	23.90	23.75	23.73	23.68	13.20	11.62	32.23	175.16
0.1220	18.41	17.94	23.79	23.64	23.62	23.57	13.10	11.54	32.18	175.13

Table S1.9 – ^{13}C-NMR chemical shifts, δ, of $[P_{4444}][C_2COO]$-water mixtures at 300 K.

	$[P_{4444}]^+$							$[C_2COO]^-$		
	α		β		γ		δ	$-CH_3$	$-CH_2-$	$-COO^-$
x_w	δ / ppm		δ / ppm		δ / ppm		δ / ppm	δ / ppm		
0.2174	18.46	17.99	24.15	24.00	23.88	23.88	13.56	11.66	31.99	176.18
0.3173	18.37	17.89	24.09	23.93	23.82	23.82	13.49	11.62	31.98	176.01
0.4060	18.43	17.96	24.13	23.98	23.87	23.87	13.56	11.64	31.96	176.30
0.5003	18.41	17.94	24.07	23.92	23.83	23.83	13.55	11.59	31.91	176.61
0.6052	18.23	17.76	23.88	23.72	23.64	23.64	13.41	11.28	31.51	177.12
0.6686	18.19	17.72	23.82	23.67	23.58	23.58	13.40	11.19	31.39	177.57
0.7010	18.16	17.67	23.77	23.62	23.54	23.54	13.37	11.17	31.39	177.77
0.7502	18.13	17.66	23.73	23.58	23.48	23.48	13.36	11.13	31.37	178.27
0.8024	18.07	17.59	23.65	23.50	23.37	23.37	13.29	10.96	31.13	178.88
0.8336	18.06	17.59	23.63	23.47	23.32	23.32	13.27	10.86	30.99	179.37
0.8573	18.05	17.57	23.60	23.44	23.27	23.27	13.24	10.80	30.94	179.77
0.9009	18.02	17.54	23.54	23.39	23.17	23.17	13.16	10.73	30.90	180.68
0.9502	17.97	17.50	23.50	23.35	23.02	23.02	13.05	10.66	30.91	182.32

Table S1.10 – ^{13}C-NMR chemical shifts, δ, of the dry $[P_{4444}][C_7COO]$ and water mixtures at 300 K.

	$[P_{4444}]^+$							$[C_7COO]^-$							
	α		β		γ		δ	C1 (CH_3)	C2 (CH_2)	C3 (CH_2)	C4 (CH_2)	C5 (CH_2)	C6 (CH_2)	C7 (CH_2)	C8 (COO^-)
x_w	δ / ppm		δ / ppm		δ / ppm		δ / ppm	δ / ppm							
0	18.45	17.98	24.22	24.06	23.94	23.90	13.54	13.96	22.73	27.73	29.68	30.39	32.10	39.99	174.78
0.1143	18.46	17.99	24.20	24.05	23.94	23.90	13.54	13.97	22.74	27.69	29.68	30.39	32.10	39.89	174.92
0.2055	18.45	17.98	24.17	24.02	23.93	23.90	13.53	13.96	22.73	27.64	29.67	30.37	32.10	39.80	175.08
0.2516	18.44	17.97	24.15	24.00	23.91	23.88	13.52	13.96	22.73	27.60	29.66	30.36	32.09	39.74	175.20
0.3404	18.43	17.96	24.12	23.97	23.90	23.86	13.52	13.96	22.73	27.55	29.65	30.34	32.09	39.64	175.37
0.4101	18.40	17.93	24.09	23.93	23.87	23.83	13.51	13.95	22.72	27.48	29.63	30.32	32.08	39.54	175.56
0.5029	18.38	17.91	24.04	23.89	23.84	23.98	13.51	13.96	22.73	27.47	29.64	30.33	32.09	39.55	175.86
0.5992	18.31	17.84	23.95	23.80	23.76	23.72	13.48	13.95	22.72	27.32	29.60	30.27	32.07	39.32	176.38
0.6734	18.25	17.77	23.88	27.72	23.68	23.63	13.45	13.93	22.70	27.18	29.56	30.22	32.05	39.12	176.89
0.6975	18.23	17.76	23.85	23.69	23.64	23.60	13.44	13.93	22.70	27.13	29.55	30.19	32.05	39.04	177.12
0.7524	18.19	17.72	23.79	23.63	23.57	23.53	13.40	13.92	22.68	27.01	29.51	30.13	32.02	38.88	177.62
0.7990	18.18	17.71	23.74	23.58	23.50	23.46	13.36	13.91	22.67	26.90	29.47	30.07	32.01	38.72	178.17
0.8348	18.18	17.70	23.70	23.55	23.45	23.40	13.33	13.91	22.66	26.80	29.43	30.02	31.99	38.59	178.66
0.8569	18.18	17.70	23.68	23.53	23.41	23.36	13.30	13.91	22.66	26.74	29.41	29.98	31.98	38.50	179.02
0.9003	18.17	17.70	23.62	23.47	23.31	23.27	13.21	13.91	22.64	26.60	29.34	29.88	31.95	38.32	179.78
0.9503	18.16	17.68	23.56	23.41	23.17	23.12	13.06	13.89	22.61	26.45	29.26	29.76	31.91	38.10	180.78

Table S1.11 – *^{31}P-NMR chemical shifts, δ, of the dry $[P_{4444}][C_1COO]$ and low water content mixtures 353 K.*

	^{31}P
x_w	δ / ppm
0	33.47
0.1312	33.37
0.2201	33.24
0.2606	33.27

Table S1.12 – *^{31}P-NMR chemical shifts, δ, of $[P_{4444}][C_1COO]$-water mixtures 300 K.*

	^{31}P
x_w	δ / ppm
0.3014	32.91
0.3466	32.88
0.4447	32.84
0.5050	32.70
0.5652	32.68
0.5970	32.66
0.6700	32.64
0.7143	32.64
0.7511	32.64
0.8001	32.65
0.8383	32.66
0.8572	32.66
0.9010	32.66
0.9503	32.67

Table S1.13 – ^{31}P-NMR chemical shifts, δ, of the dry $[P_{4444}][C_2COO]$ and low water content mixtures 333 K.

	^{31}P
x_w	δ / ppm
0	33.37
0.1220	33.25

Table S1.14 – *^{31}P-NMR chemical shifts, δ, of $[P_{4\,4\,4\,4}][C_2COO]$-water mixtures 300 K.*

	^{31}P
x_w	δ / ppm
0.2174	32.86
0.3173	32.83
0.4060	32.76
0.5003	32.64
0.6052	32.60
0.6686	32.60
0.7010	32.59
0.7502	32.62
0.8024	32.62
0.8336	32.65
0.8573	32.66
0.9009	32.66
0.9502	32.65

Table S1.15 – *^{31}P-NMR chemical shifts, δ, of the dry $[P_{4\,4\,4\,4}][C_7COO]$ and water mixtures at 300 K.*

	^{31}P
x_w	δ / ppm
0	33.11
0.1143	33.04
0.2055	32.96
0.2516	32.91
0.3404	32.84
0.4101	32.78
0.5029	32.70
0.5992	32.63
0.6734	32.61
0.6975	32.61
0.7524	32.61
0.7990	32.61
0.8348	32.60
0.8569	32.59
0.9003	32.57
0.9503	32.54

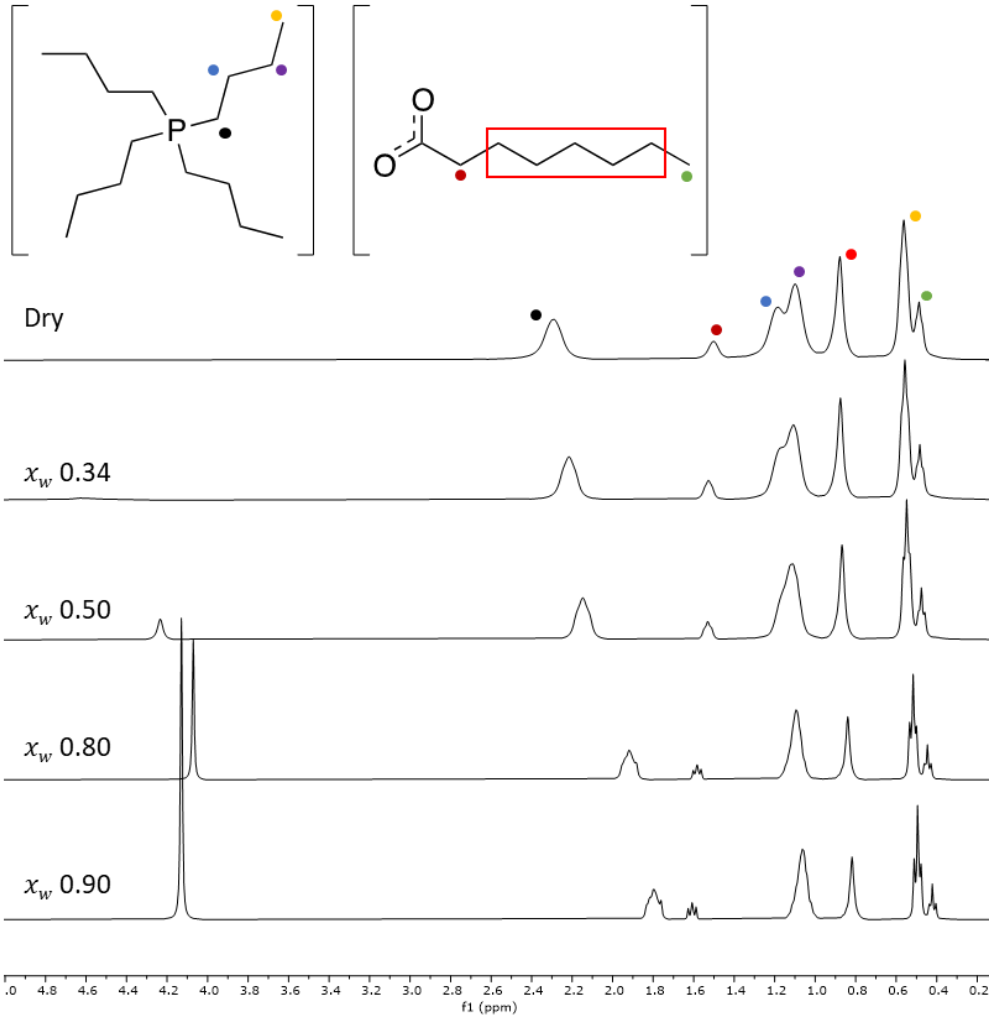

Figure S1.1 *– Stacked ^{1}H-NMR spectra of $[P_{4\,4\,4\,4}][C_7COO]$ and water mixtures at 27 ˚C (400 MHz; 27˚C; d_6-dmso internal capillary).*

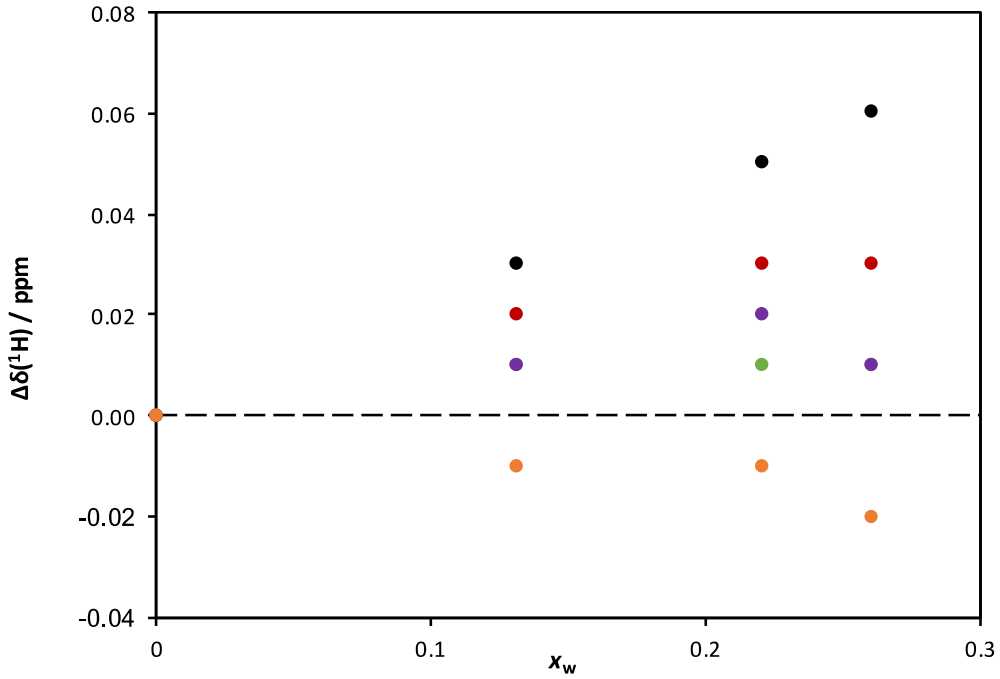

Figure S1.2 *– Deviations in ^{1}H-NMR chemical shifts, Δδ, of $[P_{4444}][C_1COO]$ and low water content mixtures as a function of mole fraction composition of water, x_w, at 353 K, (●) P–CH_2–; (●) –CH_2–; (●) –CH_2–CH_3; (●) –CH_3 of the $[P_{4444}]^+$ cation and (●) –CH_3 of the $[C_1COO]^-$ anion.*

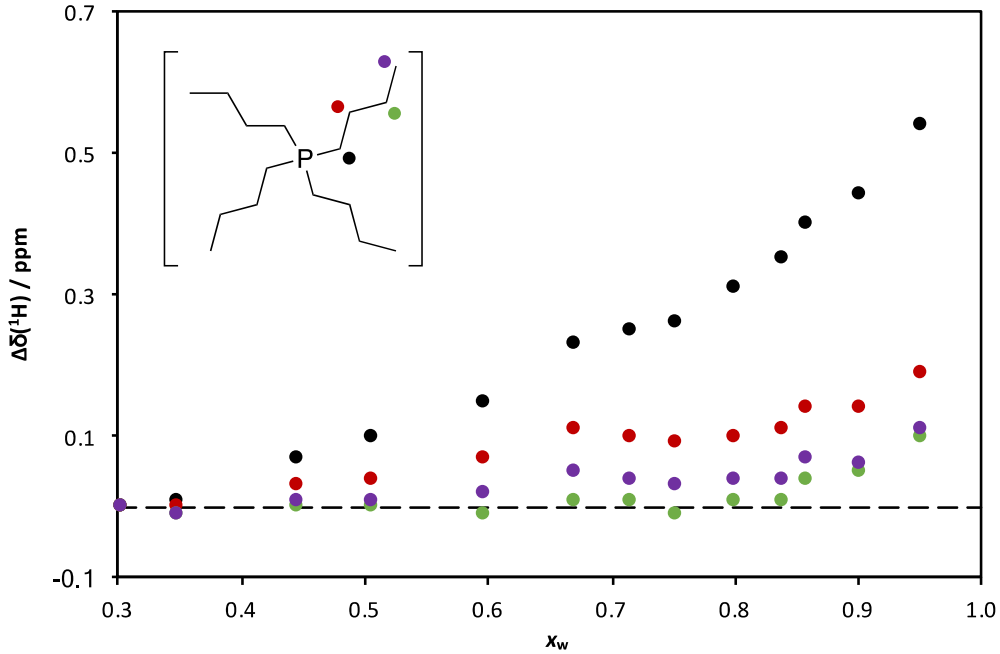

Figure S1.3 *– Deviations in ^{1}H-NMR chemical shifts, Δδ, of the $[P_{4444}]^+$ cation in $[P_{4444}][C_1COO]$-water mixtures as a function of mole fraction composition of water, x_w, at 300 K, (●) P–CH_2–; (●) –CH_2–; (●) –CH_2–CH_3; (●) –CH_3.*

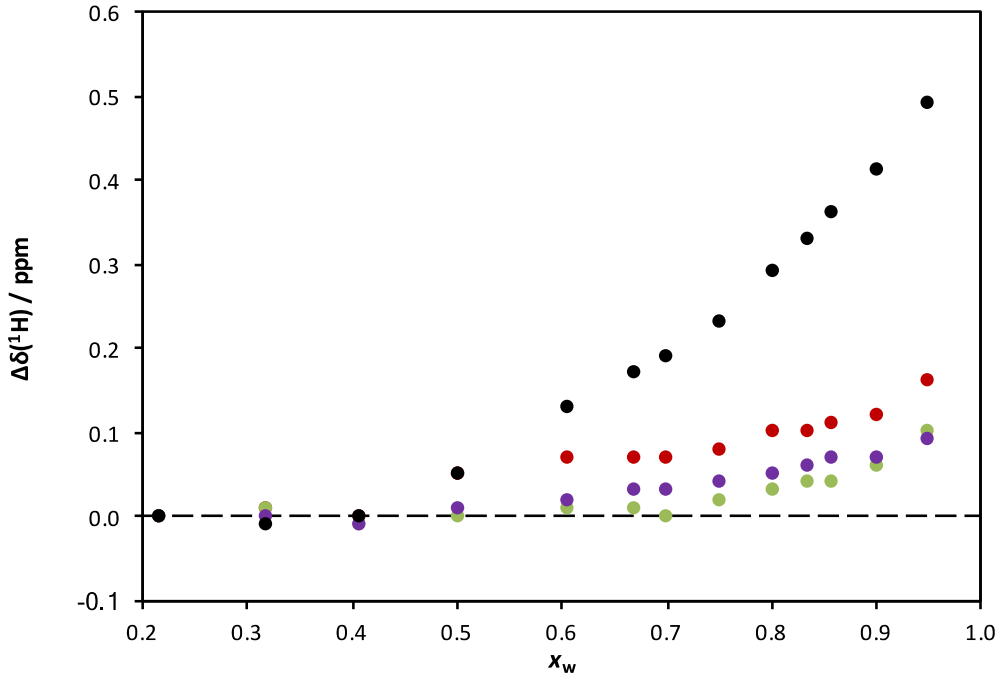

Figure S1.4 *– Deviations in ^{1}H-NMR chemical shifts, Δδ, of $[P_{4444}][C_2COO]$-water mixtures as a function of mole fraction composition of water, x_w, at 300 K, (●) P–CH_2–; (●) –CH_2–; (●) –CH_2–CH_3; (●) –CH_3 of the $[P_{4444}]^+$ cation.*

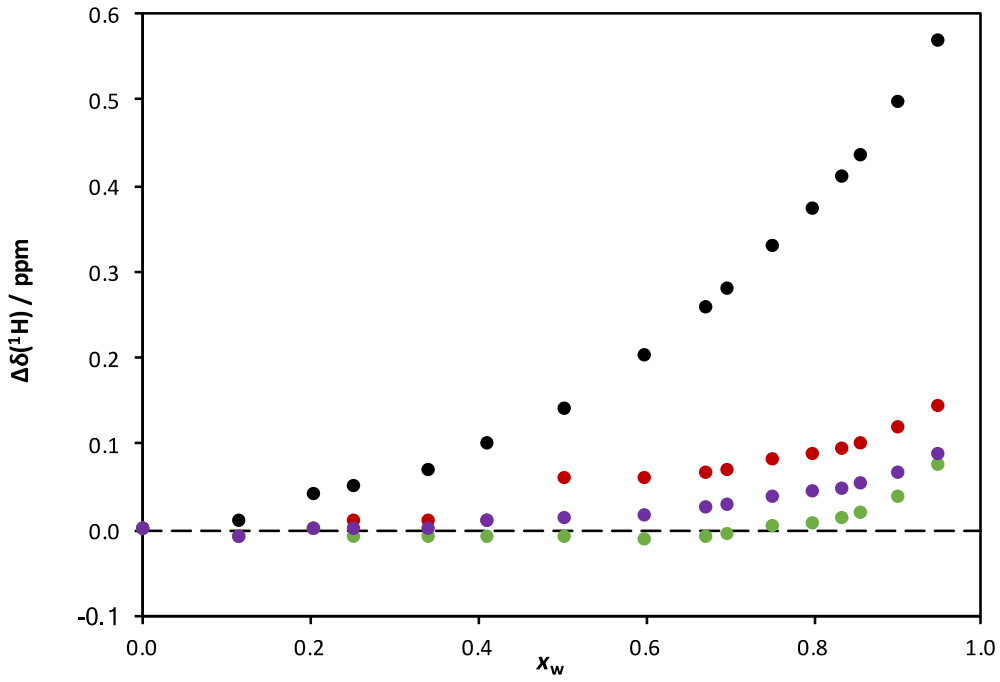

Figure S1.5 *– Deviations in ^{1}H-NMR chemical shifts, Δδ, of $[P_{4444}][C_7COO]$-water mixtures as a function of mole fraction composition of water, x_w, at 300 K, (●) P–CH_2–; (●) –CH_2–; (●) –CH_2–CH_3; (●) –CH_3 of the $[P_{4444}]^+$ cation.*

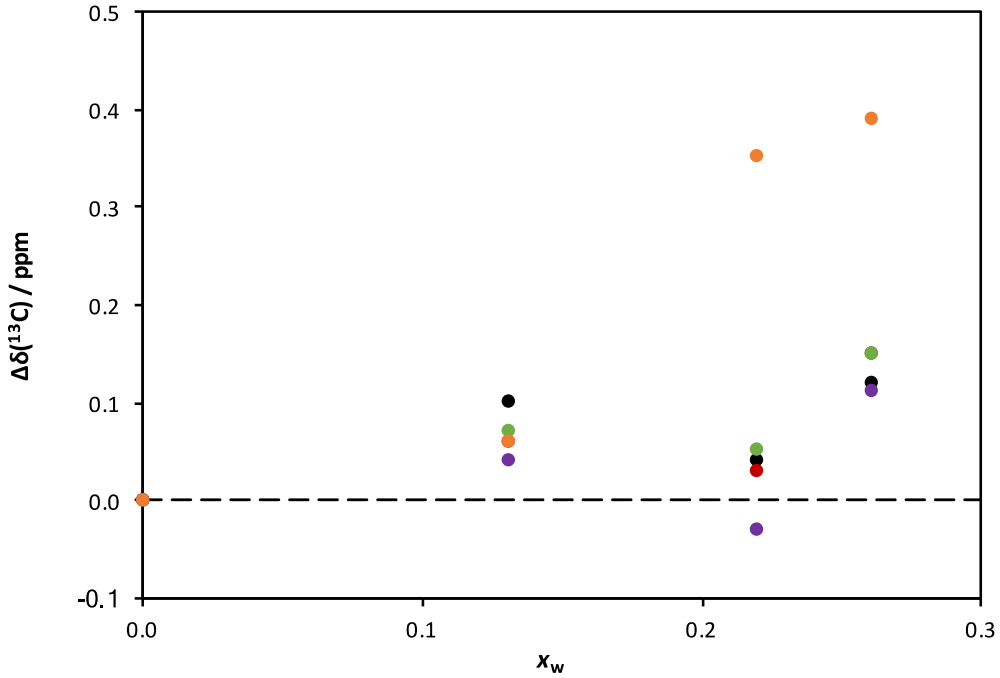

Figure S1.6 – *Deviations in ^{13}C-NMR chemical shifts, Δδ, of $[P_{4\,4\,4\,4}][C_1COO]$ and low water content mixtures as a function of mole fraction composition of water, x_w, at 353 K, (●) P–CH_2–; (●) –CH_2–; (●) –CH_2–CH_3; (●) –CH_3 of the $[P_{4\,4\,4\,4}]^+$ cation and (●) –CH_3 of the $[C_1COO]^-$ anion.*

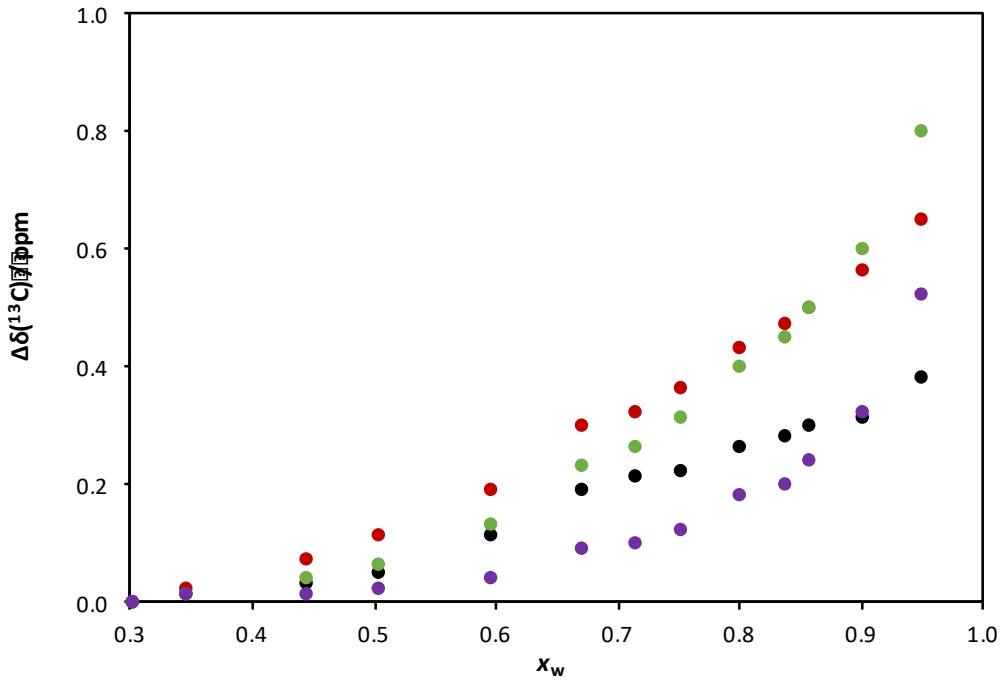

Figure S1.7 – *Deviations in ^{13}C-NMR chemical shifts, Δδ, of $[P_{4\,4\,4\,4}][C_1COO]$-water mixtures as a function of mole fraction composition of water, x_w, at 300 K, (●) P–CH_2–; (●) –CH_2–; (●) –CH_2–CH_3; (●) –CH_3 of the $[P_{4\,4\,4\,4}]^+$ cation.*

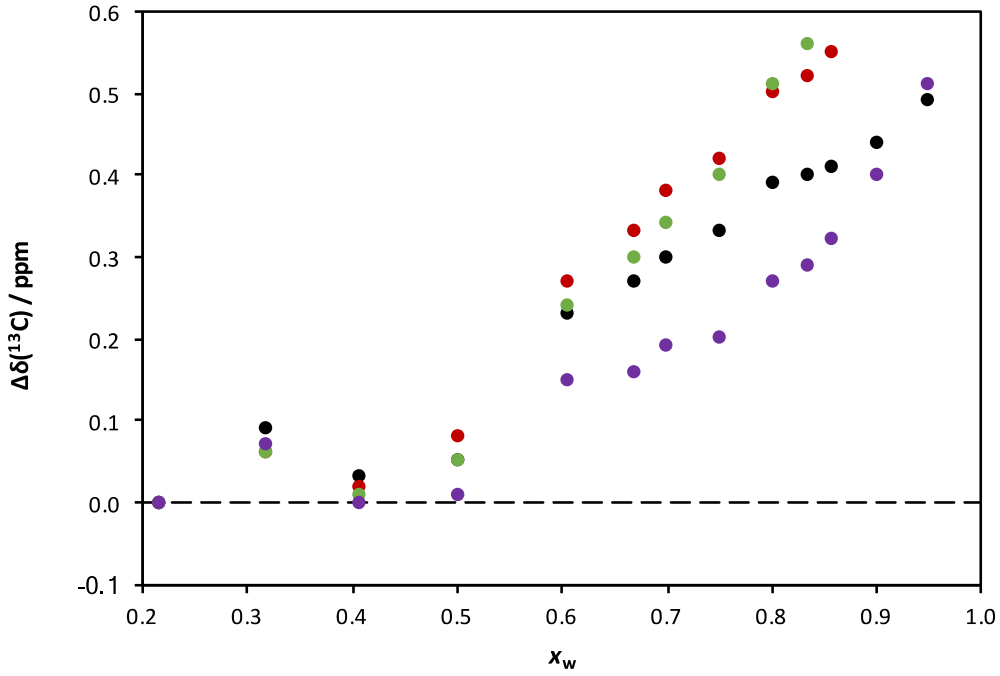

Figure S1.8 – *Deviations in ^{13}C-NMR chemical shifts, Δδ, of $[P_{4444}][C_2COO]$-water mixtures as a function of mole fraction composition of water, x_w, at 300 K, (●) P–CH_2–; (●) –CH_2–; (●) –CH_2–CH_3; (●) –CH_3 of the $[P_{4444}]^+$ cation.*

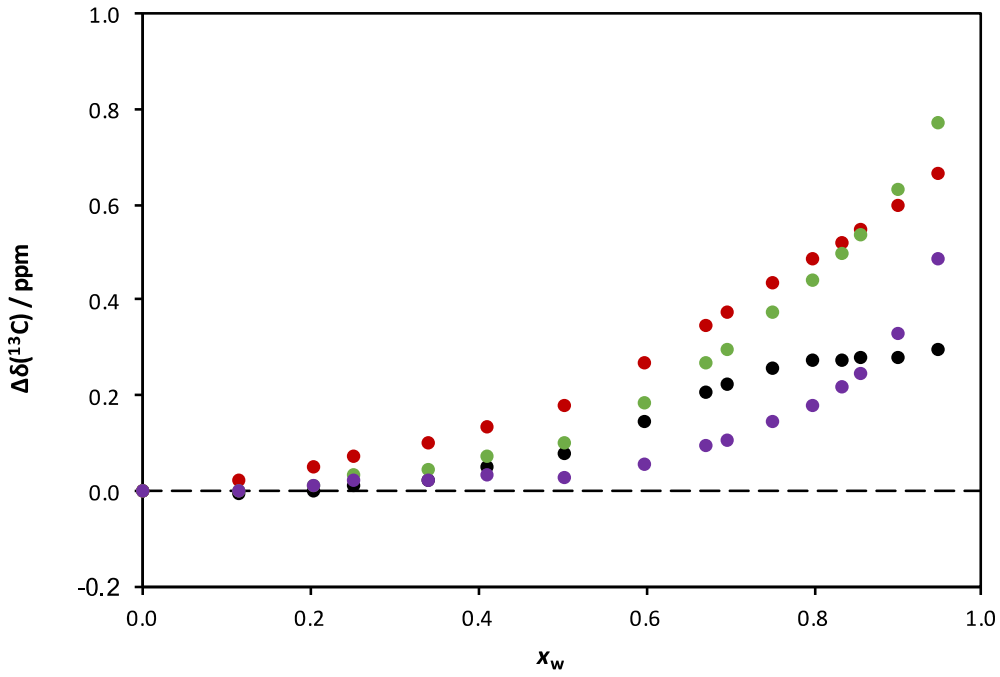

Figure S1.9 – *Deviations in ^{13}C-NMR chemical shifts, Δδ, of $[P_{4444}][C_7COO]$-water mixtures as a function of mole fraction composition of water, x_w, at 300 K, (●) P–CH_2–; (●) –CH_2–; (●) –CH_2–CH_3; (●) –CH_3 of the $[P_{4444}]^+$ cation.*

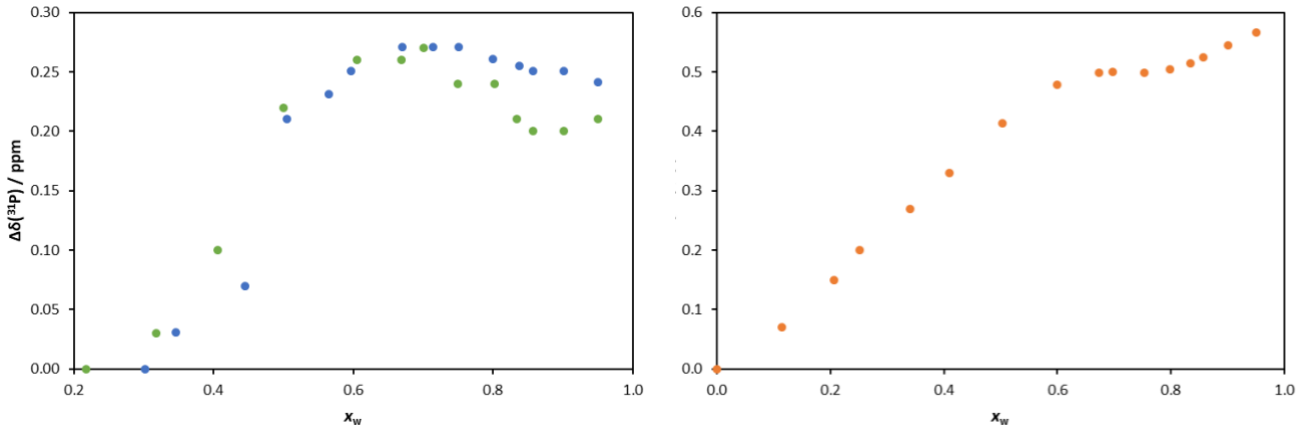

Figure S1.10 – *Deviations in ^{31}P-NMR, Δδ, of the $[P_{4444}]^+$ cation for $[P_{4444}][C_nCOO]$-water mixtures as a function of mole fraction composition of water, x_w, at 300 K, (●) $[P_{4444}][C_1COO]$; (●) $[P_{4444}][C_2COO]$; (●) $[P_{4444}][C_7COO]$.*

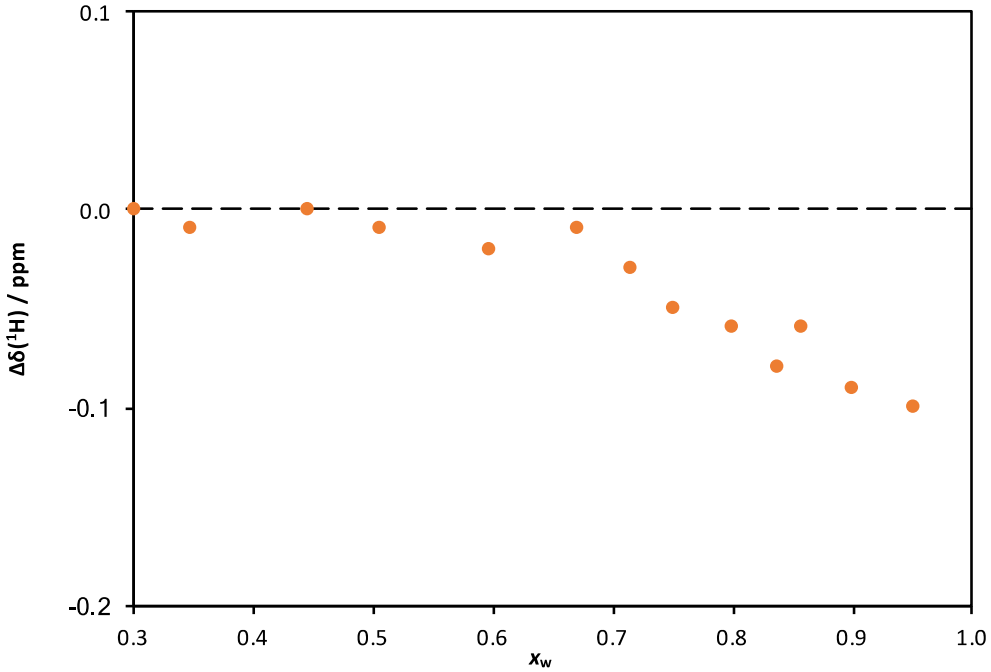

Figure S1.11 *– Deviations in ^{1}H-NMR chemical shifts, Δδ, of $[P_{4444}][C_1COO]$-water mixtures as a function of mole fraction composition of water, x_w, at 300 K, (●) –CH_3 of the $[C_1COO]^-$ anion.*

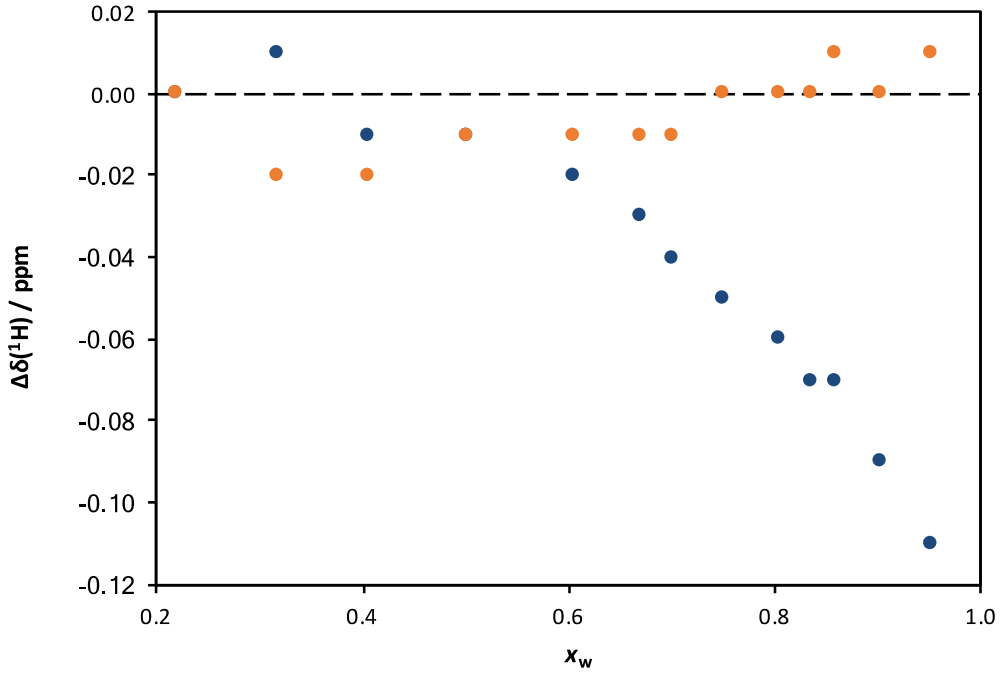

Figure S1.12 *– Deviations in ^{1}H-NMR chemical shifts, Δδ, of $[P_{4444}][C_2COO]$-water mixtures as a function of mole fraction composition of water, x_w, at 300 K, (●) $–CH_2$; (●) $–CH_3$ of the $[C_2COO]^-$ anion.*

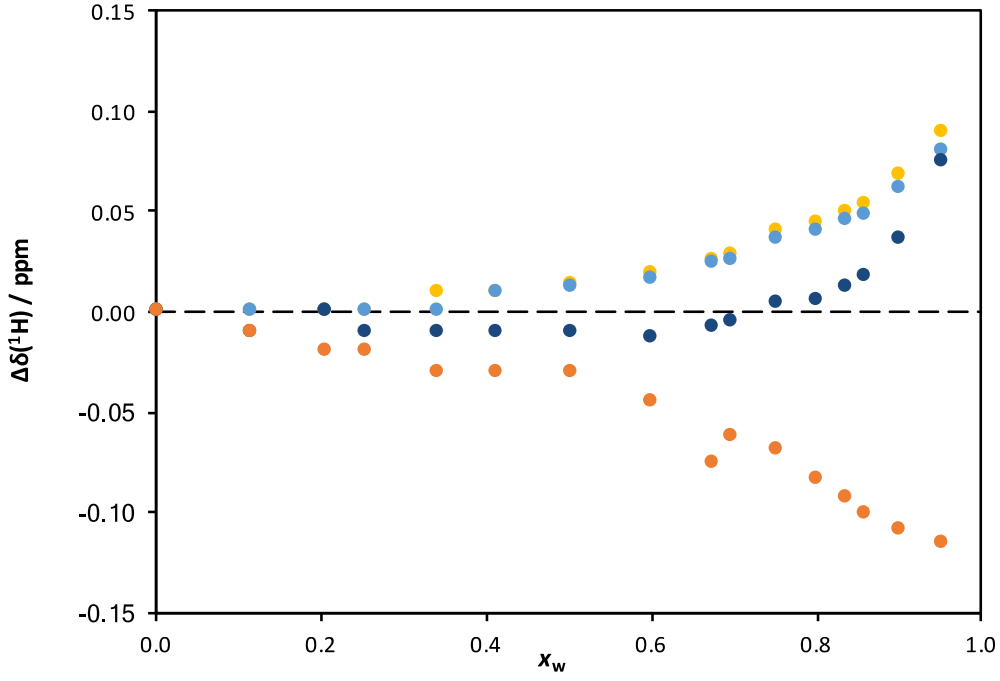

Figure S1.13 – *Deviations in ^{1}H-NMR chemical shifts, Δδ, of $[P_{4444}][C_7COO]$-water mixtures as a function of mole fraction composition of water, x_w, at 300 K, (●) $–CH_2–COO^-$; (●) $–CH_2–$;(●) $–(CH_2)_4–$; (●) $–CH_3$ of the $[C_7COO]^-$ anion.*

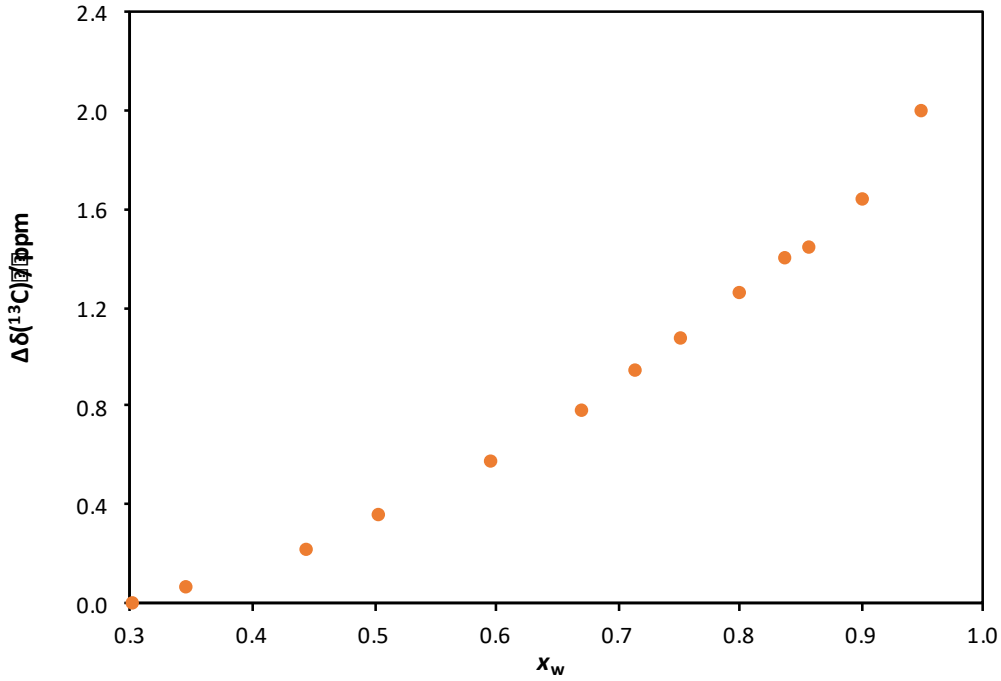

Figure S1.14 – *Deviations in ^{13}C-NMR chemical shifts, Δδ, of $[P_{4444}][C_1COO]$-water mixtures as a function of mole fraction composition of water, x_w, at 300 K, (●) –CH_3 of the $[C_1COO]^-$ anion.*

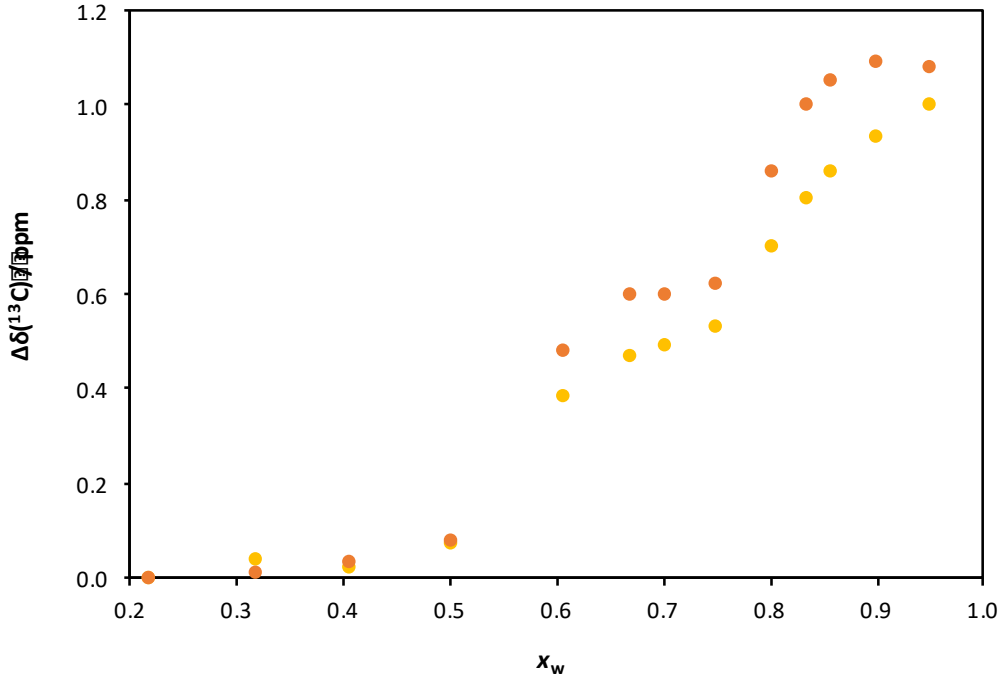

Figure S1.15 – *Deviations in ^{13}C-NMR chemical shifts, Δδ, of $[P_{4444}][C_2COO]$-water mixtures as a function of mole fraction composition of water, x_w, at 300 K, (●) –CH_3; (●) –CH_2– of the $[C_2COO]^-$ anion.*

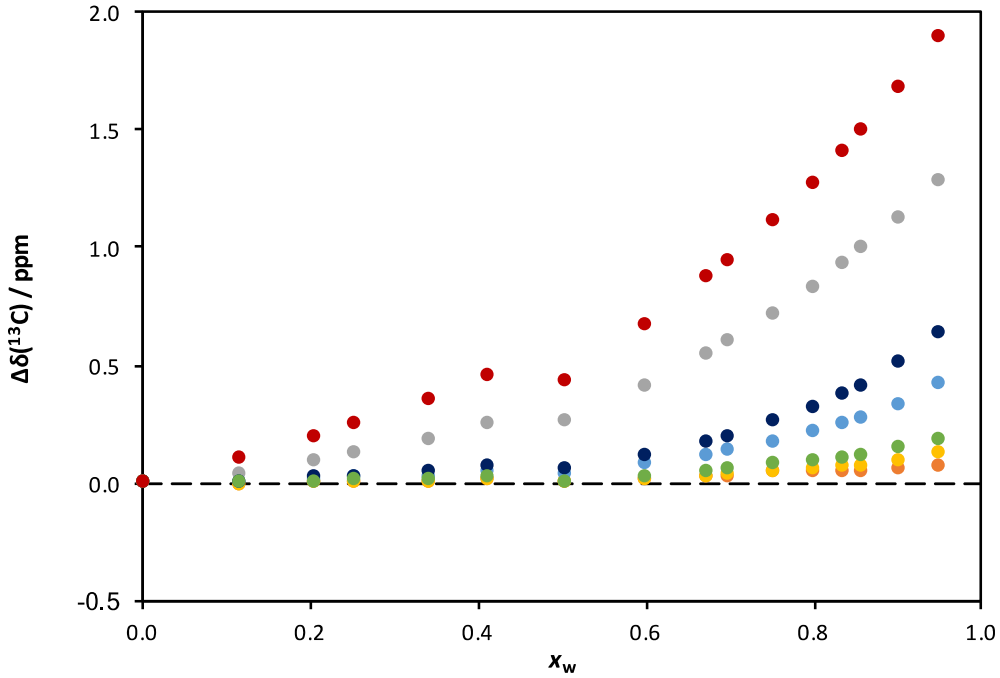

Figure S1.16 *– Deviations in ^{13}C-NMR chemical shifts, Δδ, of [P4 4 4 4][C7COO]-water mixtures as a function of mole fraction composition of water, x_w, at 300 K,(●) C1 (CH_3); (●) C2 (CH_2); (●) C3 (CH_2); (●) C4 (CH_2); (●) C5 (CH_2); (●) C6 (CH_2);(●) C7 (CH_2–COO^-); of the $[C_7COO]^-$ anion.*

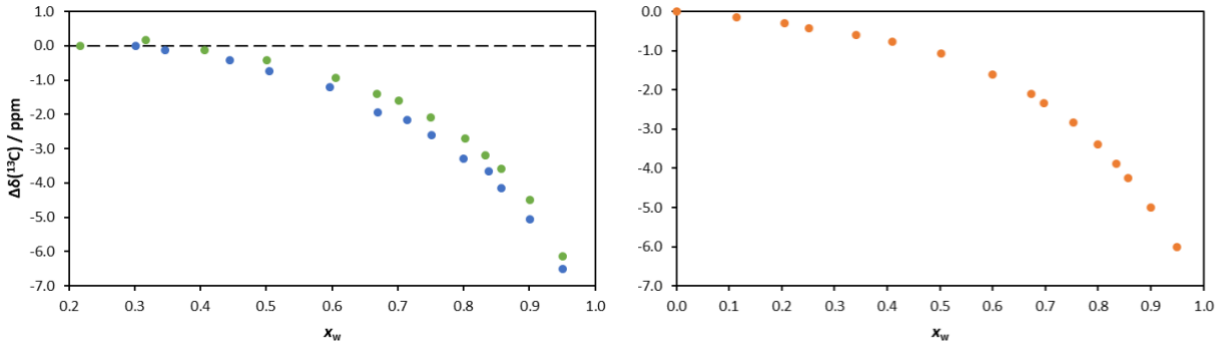

Figure S1.17 – *Deviations in ^{13}C-NMR, Δδ, of the COO^- environment for [P4 4 4 4][CnCOO]-water mixtures as a function of mole fraction composition of water, x_w, at 300 K, (●) [P4 4 4 4][C1COO]; (●) [P4 4 4 4][C2COO]; (●) [P4 4 4 4][C7COO].*

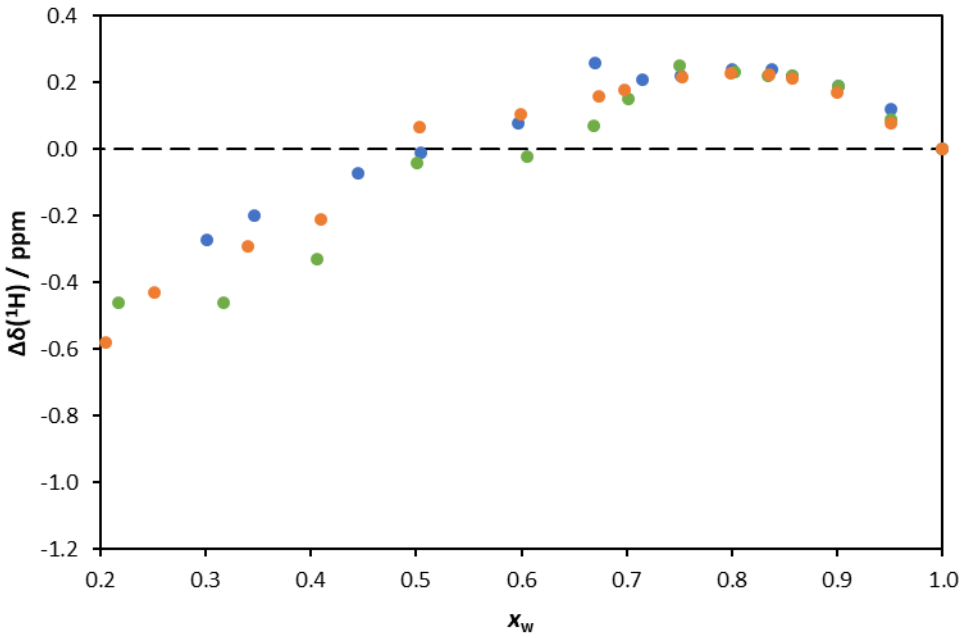

Figure S1.18 – *Deviations in ^{1}H-NMR chemical shifts, Δδ, of water as a function of mole fraction composition, x_w, in $[P_{4444}][C_nCOO]$ ionic liquids at 300 K, (●) $[P_{4444}][C_1COO]$; (●) $[P_{4444}][C_2COO]$; (●) $[P_{4444}][C_7COO]$.*

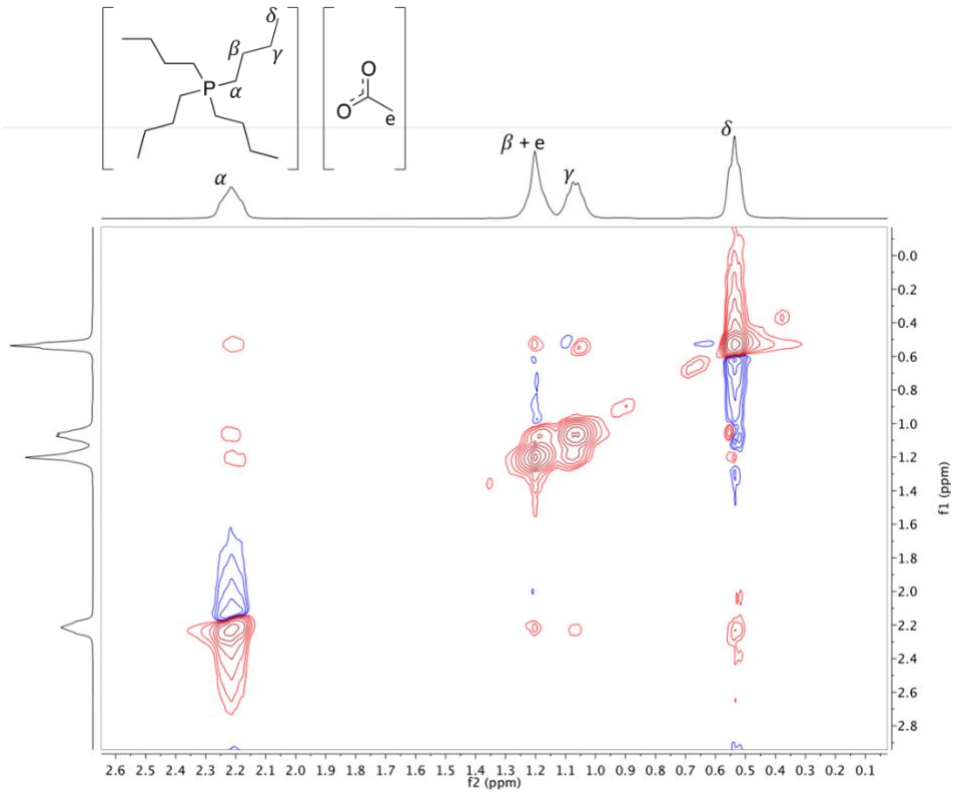

Figure S1.19 – *^{1}H-^{1}H NOESY of pure $[P_{4444}][C_1COO]$ at 353 K.*

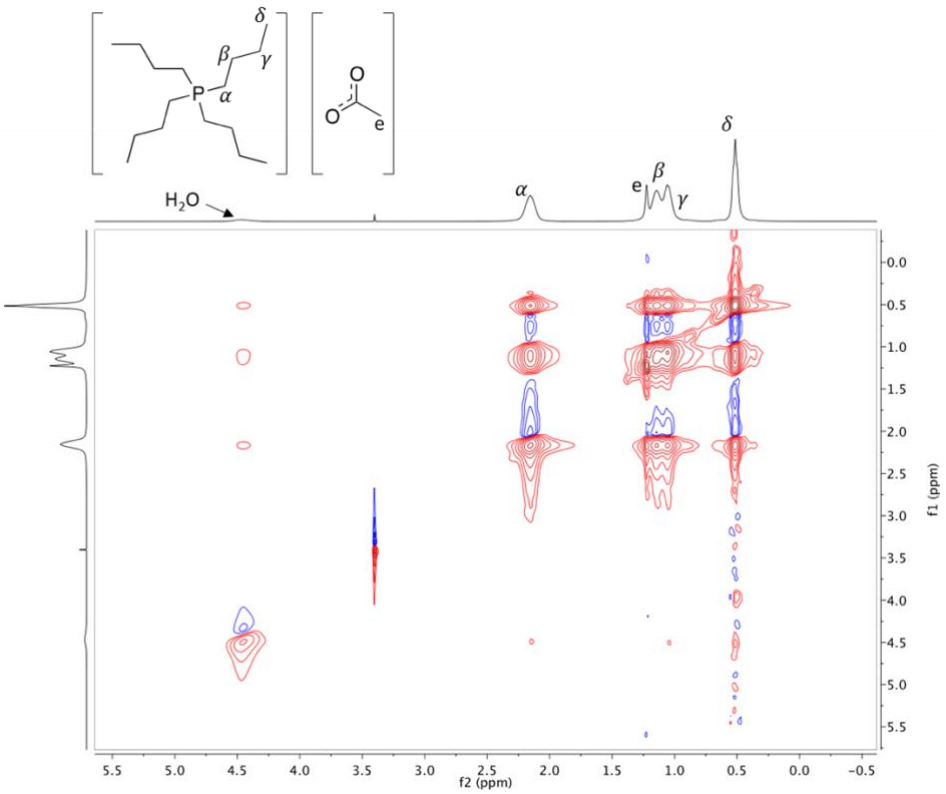

Figure S1.20 – *^{1}H-^{1}H NOESY of [P_{4444}][C_1COO]-water mixture at x_w 0.35 water content, 300 K.*

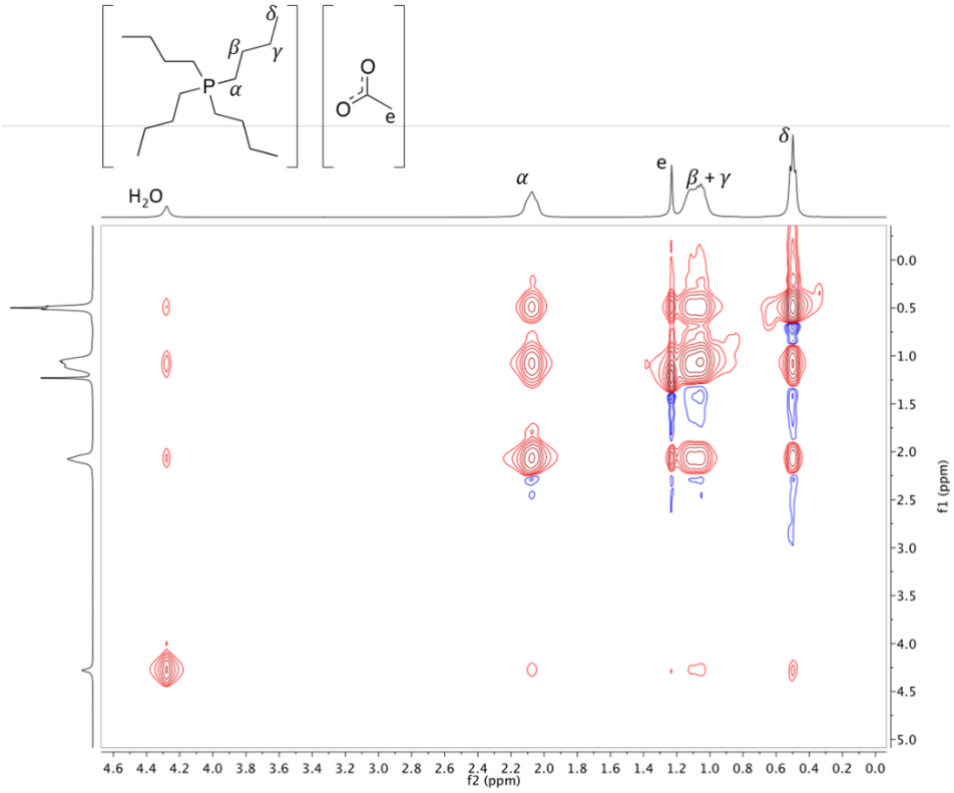

Figure S1.21 – *^{1}H-^{1}H NOESY of [P_{4444}][C_1COO]-water mixture at x_w 0.50 water content, 300 K.*

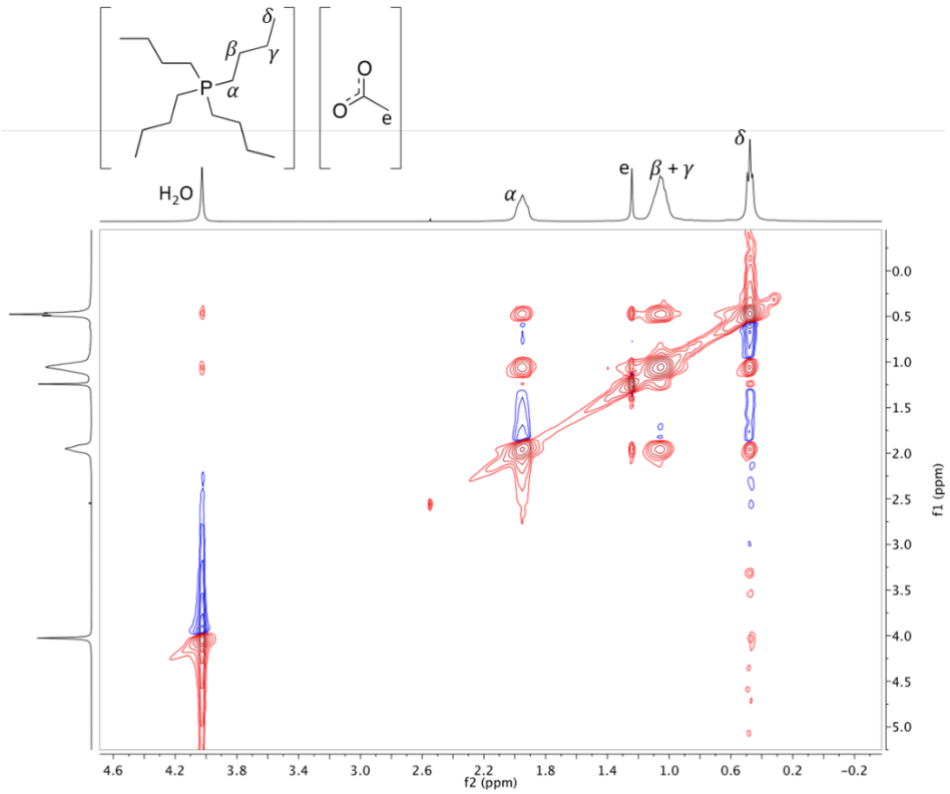

Figure S1.22 – *^{1}H-^{1}H NOESY of [P$_{4444}$][C$_1$COO]-water mixture at x_w 0.67 water content, 300 K.*

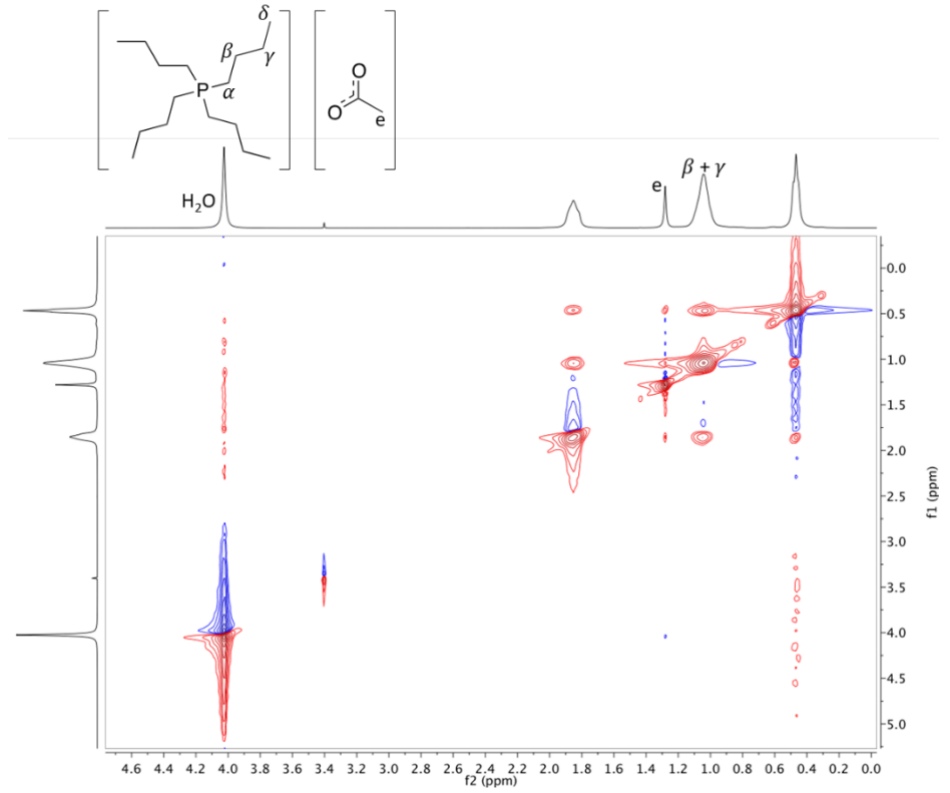

Figure S1.23 – *^{1}H-^{1}H NOESY of [P$_{4444}$][C$_1$COO]-water mixture at x_w 0.80 water content, 300 K.*

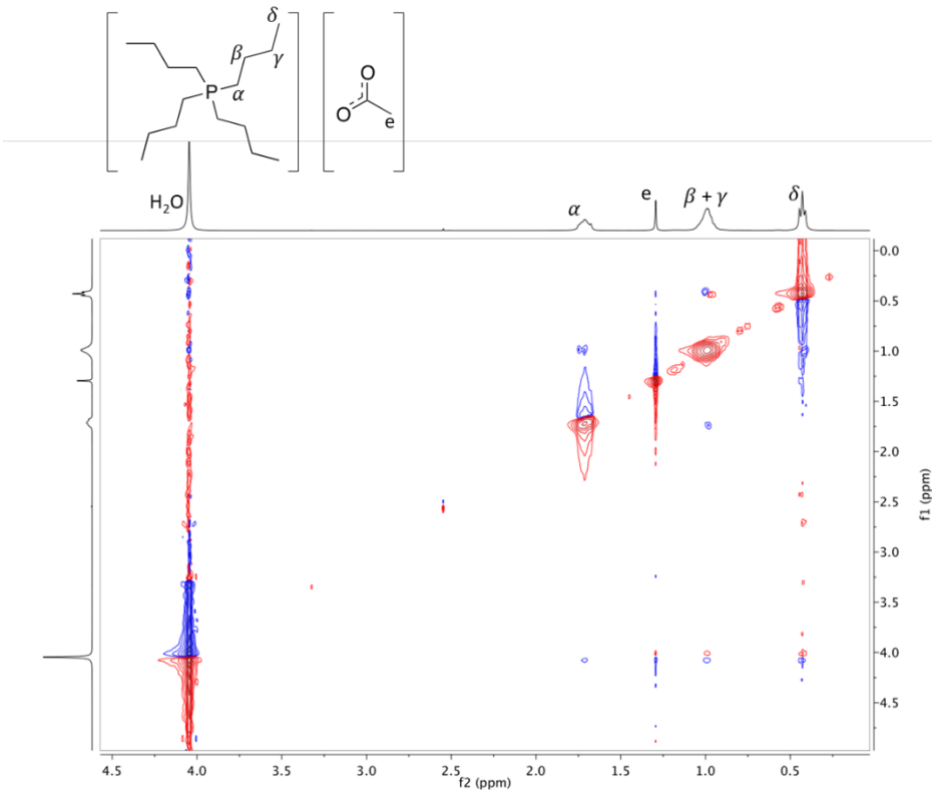

Figure S1.24 – *^{1}H-^{1}H NOESY of [P$_{4444}$][C$_1$COO]-water mixture at x_w 0.90 water content, 300 K.*

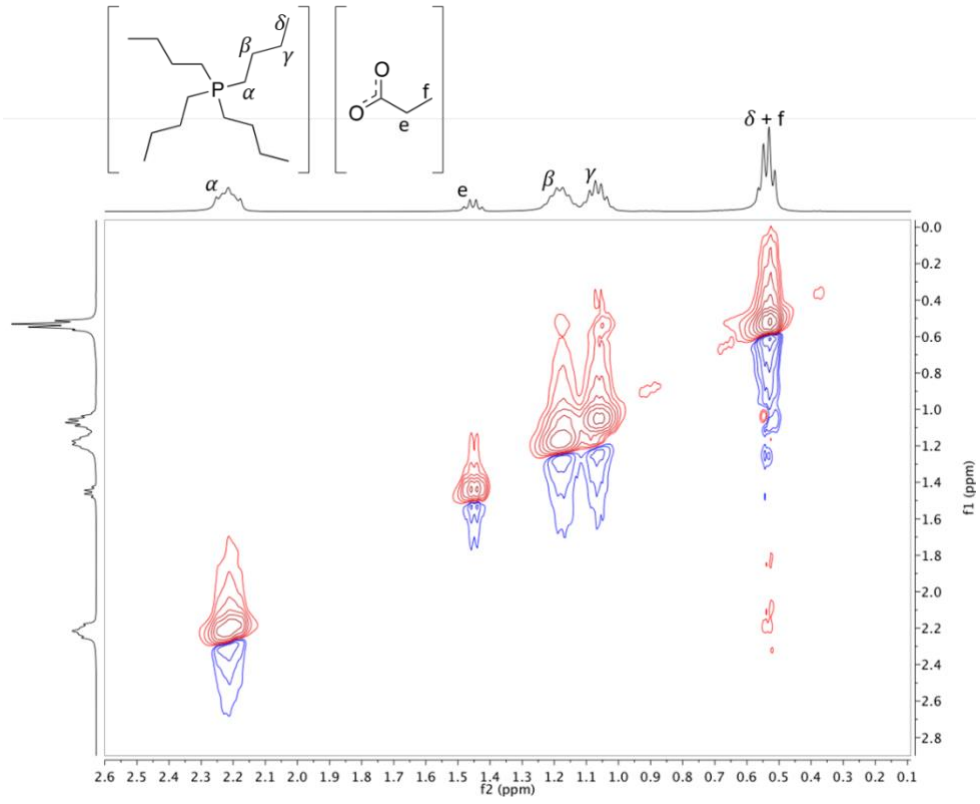

Figure S1.25 – *^{1}H-^{1}H NOESY of pure [P$_{4444}$][C$_2$COO] at 353 K.*

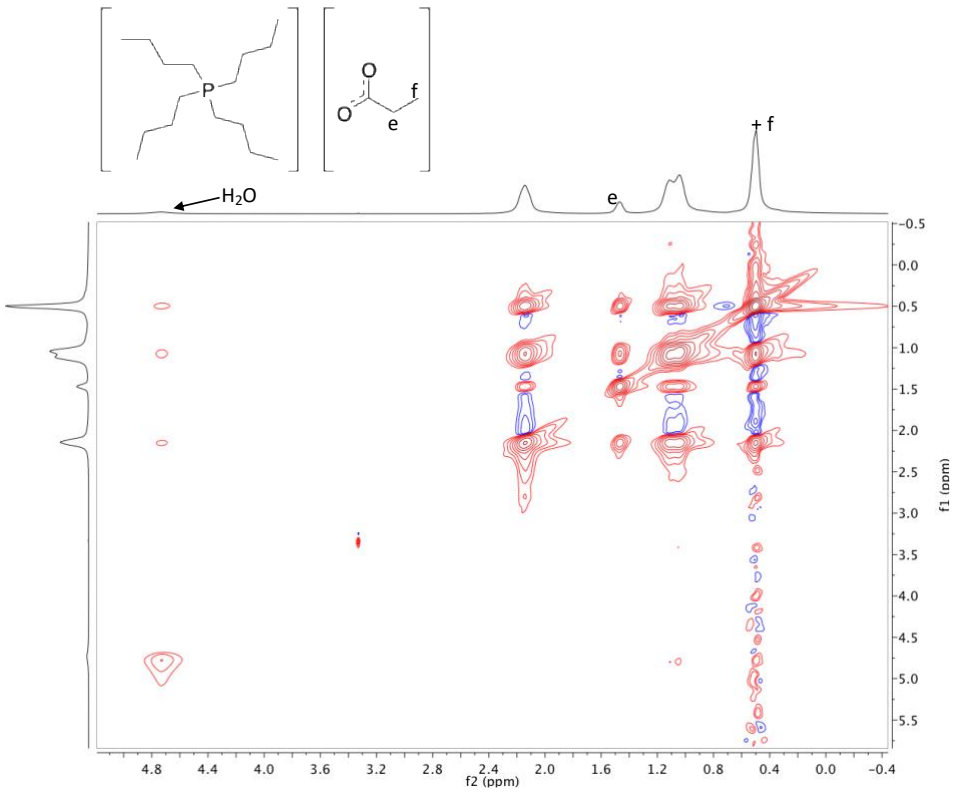

Figure S1.26 – *^{1}H-^{1}H NOESY of [$P_{4\,4\,4\,4}$][C_2COO]-water mixture at x_w 0.34 water content, 300 K.*

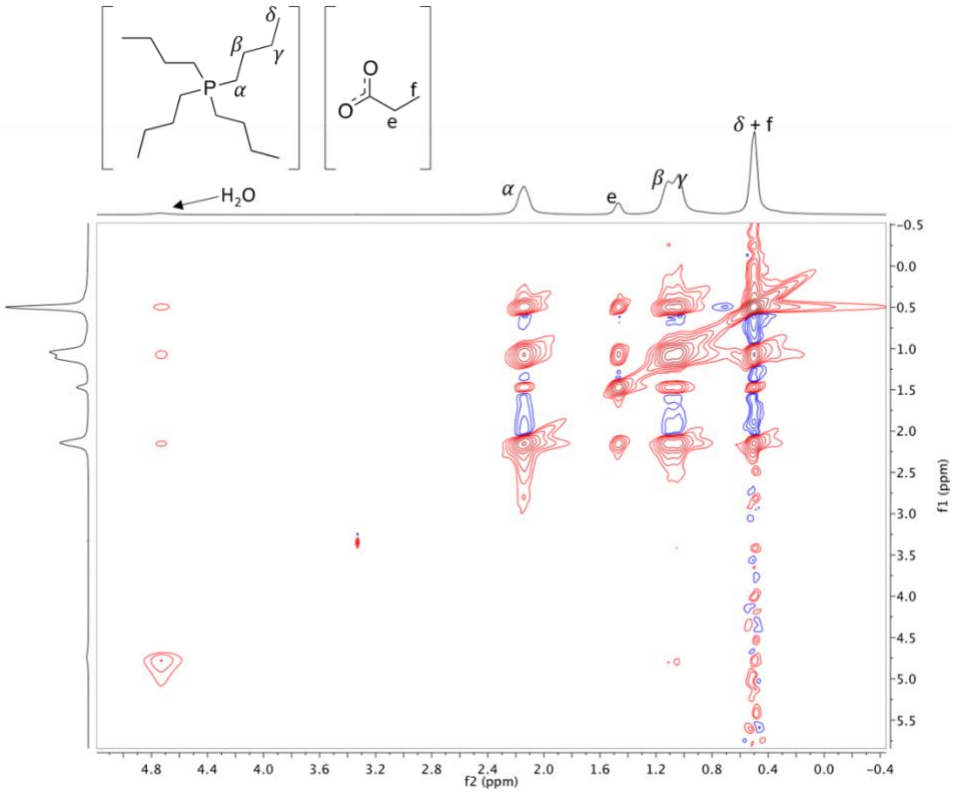

Figure S1.27 – *^{1}H-^{1}H NOESY of [$P_{4\,4\,4\,4}$][C_2COO]-water mixture at x_w 0.50 water content, 300 K.*

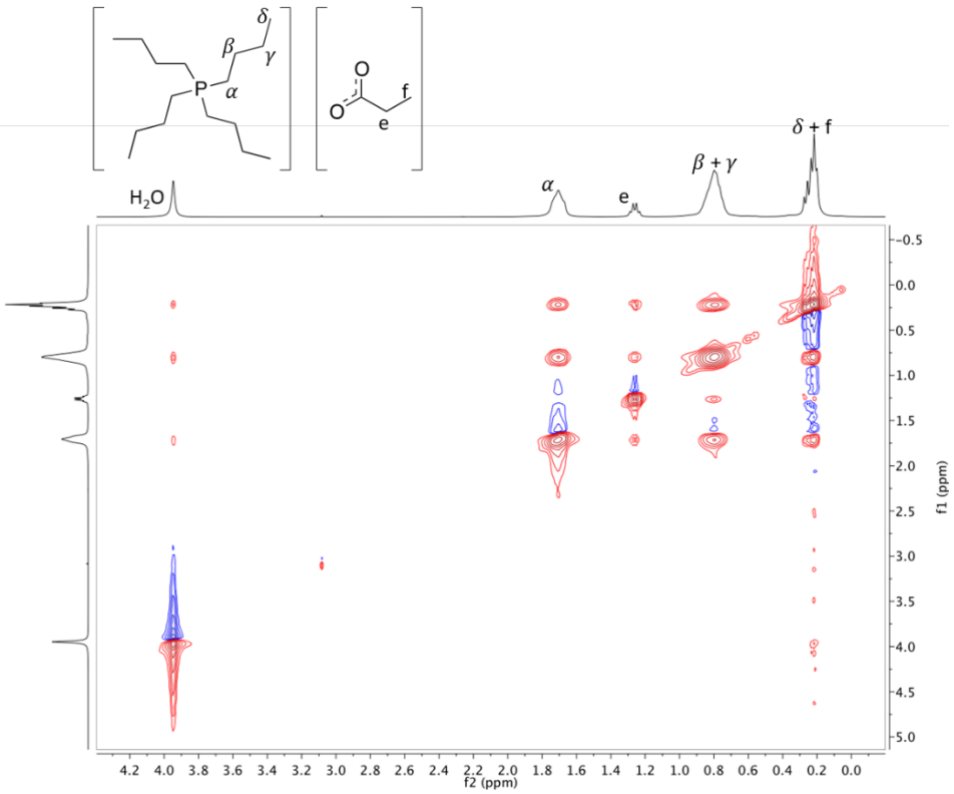

Figure S1.28 – *^{1}H-^{1}H NOESY of [P_{4444}][C_2COO]-water mixture at x_w 0.67 water content, 300 K.*

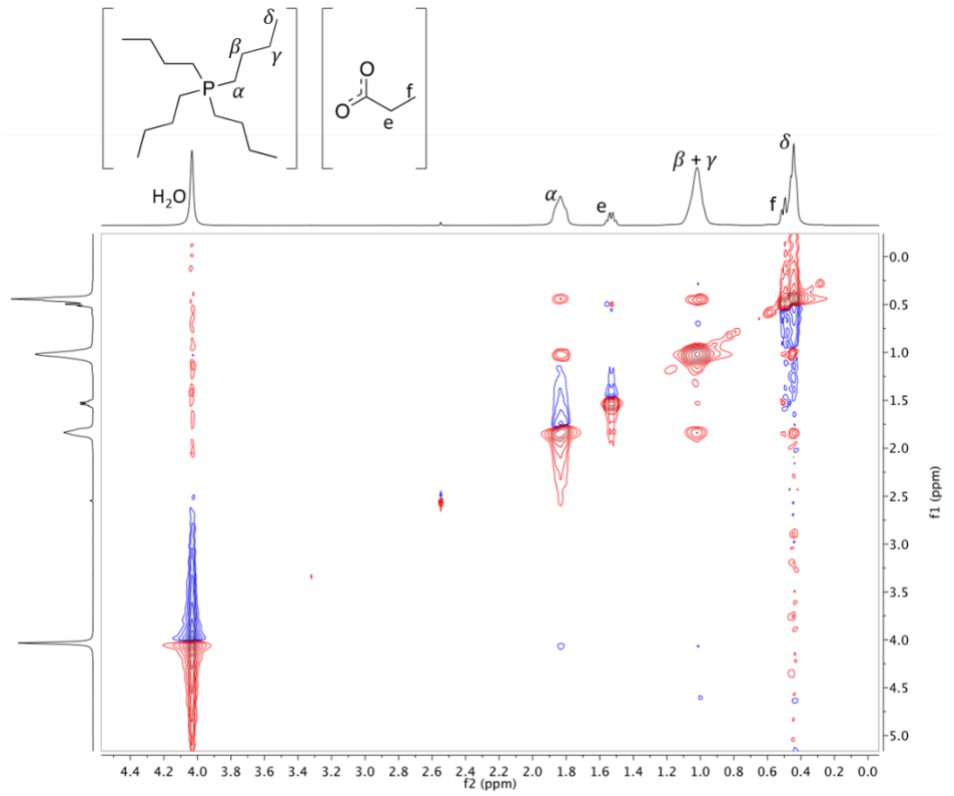

Figure S1.29 – *^{1}H-^{1}H NOESY of [P_{4444}][C_2COO]-water mixture at x_w 0.80 water content, 300 K.*

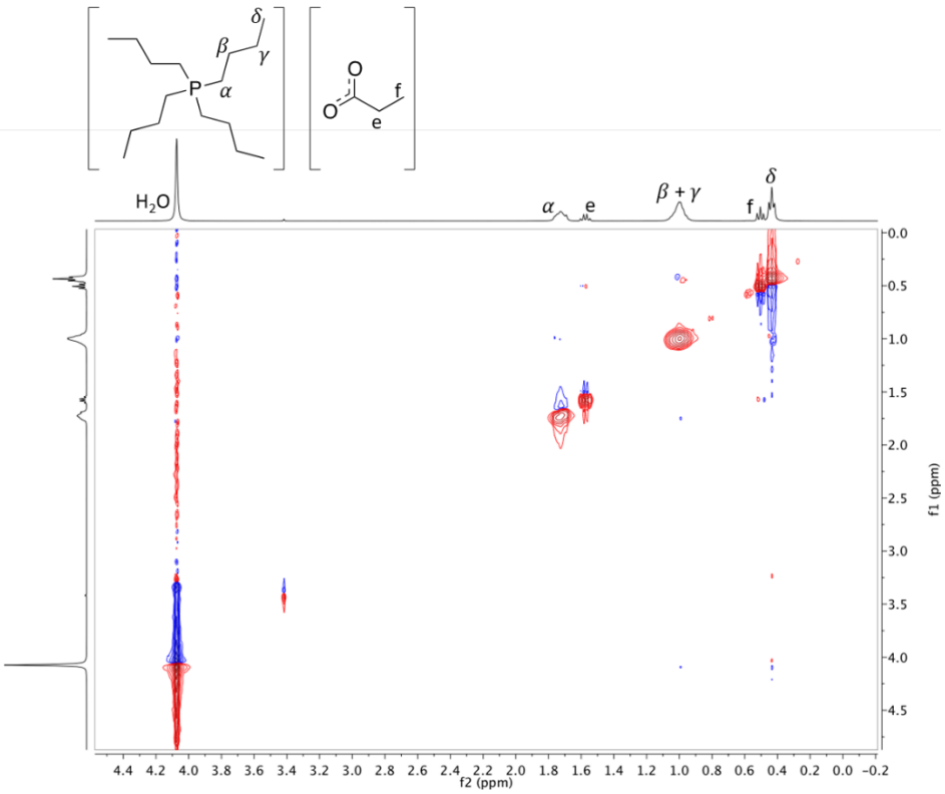

Figure S1.30 – *^{1}H-^{1}H NOESY of [P_{4444}][C_2COO]-water mixture at x_w 0.90 water content, 300 K.*

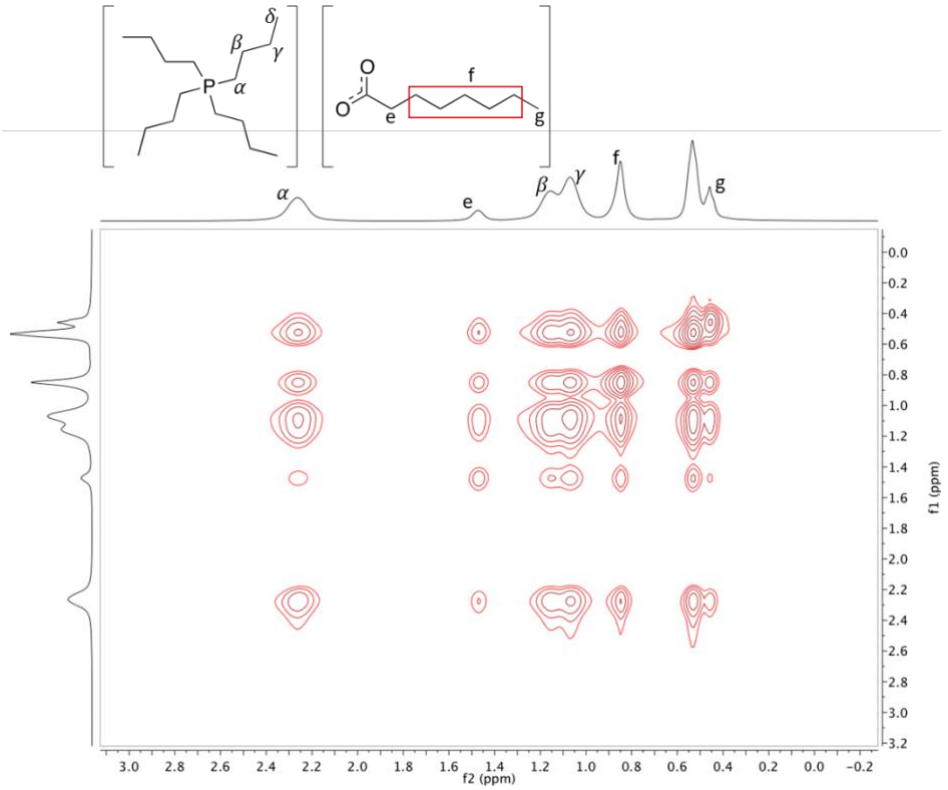

Figure S1.31 – *^{1}H-^{1}H NOESY of pure [P_{4444}][C_7COO] at 300 K.*

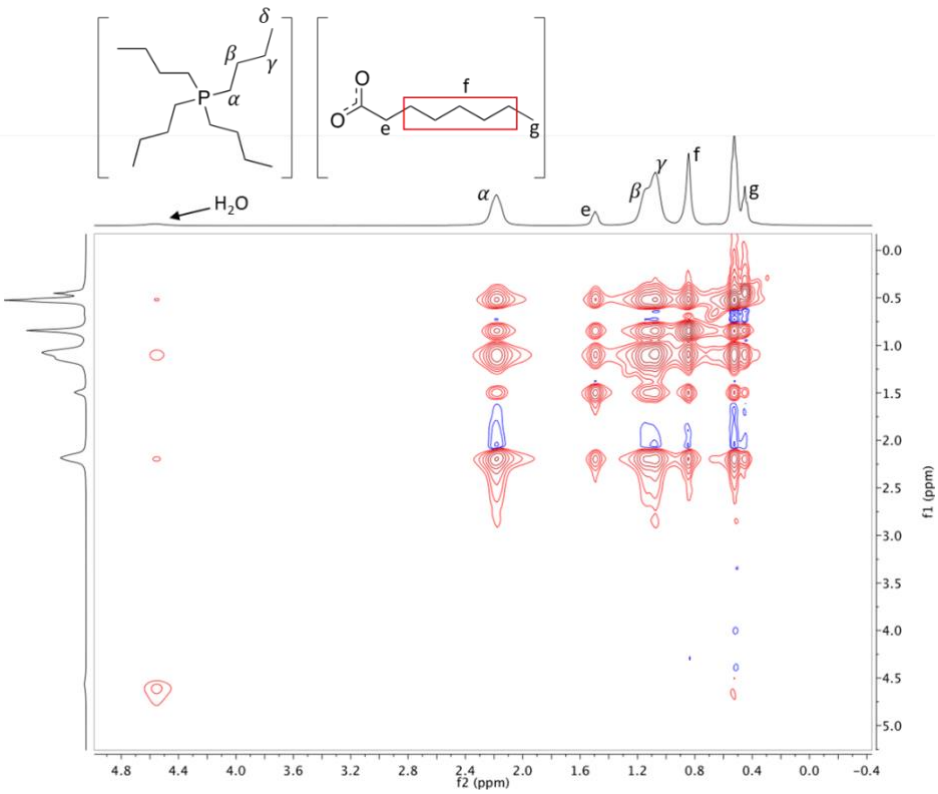

Figure S1.32 – *^{1}H-^{1}H NOESY of [P_{4444}][C_7COO]-water mixture at x_w 0.34 water content, 300 K.*

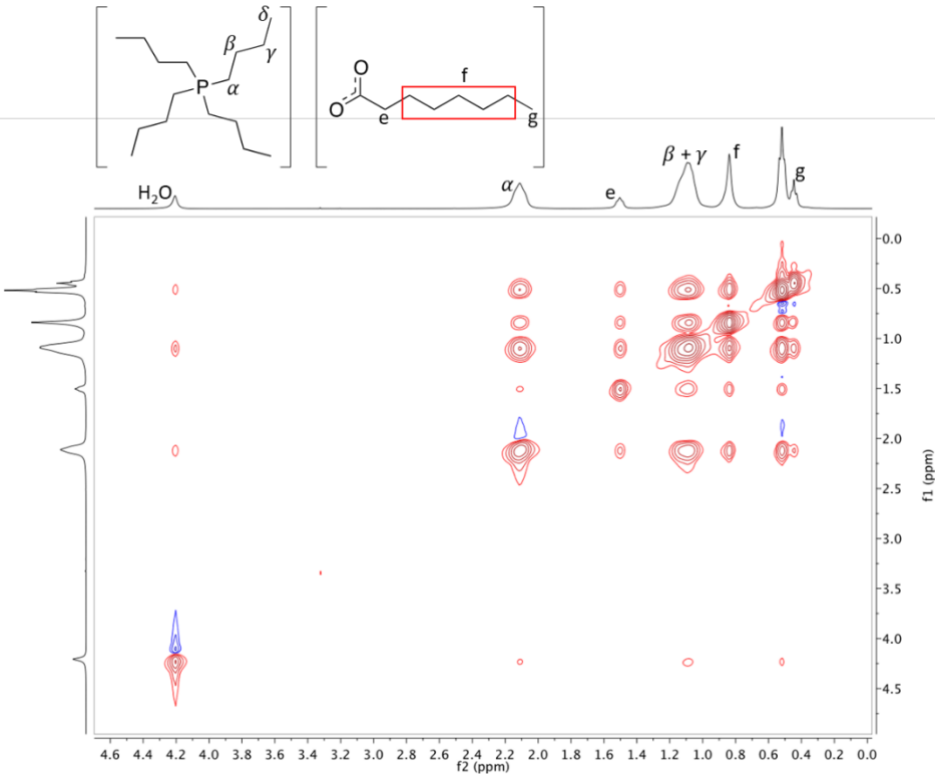

Figure S1.33 – *^{1}H-^{1}H NOESY of [P_{4444}][C_7COO]-water mixture at x_w 0.50 water content, 300 K.*

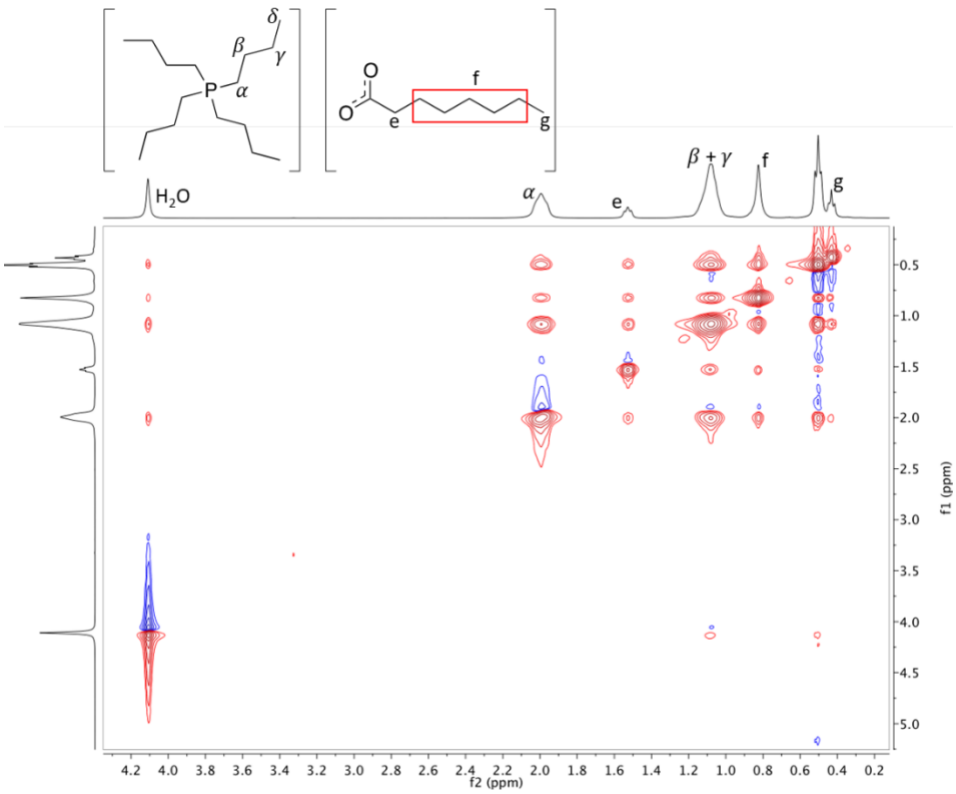

Figure S1.34 – *^{1}H-^{1}H NOESY of [P_{4444}][C_7COO]-water mixture at x_w 0.67 water content, 300 K.*

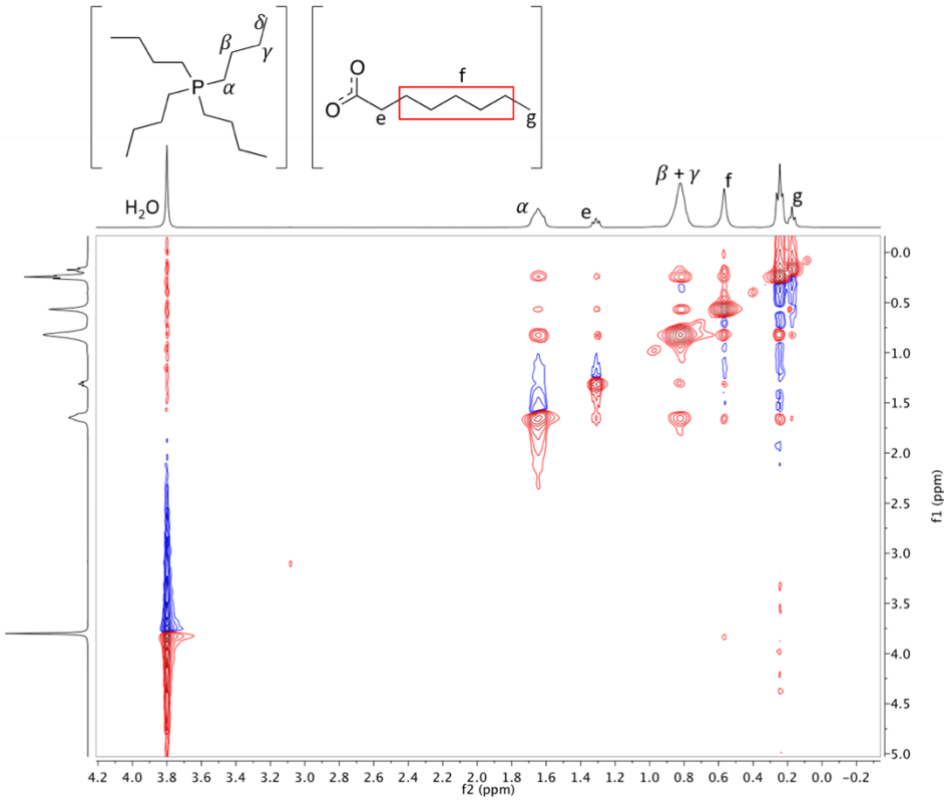

Figure S1.35 – *^{1}H-^{1}H NOESY of [P_{4444}][C_7COO]-water mixture at x_w 0.80 water content, 300 K.*

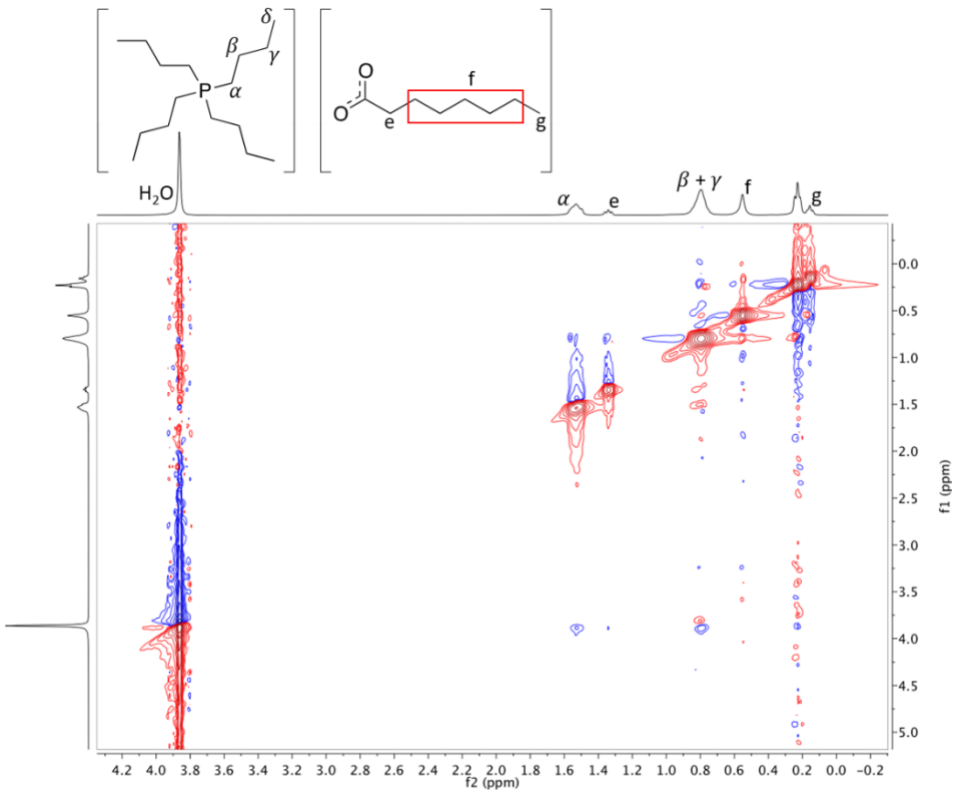

Figure S1.36 – *^{1}H-^{1}H NOESY of [P_{4444}][C_7COO]-water mixture at x_w 0.90 water content, 300 K.*

2. ATR-IR Spectroscopy

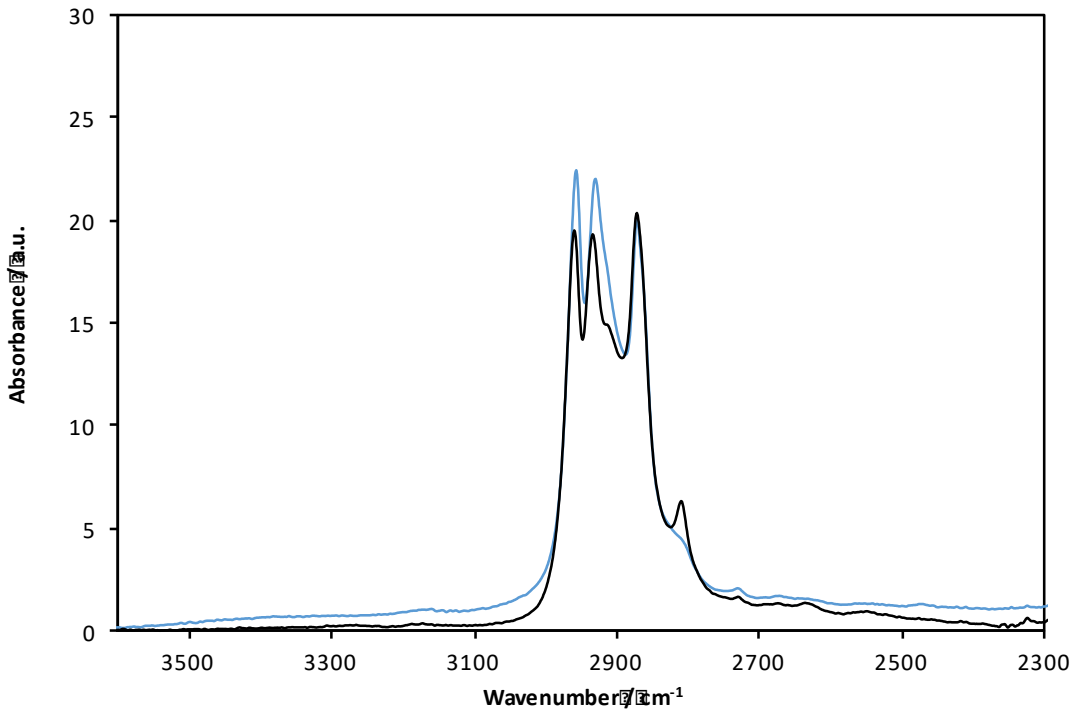

Figure S2.1 – *IR spectra of dry (–) [P_{4444}][C_1COO] and (–) [P_{4444}]Cl, 3600-2300 cm^{-1}.*

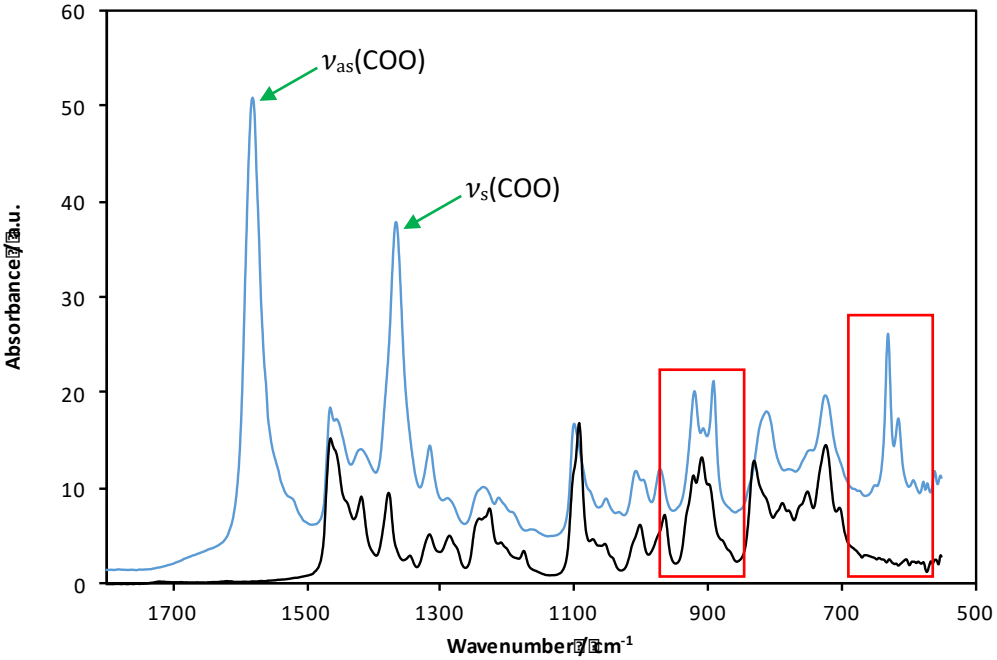

Figure S2.2 *– IR spectra of dry (–) $[P_{4444}][C_1COO]$ and (–) $[P_{4444}]Cl$, 1800-500 cm^{-1}.*

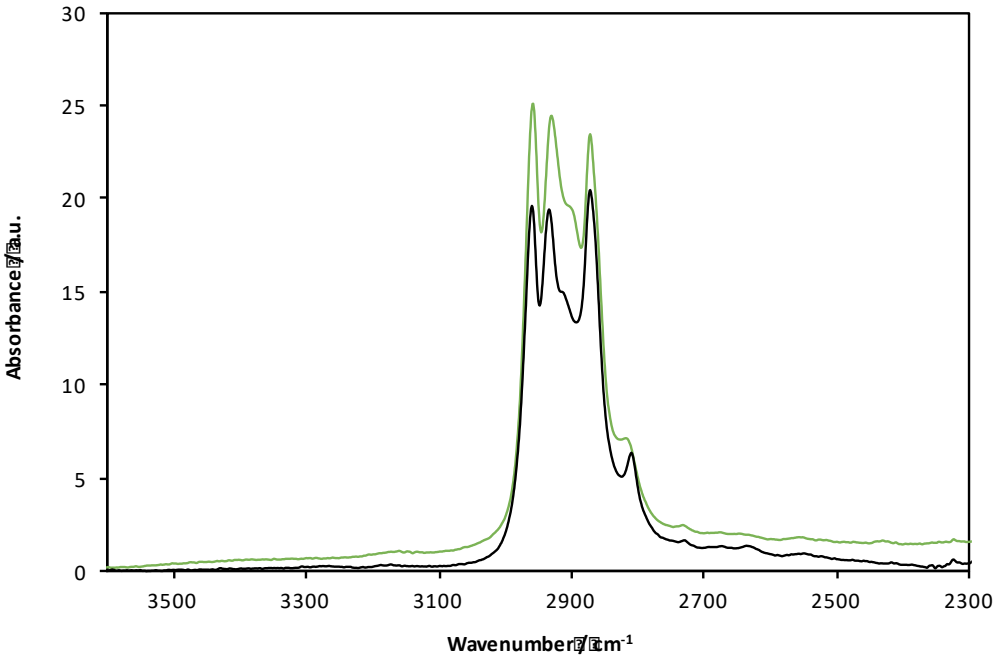

Figure S2.3 *– IR spectra of dry (–) $[P_{4444}][C_2COO]$ and (–) $[P_{4444}]Cl$, 3600-2300 cm^{-1}.*

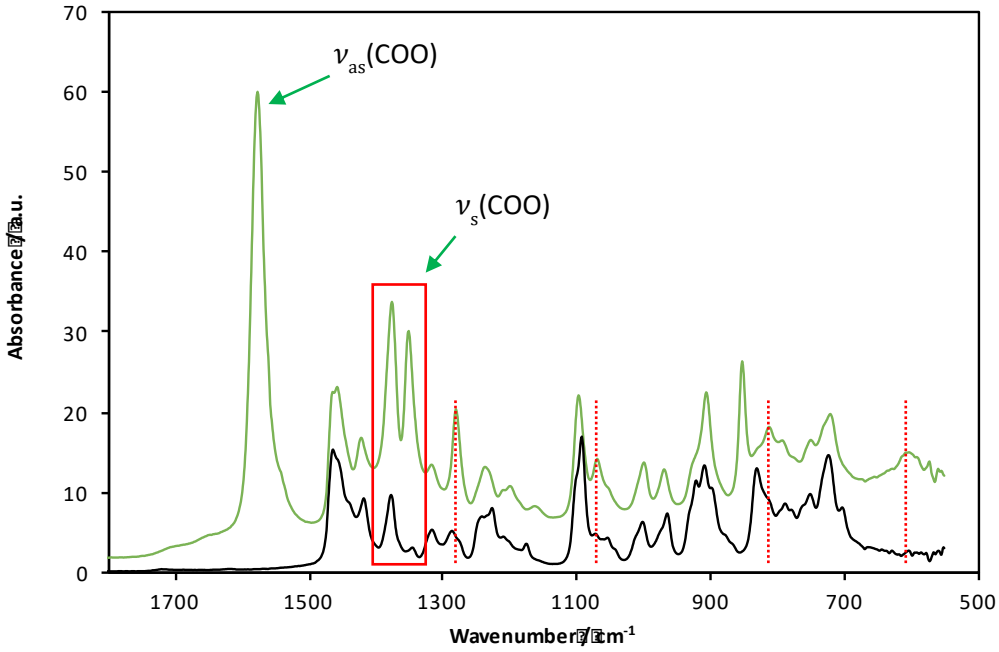

Figure S2.4 – *IR spectra of dry (–) $[P_{4444}][C_2COO]$ and (–) $[P_{4444}]Cl$, 1800-500 cm^{-1}.*

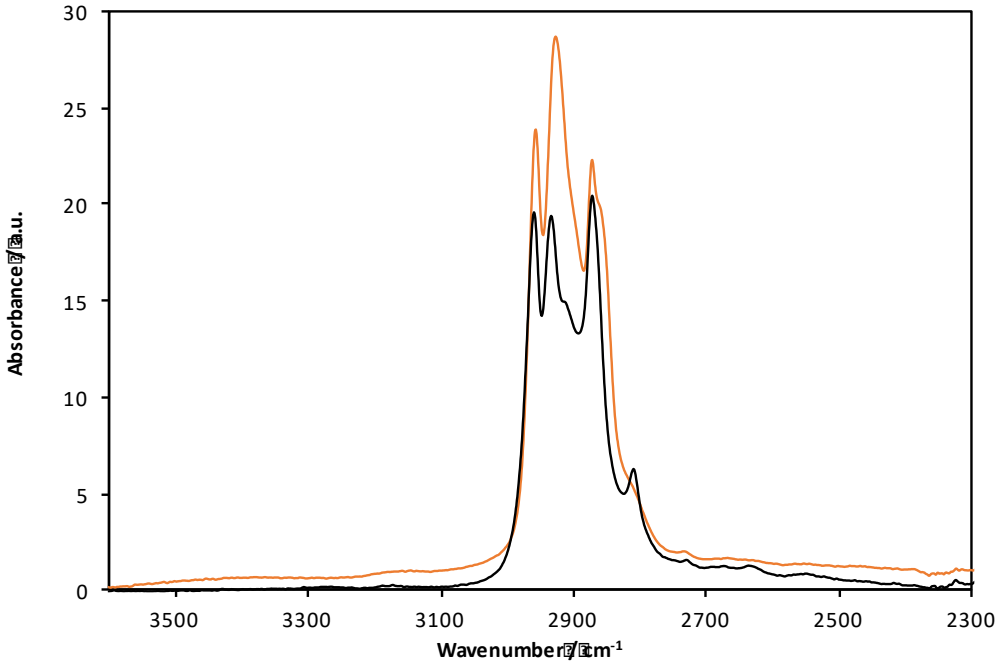

Figure S2.5 – *IR spectra of dry (–) $[P_{4444}][C_7COO]$ and (–) $[P_{4444}]Cl$, 3600-2300 cm^{-1}.*

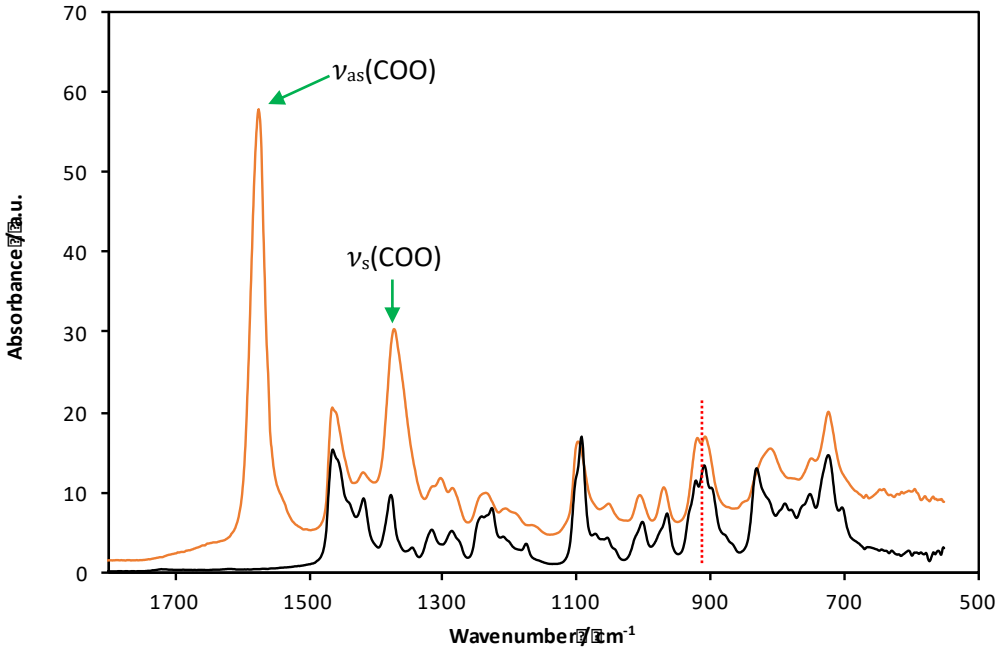

Figure S2.6 – *IR spectra of dry (–) $[P_{4444}][C_7COO]$ and (–) $[P_{4444}]Cl$, 1800-500 cm^{-1}.*

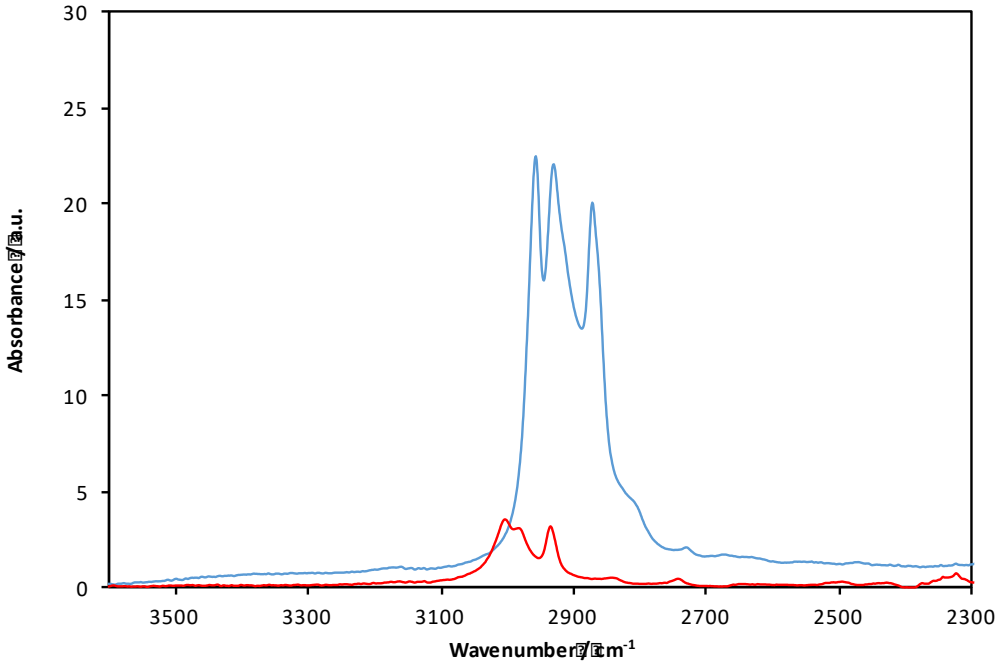

Figure S2.7 – *IR spectra of (–) $[P_{4444}][C_1COO]$ and (–) sodium ethanoate, 3600-2300 cm^{-1}.*

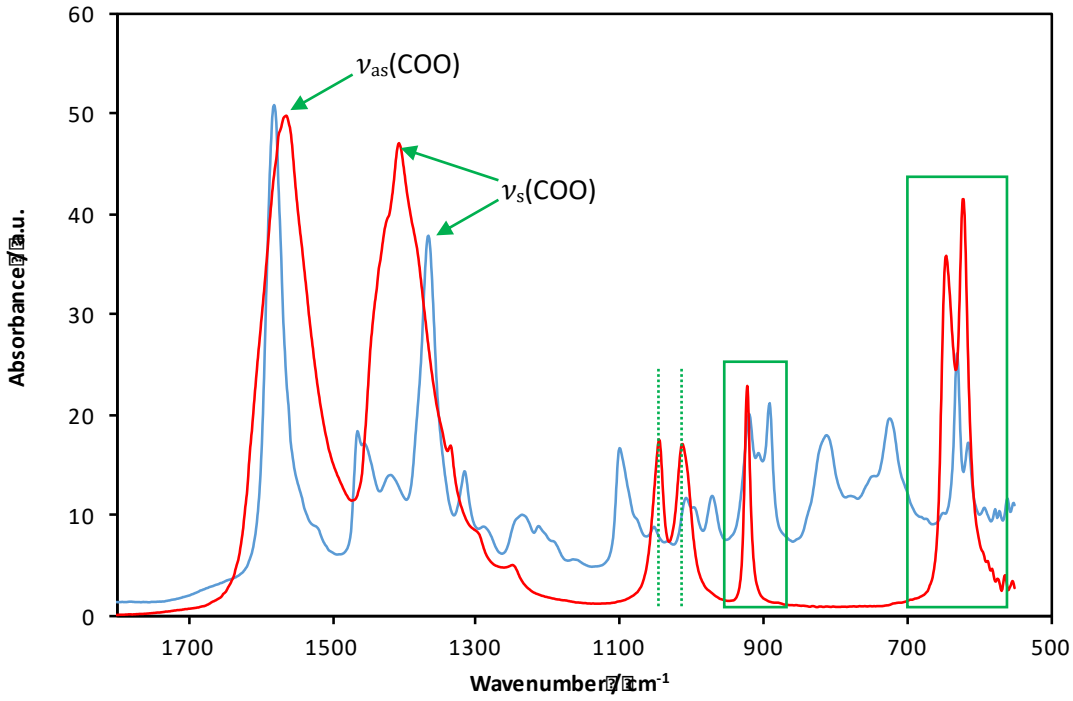

Figure S2.8 – *IR spectra of (–) $[P_{4444}][C_1COO]$ and (–) sodium ethanoate, 1800-500 cm^{-1}.*

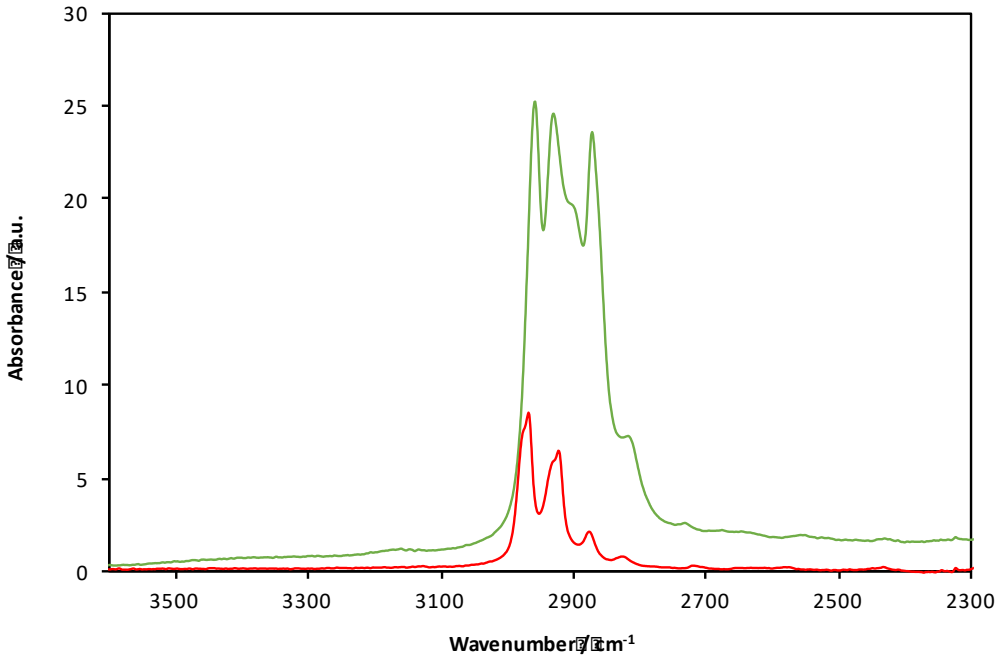

Figure S2.9 – *IR spectra of (–) $[P_{4444}][C_2COO]$ and (–) potassium propanoate, 3600-1800 cm^{-1}.*

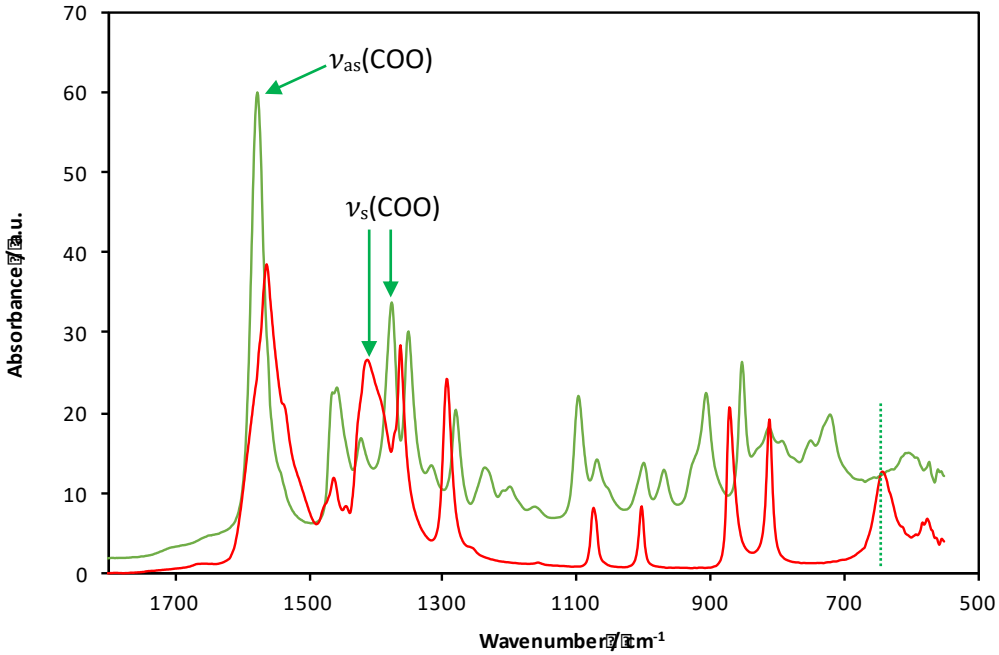

Figure S2.10 – *IR spectra of (–) [P_{4444}][C_2COO] and (–) potassium propanoate, 1800-500 cm^{-1}.*

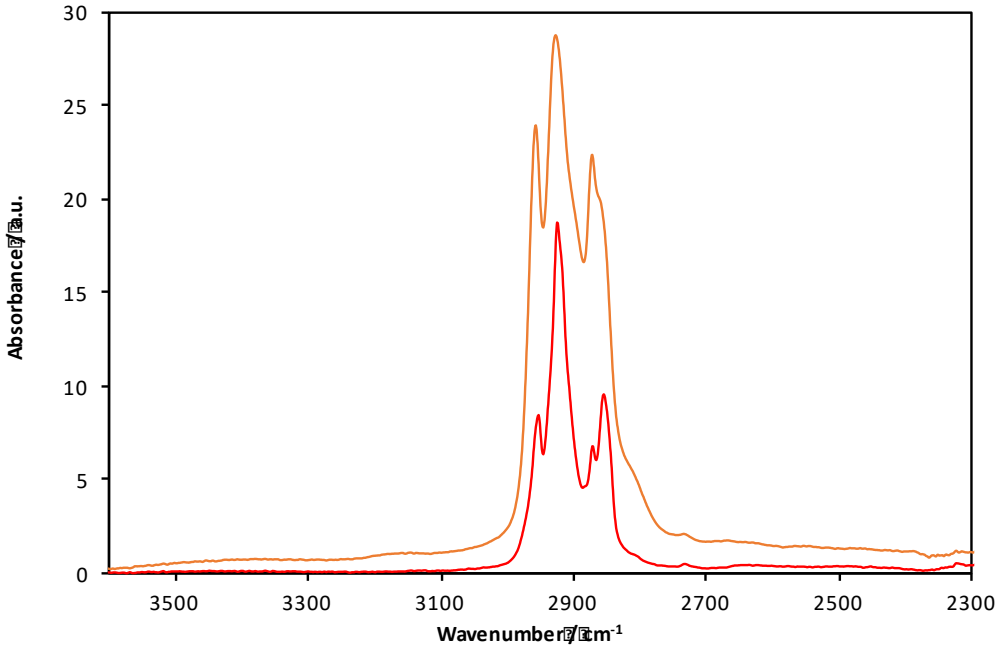

Figure S2.11 – *IR spectra of (–) [P_{4444}][C_7COO] and (–) potassium octanoate, 3600-2300 cm^{-1}.*

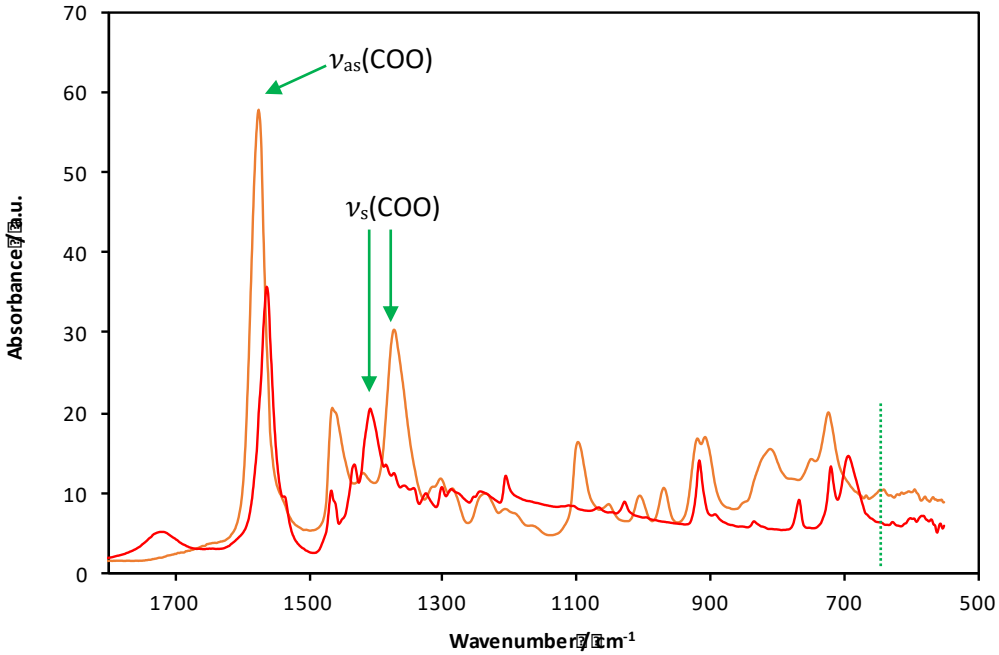

Figure S2.12 – *IR spectra of (–) $[P_{4\,4\,4\,4}][C_7COO]$ and (–) potassium octanoate, 1800-500 cm^{-1}.*

Table S2.1 – *Experimental IR vibrational bands of $[C_1COO]^-$ in dry $[P_{4444}][C_1COO]$ and NaC_1COO, accompanied by literature values of NaC_1COO.*

Mode Assignment	Wavenumber / cm^{-1}		
	$[P_{4444}][C_1COO]$	NaC_1COO exp	NaC_1COO lit.
ν(C-H)	2956 - 2870	3000, 2979, 2932	2989, 2936[2] 3000, 2955[3]
ν_{as}(COO)	1581	1561	1578[2] 1583[3]
$\omega(CH_3)$	–	–	1498[2]
$\tau(CH_3)$	–	–	1443[2] 1440[3]
$\rho(CH_3)$	–	–	1430[2]
ν_s(COO)	1366	1405	1414[2] 1421[3]
$\delta(CH_3)$	1329	1333	1333[3]
$\rho(CH_3)$	–	1043	1042[2] 1043[3]
$\rho(CH_3)$	1001	1010	1009[2] 1012[3]
ν(CC)	920	923	924[2, 3]
?	890	–	–
δ(COO)	630	643	646[2] 650[3]
ω(COO)	611	620	615[2]

Table S2.2 – *Experimental IR vibrational bands of $[C_2COO]^-$ in dry $[P_{4444}][C_2COO]$ and potassium propanoate, accompanied by literature values of sodium propanoate.*

Mode Assignment	Wavenumber / cm^{-1}		
	$[P_{4444}][C_2COO]$	KC_2COO exp	NaC_2COO lit.
ν(C-H)	2956 - 2870	2967, 2921, 2873	2974, 2953, 2937[4]
ν_{as}(COO)	1577	1561	1573, 1565, 1553[3] 1563[4]
ν_s(COO)	1378	1410	1429[3] 1428[4]
$\omega(CH_3)$	1353	1362	1369[4]
$\omega(CH_2)$	1289	1293	1301[4]
ν(C-CH_3) + $\rho(CH_3)$	1095	1072	1076[3] 1077[4]
ν(C-CH_3)	997	1001	1009[4]
ν(CC)	905	–	920[4]
ν(C-COO)	851	869	880[3] 881[4]
$\rho(CH_2)$	810	810	815[3]
δ(COO)	603	639	647[4]

Table S2.3 – *Experimental IR vibrational bands of $[C_7COO]^-$ in dry $[P_{4444}][C_7COO]$ and potassium octanoate.*

Mode Assignment	Wavenumber / cm^{-1}	
	$[P_{4444}][C_7COO]$	KC_7COO exp
ν(C-H)	2956 - 2870	2951, 2923, 2868, 2852
ν_{as}(COO)	1575	1561
ν_s(COO)	1372	1405
$\omega(CH_2)$	1214	1202
ν(CC)	915	914
ν(C-COO)	768	764
$\rho(CH_2)$	746	717
δ(COO)	689	689

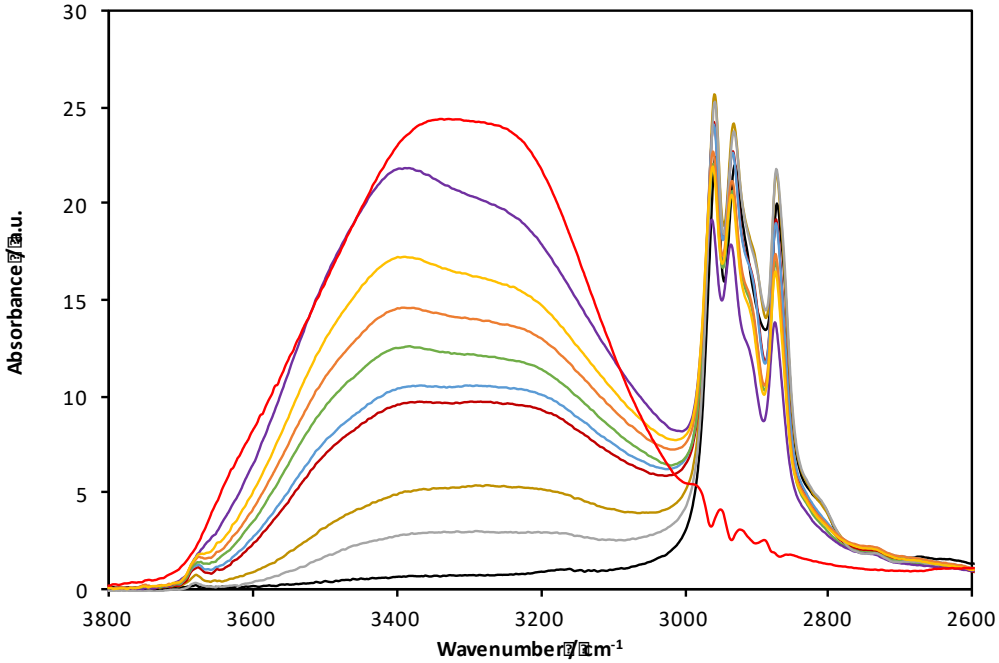

Figure S2.13 – *Expansion of infrared spectra (3800 – 2600 cm^{-1}) of [$P_{4\,4\,4\,4}$][C_1COO]-water mixtures, at: (–) x_w 0.00; (–) x_w 0.30; (–) x_w 0.51; (–) x_w 0.67; (–) x_w 0.75; (–) x_w 0.80; (–) x_w 0.83; (–) x_w 0.86; (–) x_w 0.90; and (–) x_w 1.00.*

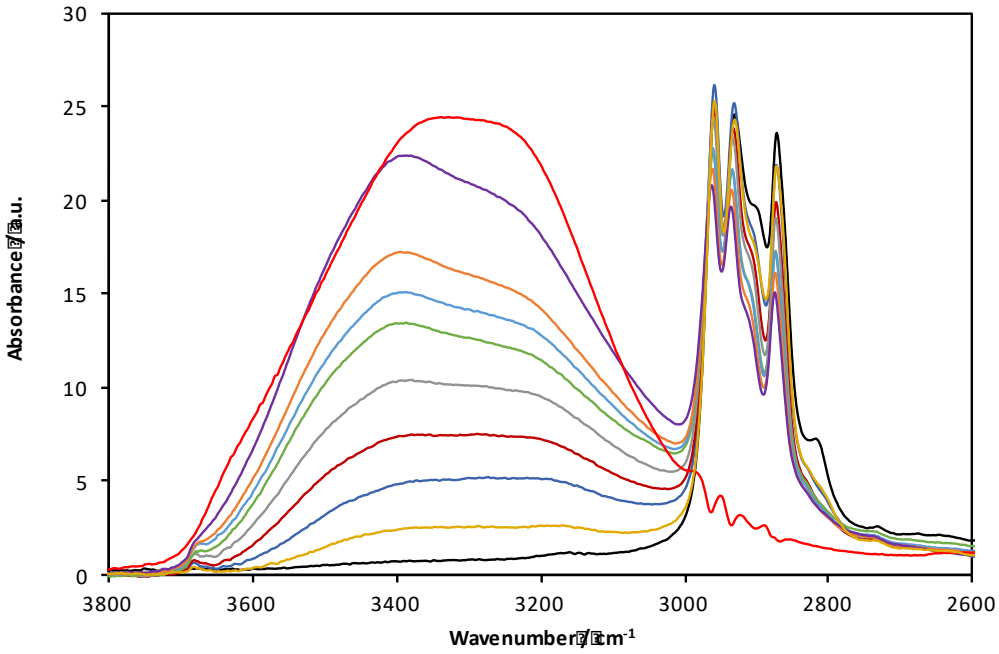

Figure S2.14 – *Expansion of infrared spectra (3800 – 2600 cm^{-1}) of [$P_{4\,4\,4\,4}$][C_2COO]-water mixtures, at: (–) x_w 0.00; (–) x_w 0.32; (–) x_w 0.50; (–) x_w 0.67; (–) x_w 0.75;(–) x_w 0.80; (–) x_w 0.83; (–) x_w 0.86; (–) x_w 0.90; and (–) x_w 1.00.*

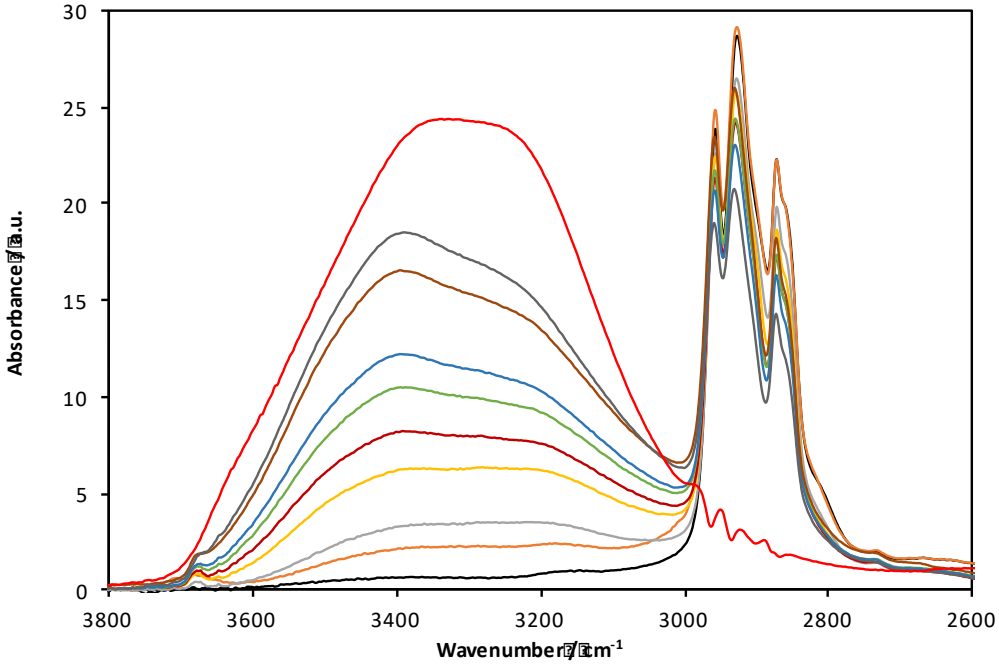

Figure S2.15 – *Expansion of infrared spectra (3800 – 2600 cm^{-1}) of [$P_{4\,4\,4\,4}$][C_7COO]-water mixtures, at: (–) x_w 0.00; (–) x_w 0.34; (–) x_w 0.51; (–) x_w 0.67; (–) x_w 0.75;(–) x_w 0.80; (–) x_w 0.83; (–) x_w 0.86; (–) x_w 0.90; and (–) x_w 1.00.*

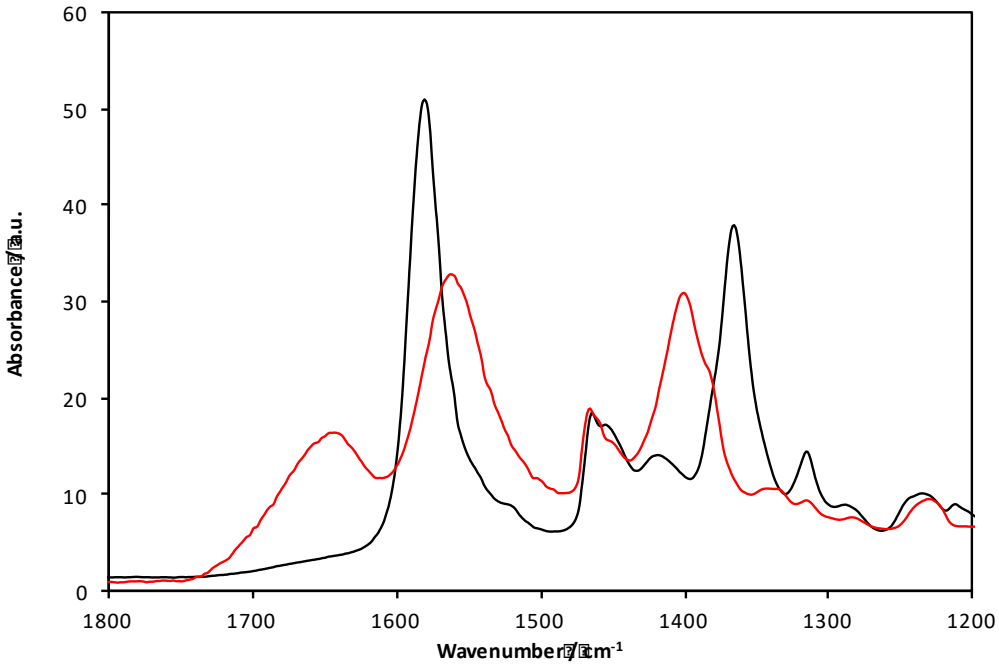

Figure S2.16 – *Expansion of infrared spectra (1800 – 1200 cm^{-1}) depicting ν_{as}(COO) and ν_s(COO) vibrational modes of [$P_{4\,4\,4\,4}$][C_1COO]-water mixtures, at: (–) x_w 0.00; and (–) x_w 0.90.*

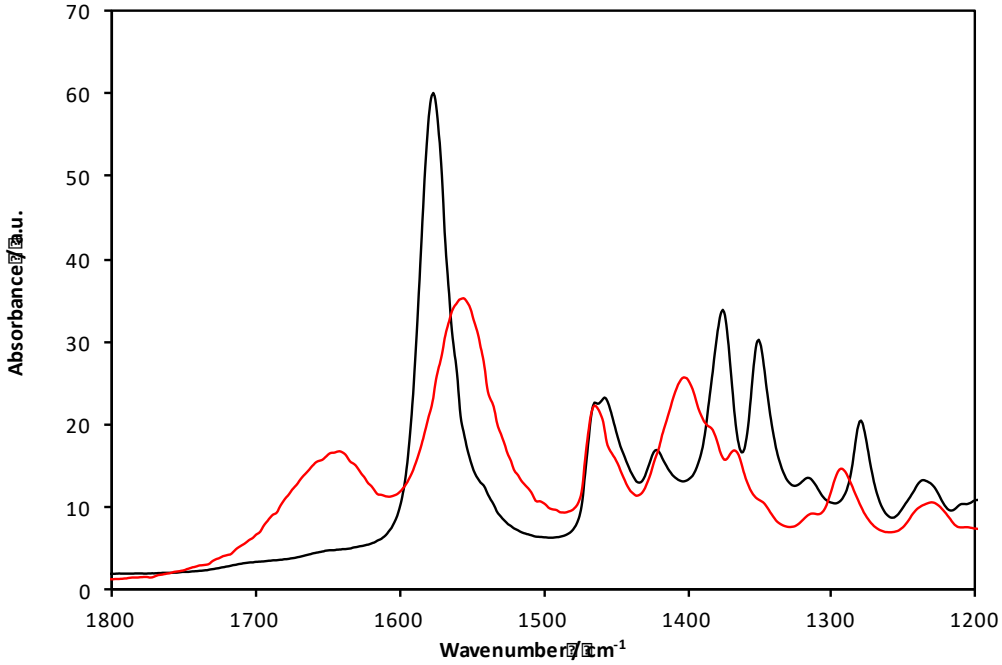

Figure S2.17 – *Expansion of infrared spectra (1800 – 1200 cm^{-1}) depicting ν_{as}(COO) and ν_{s}(COO) vibrational modes of [P$_{4\,4\,4\,4}$][C$_2$COO]-water mixtures, at: (–) x_w 0.00; and (–) x_w 0.90.*

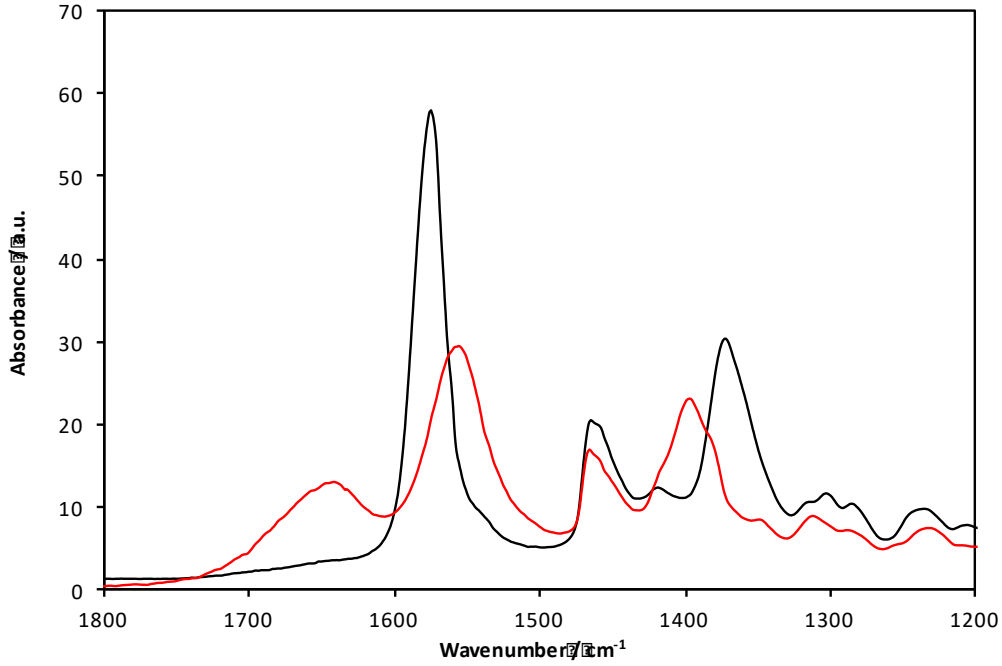

Figure S2.18 – *Expansion of infrared spectra (1800 – 1200 cm^{-1}) depicting ν_{as}(COO) and ν_{s}(COO) vibrational modes of [P$_{4\,4\,4\,4}$][C$_7$COO]-water mixtures, at: (–) x_w 0.00; and (–) x_w 0.90.*

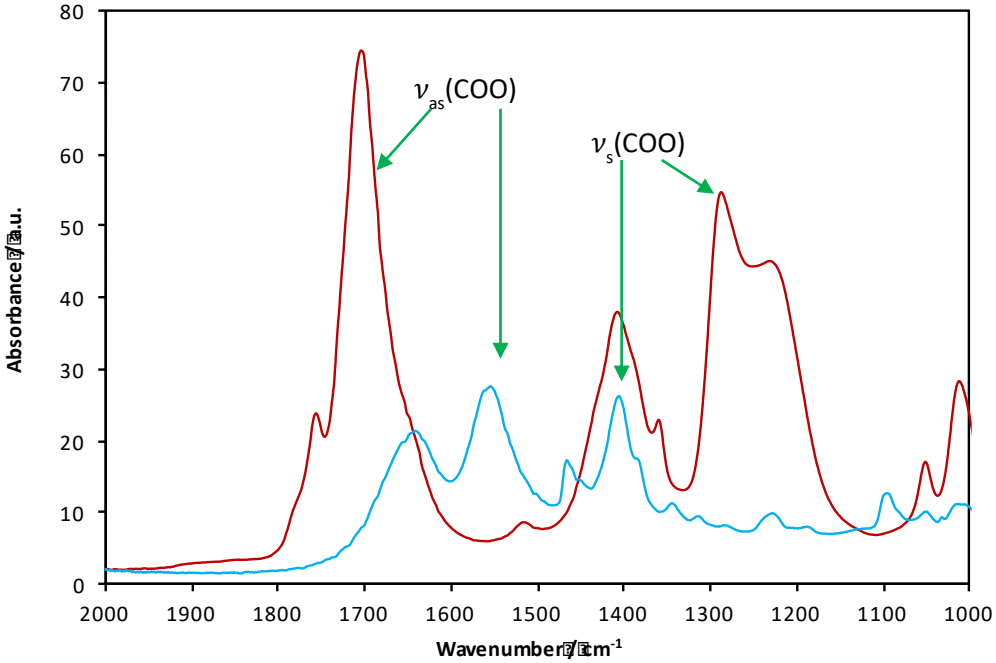

Figure S2.19 – *Comparison of infrared spectra of (–) [P_{4444}][C_1COO]-water mixture at x_w 0.95 and (–) ethanoic acid.*

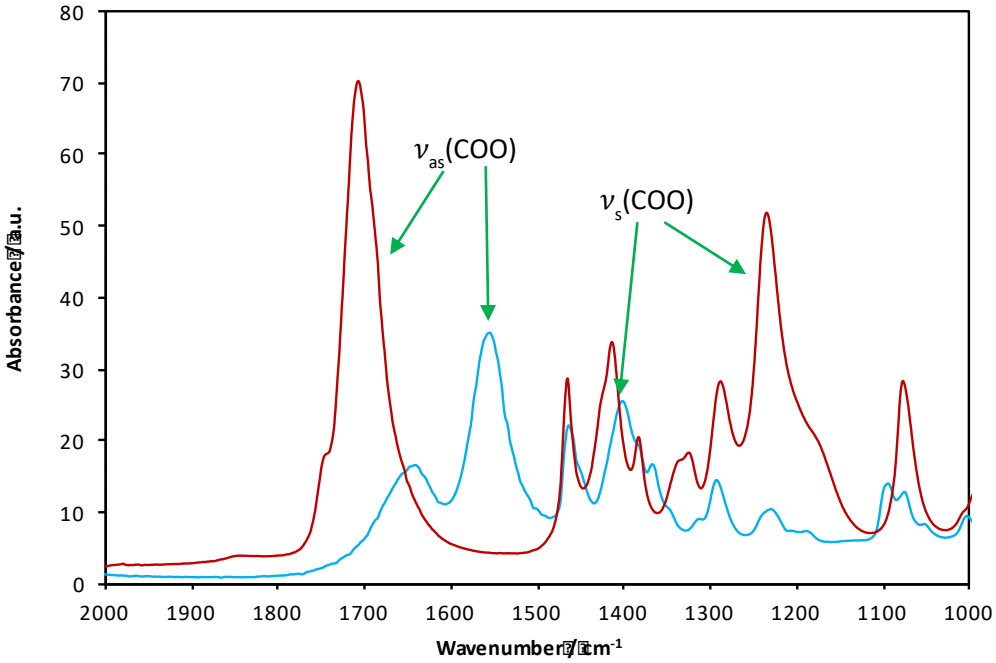

Figure S2.20 – *Comparison of infrared spectra of (–) [P_{4444}][C_2COO]-water mixture at x_w 0.95 and (–) propanoic acid.*

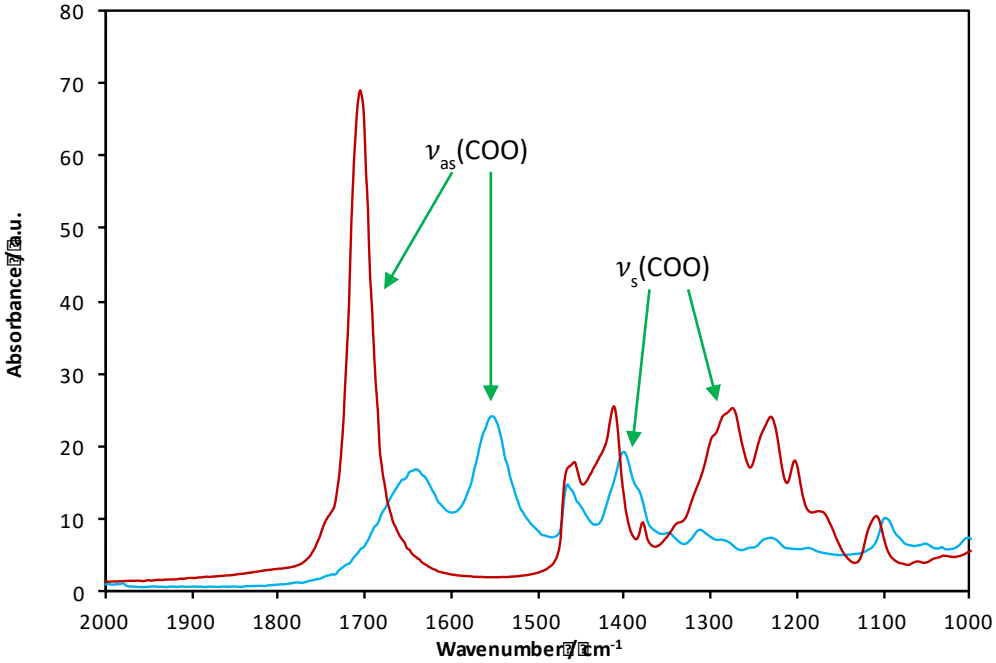

Figure S2.21 – *Comparison of infrared spectra of (–) $[P_{4\,4\,4\,4}][C_7COO]$-water mixture at x_w 0.95 and (–) octanoic acid.*

3. $[P_{4\,4\,4\,4}][C_nCOO]$-D_2O Mixtures

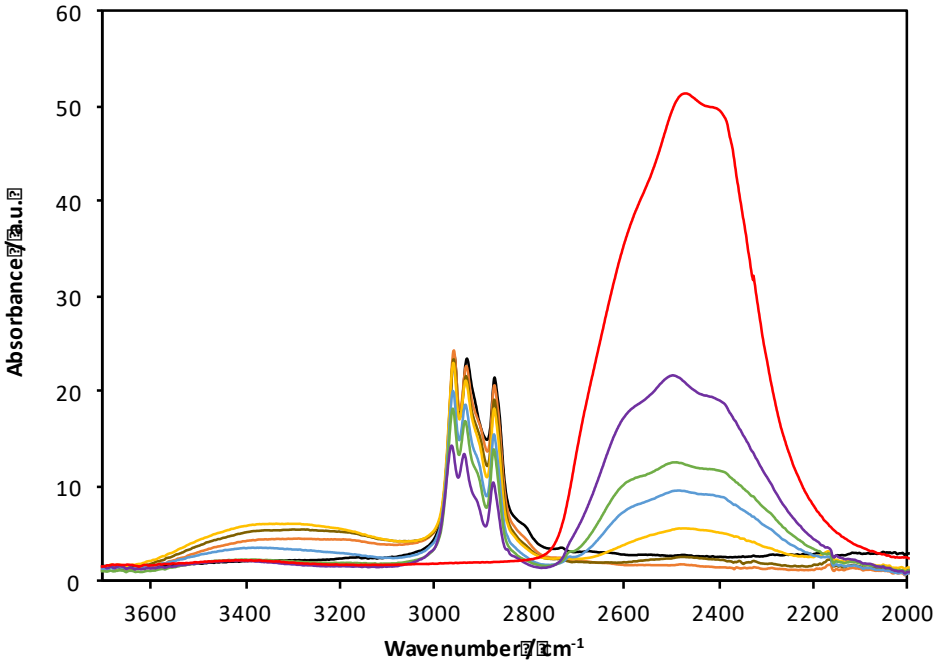

Figure S3.1 *– Expansion of infrared spectra (3700 – 2000 cm^{-1}) of $[P_{4\,4\,4\,4}][C_1COO]$-D_2O mixtures, at: (–) x_D 0.00; (–) x_D 0.34; (–) x_D 0.51; (–) x_D 0.67; (–) x_D 0.75; (–) x_D 0.80; (–) x_D 0.90; and (–) x_D 1.00.*

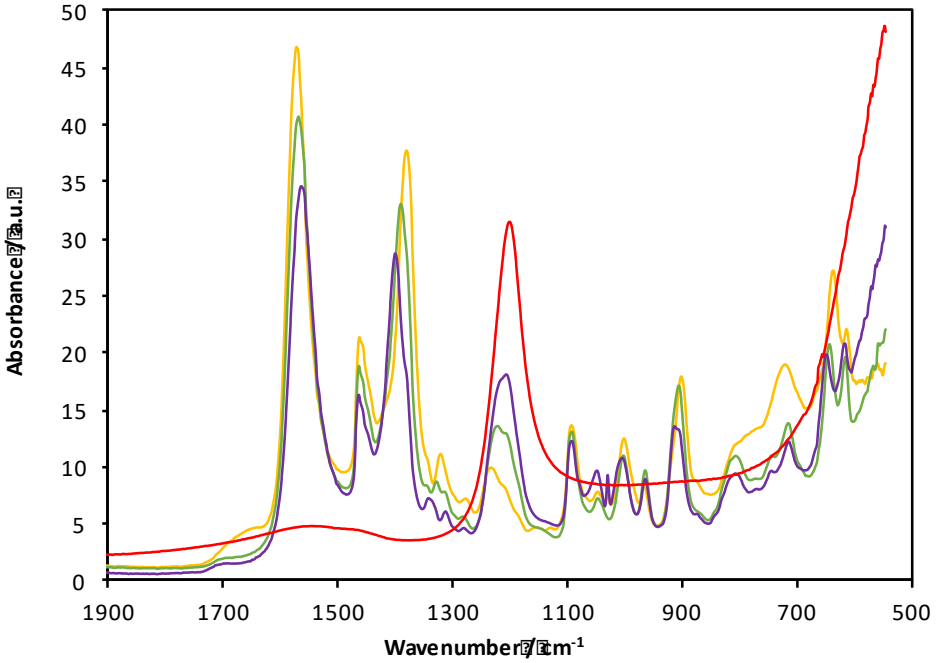

Figure S3.2 *– Expansion of infrared spectra (1900 – 500 cm^{-1}) of $[P_{4\,4\,4\,4}][C_1COO]$-D_2O mixtures, at: (–) x_D 0.67; (–) x_D 0.80; (–) x_D 0.90; and (–) x_D 1.00.*

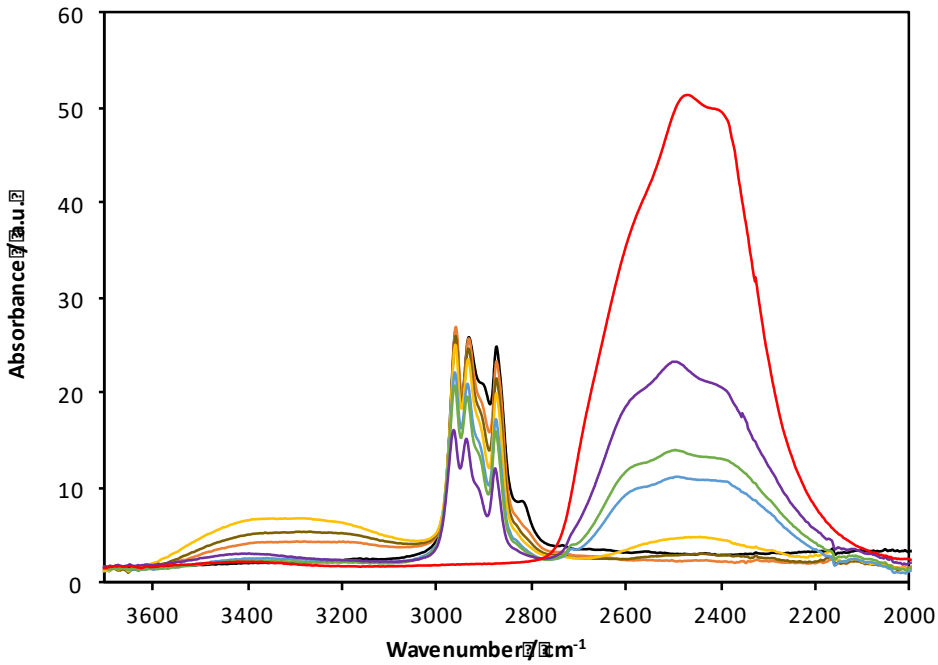

Figure S3.3 – *Expansion of infrared spectra (3700 – 2000 cm^{-1}) of $[P_{4444}][C_2COO]$-D_2O mixtures, at: (–) x_D 0.00; (–) x_D 0.34; (–) x_D 0.51; (–) x_D 0.67; (–) x_D 0.75; (–) x_D 0.80; (–) x_D 0.90; and (–) x_D 1.00.*

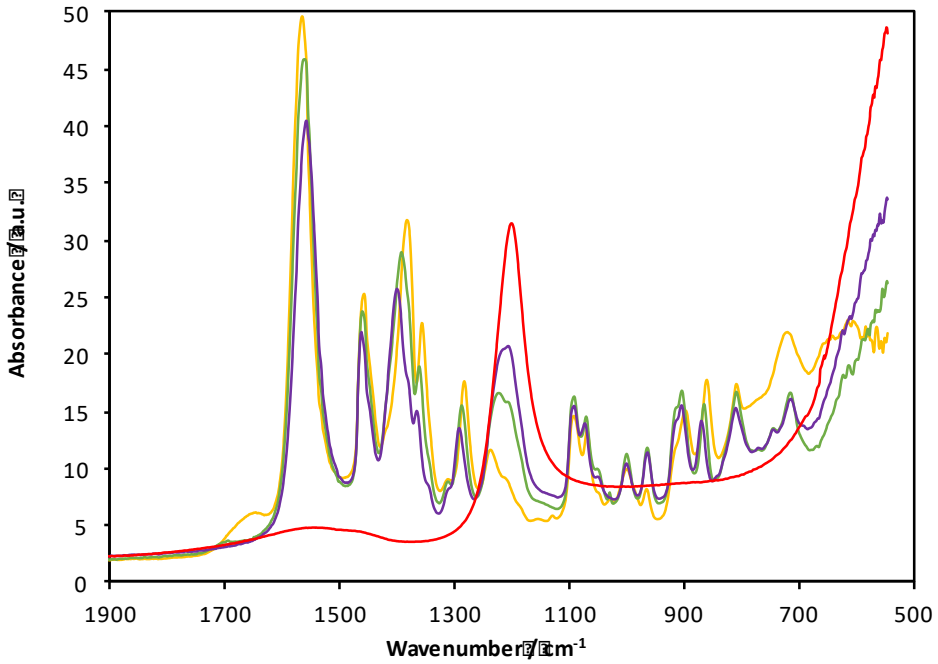

Figure S3.4 – *Expansion of infrared spectra (1900 – 500 cm^{-1}) of $[P_{4444}][C_2COO]$-D_2O mixtures, at: (–) x_D 0.67; (–) x_D 0.80; (–) x_D 0.90; and (–) x_D 1.00.*

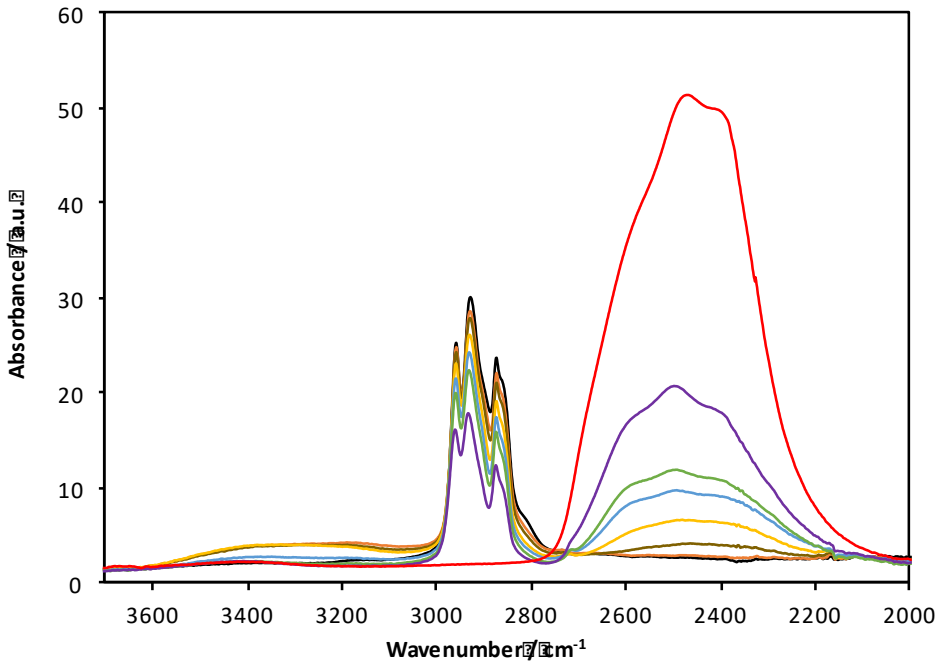

Figure S3.5 – *Expansion of infrared spectra (3700 – 2000 cm^{-1}) of $[P_{4444}][C_7COO]$-D_2O mixtures, at: (–) x_D 0.00; (–) x_D 0.34; (–) x_D 0.50; (–) x_D 0.67; (–) x_D 0.75; (–) x_D 0.80; (–) x_D 0.90; and (–) x_D 1.00.*

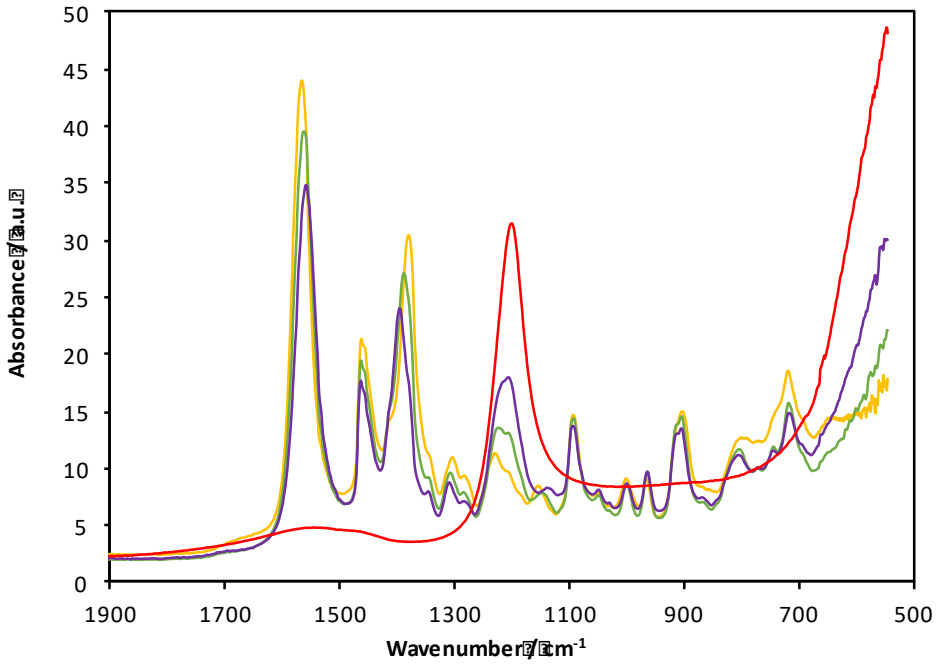

Figure S3.6 – *Expansion of infrared spectra (1900 – 500 cm^{-1}) of $[P_{4444}][C_7COO]$-D_2O mixtures, at: (–) x_D 0.67; (–) x_D 0.80; (–) x_D 0.90; and (–) x_D 1.00.*

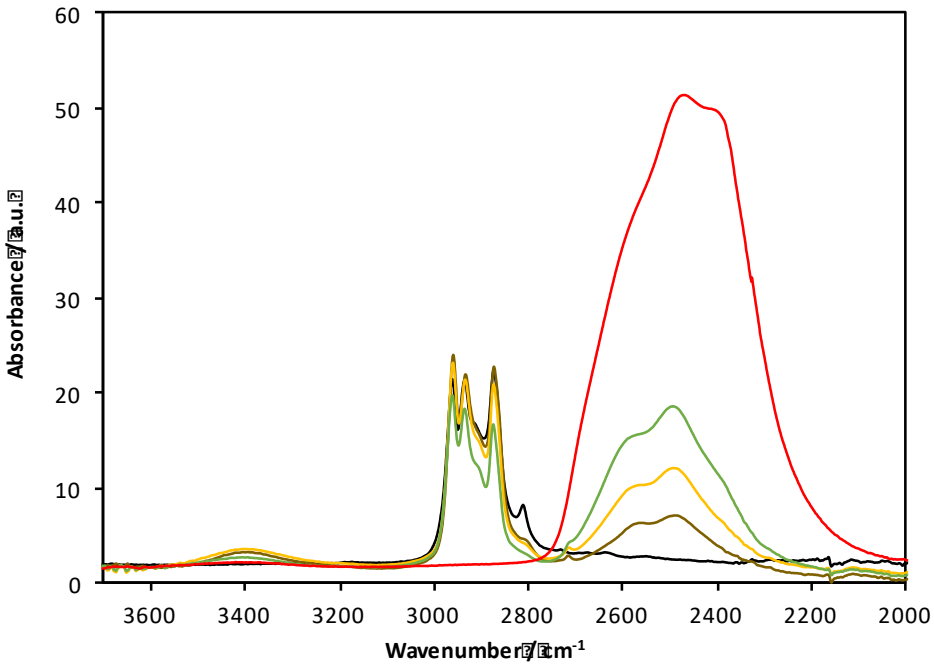

Figure S3.7 – *Expansion of infrared spectra (3700 – 2000 cm^{-1}) of $[P_{4444}]Cl$-D_2O mixtures, at: (–) x_D 0.00; (–) x_D 0.50; (–) x_D 0.67; (–) x_D 0.80; and (–) x_D 1.00.*

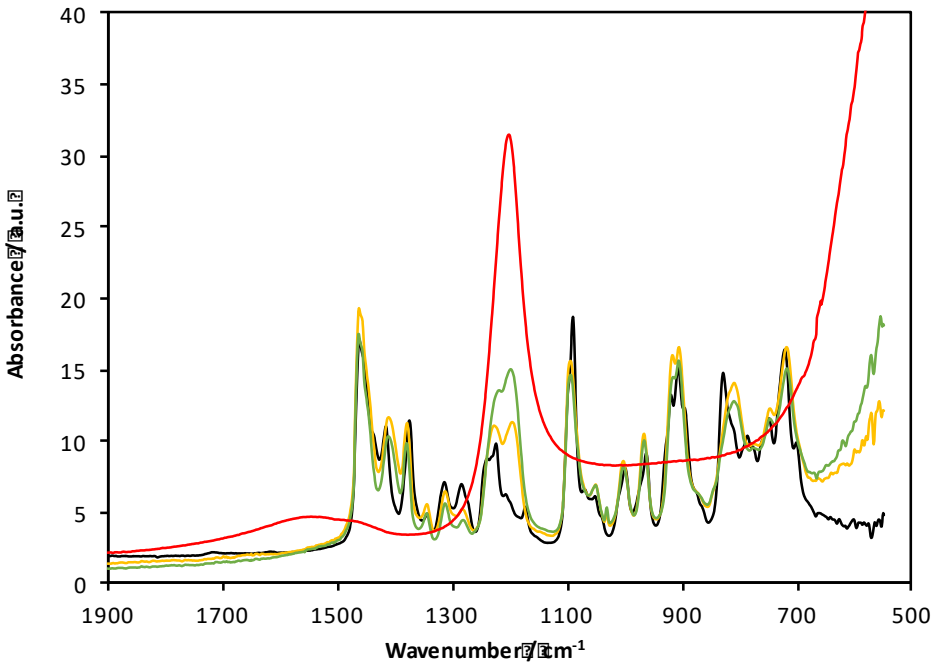

Figure S3.8 – *Expansion of infrared spectra (1900 – 500 cm^{-1}) of $[P_{4444}]Cl$-D_2O mixtures, at: (–) x_D 0.67; (–) x_D 0.80; and (–) x_D 1.00.*

Table S3.1 – *^{1}H-NMR chemical shifts, δ, and peak integration of water and α-H of the cation in $[P_{4444}][C_1COO]$-D_2O, as a function of D_2O content, x_D.*

	Water		α-H	
x_D	δ / ppm	∫^{1}H	δ / ppm	∫^{1}H
0			2.21	8.00
0.1011	3.87	0.15	2.19	7.40
0.1992	4.48	0.65	2.16	7.36
0.3368	4.41	0.93	2.14	6.80
0.4166	4.17	1.24	2.11	6.97
0.5124	4.28	1.71	2.05	6.21
0.6078	4.08	2.13	2.00	5.07
0.6680	4.12	2.46	5.76	1.95
0.7073	4.01	3.06	1.92	5.19
0.7501	4.06	0.73	1.88	7.07
0.8001	4.05	0.19	1.83	7.38
0.8383	3.97	0.27	1.79	7.79
0.8572	4.02	0.16	1.76	7.91
0.9001	4.06	0.33	1.70	7.96

Values in red were obtained at 353 K, and black at 300 K.

Table S3.2 – *^{1}H-NMR chemical shifts, δ, and peak integration of water and α-H of the cation in $[P_{4444}][C_2COO]$-D_2O, as a function of D_2O content, x_D.*

	Water		α-H	
x_w	δ / ppm	∫^{1}H	δ / ppm	∫^{1}H
0			2.21	7.98
0.1114	4.02	0.18	2.24	7.52
0.2174	3.93	0.48	2.21	7.21
0.3441	4.15	0.79	2.14	6.87
0.4013	4.60	0.90	2.10	6.61
0.5049	4.45	1.31	2.05	6.56
0.6203	4.29	1.57	1.98	5.99
0.6722	4.06	2.50	1.95	5.05
0.7039	4.18	1.24	1.92	6.36
0.7504	4.15	0.60	1.88	7.12
0.7998	4.09	0.16	1.83	7.57
0.8349	4.07	0.24	7.46	1.83
0.8578	3.99	0.20	1.76	7.66
0.9014	4.04	0.43	1.71	7.51

Values in red were obtained at 333 K, and black at 300 K.

Table S3.3 – *^{1}H-NMR chemical shifts, δ, and peak integration of water and α-H of the cation in $[P_{4444}][C_7COO]$-D_2O, as a function of D_2O content, x_D.*

	Water		α-H	
x_w	δ / ppm	∫^{1}H	δ / ppm	∫^{1}H
0			2.25	7.99
0.2017	4.52	0.61	2.21	7.24
0.3375	4.38	1.02	2.16	6.76
0.4081	4.36	0.87	2.14	6.55
0.4992	4.30	1.34	2.10	6.54
0.6016	4.23	1.35	2.03	6.34
0.6683	4.17	1.32	1.98	6.35
0.7002	4.15	0.29	1.96	7.52
0.7493	4.10	0.44	1.92	7.14
0.8004	4.08	0.40	1.87	7.32
0.8334	4.06	0.21	1.84	7.76
0.9003	4.12	0.14	1.76	7.80

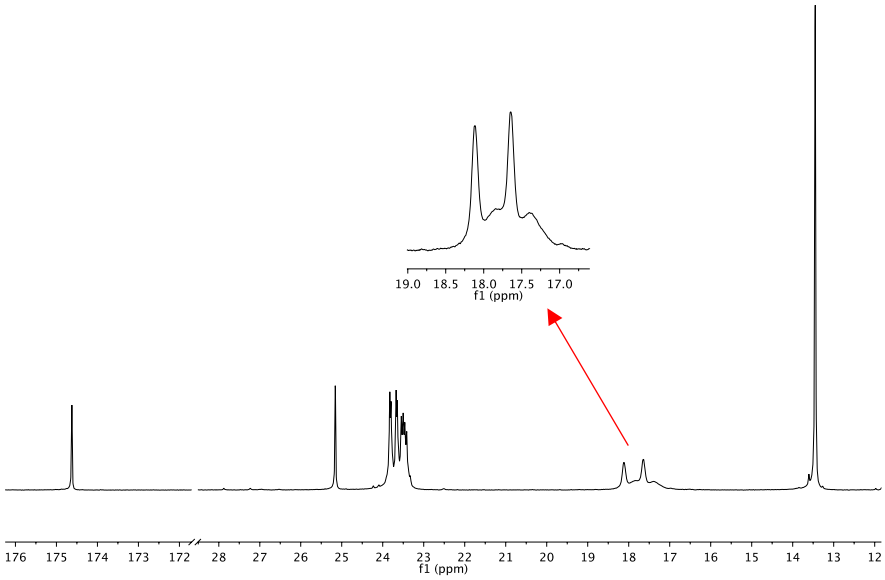

Figure S3.9 – *^{13}C-NMR spectrum of $[P_{4444}][C_1COO]$-D_2O mixture at x_D 0.67, highlighting the peak broadening from ^{13}C-^{2}H coupling on the α position of the cation (100.6 MHz; 27 ˚C; d_6-dmso internal capillary).*

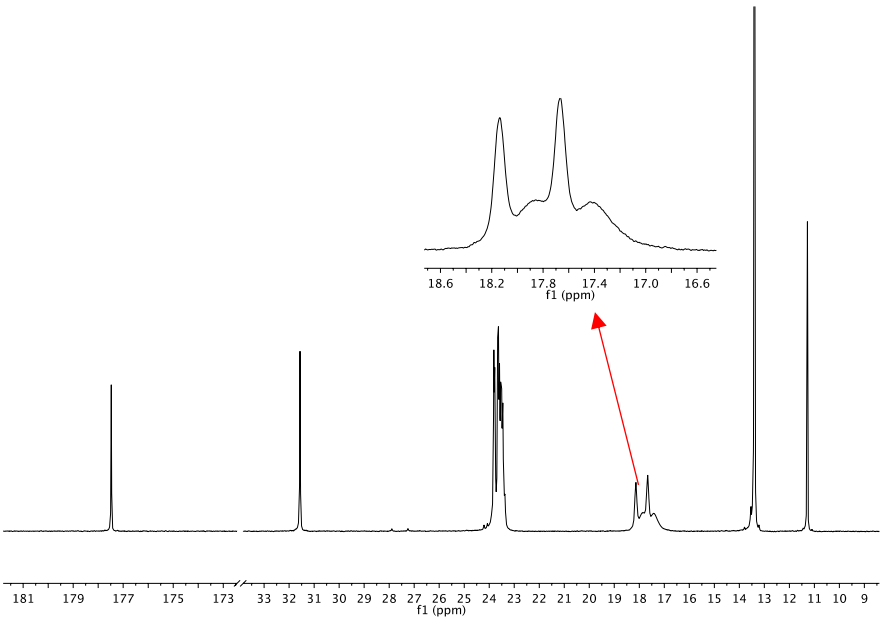

Figure S3.10 – *^{13}C-NMR spectrum of [P_{4444}][C_2COO]-D_2O mixture at x_D 0.67, highlighting the peak broadening from ^{13}C-^{2}H coupling on the α position of the cation (100.6 MHz; 27 ˚C; d_6-dmso internal capillary).*

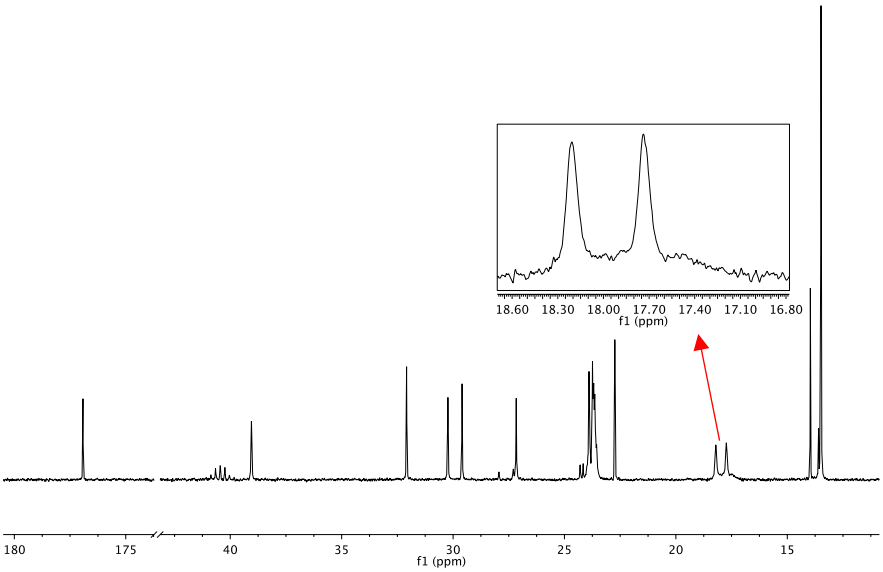

Figure S3.11 – *^{13}C-NMR spectrum of [P_{4444}][C_7COO]-D_2O mixture at x_D 0.67, highlighting the peak broadening from ^{13}C-^{2}H coupling on the α position of the cation (100.6 MHz; 27 ˚C; d_6-dmso internal capillary).*

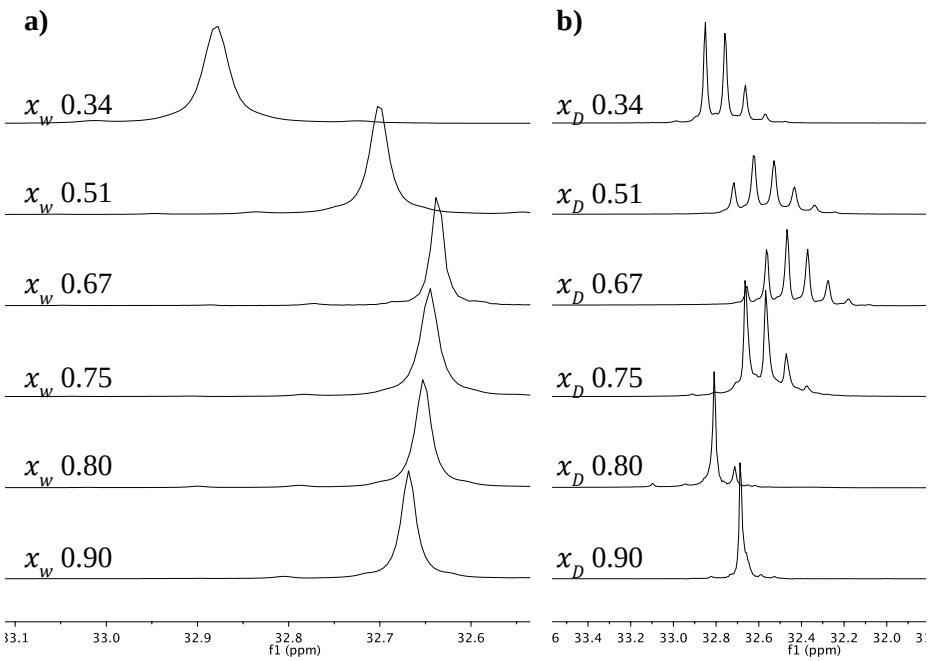

Figure S3.12 *– Stacked ^{31}P-NMR spectra of [$P_{4\,4\,4\,4}$][C_1COO], (a) water mixtures; (b) D_2O mixtures (161.9 MHz; 27 ˚C; d_6-dmso internal capillary).*

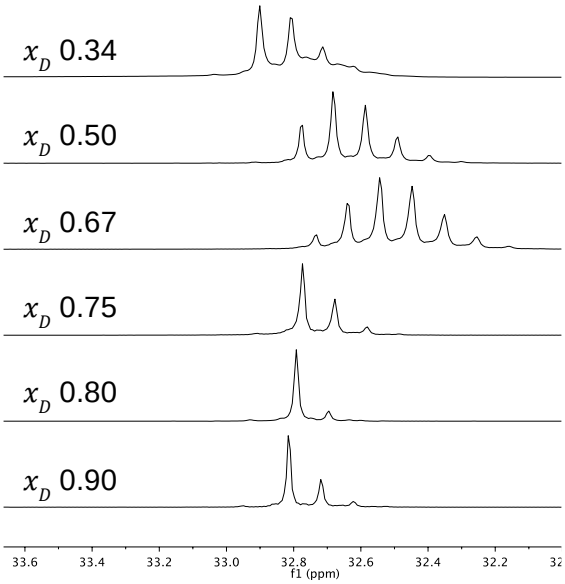

Figure S3.13 – *Stacked ^{31}P-NMR spectra of [$P_{4\,4\,4\,4}$][C_2COO] D_2O mixtures (161.9 MHz; 27 ˚C; d_6-dmso internal capillary).*

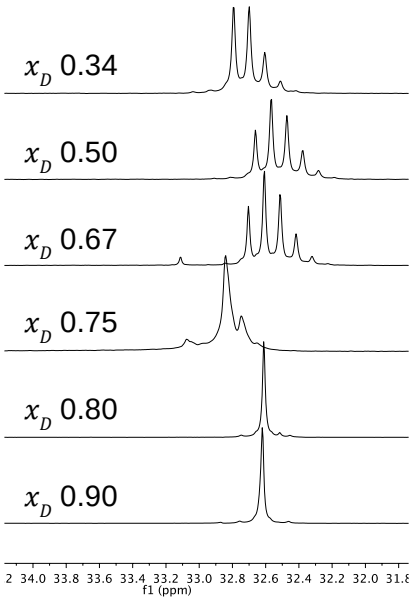

Figure S3.14 – *Stacked ^{31}P-NMR spectra of [$P_{4\,4\,4\,4}$][C_7COO] D_2O mixtures (161.9 MHz; 27 ˚C; d_6-dmso internal capillary).*

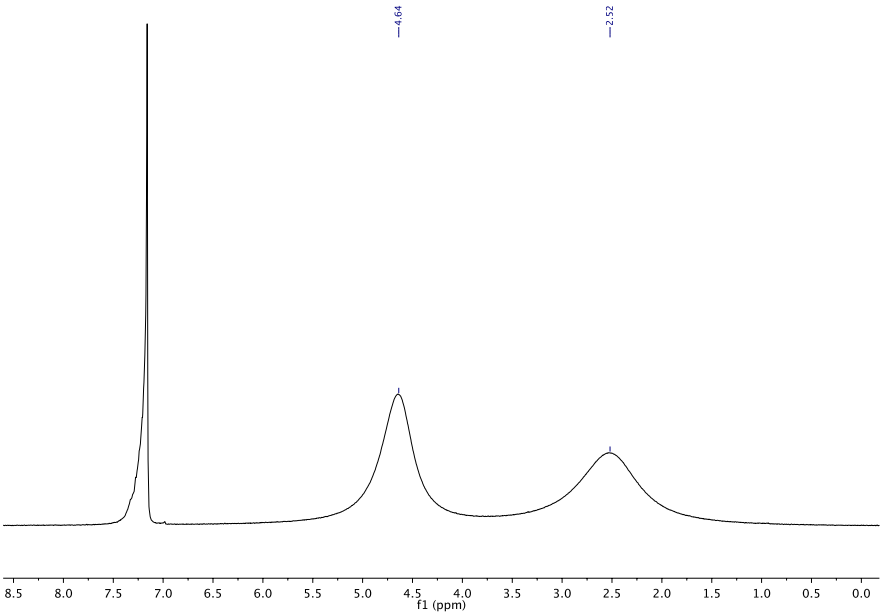

Figure S3.15 *– Deuterium, ^{2}H, NMR spectrum of [$P_{4\,4\,4\,4}$][C_1COO]-D_2O mixture at x_D 0.67, representing a D_2O signal at 4.64 ppm and an exchanged ^{2}H on the α-H of the cation at 2.52 ppm (92.12 MHz; 27 ˚C; C_6D_6 internal capillary, 7.16 ppm).*

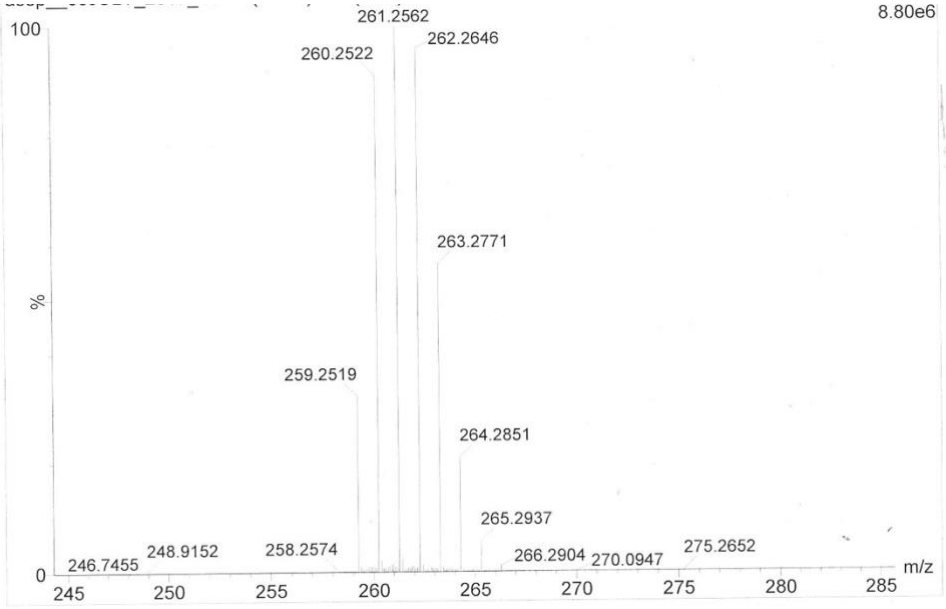

Figure S3.16 – *Mass spectrum of $[P_{4444}][C_1COO]$-D_2O mixture, x_D 0.67, in ES^+ mode, representing deuteriated forms of the $[P_{4444}]^+$ cation, 260-264 m/z.*

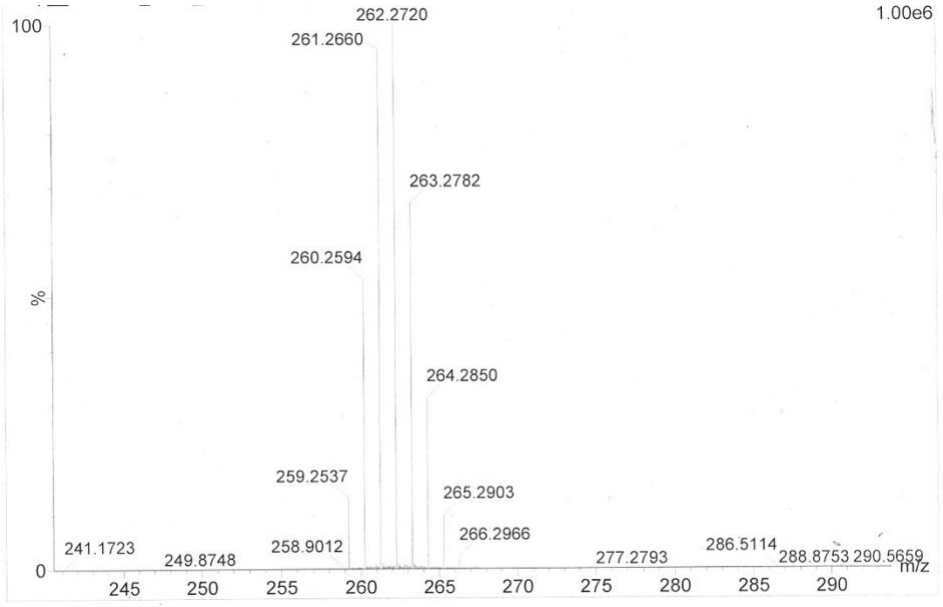

Figure S3.17 – *Mass spectrum of $[P_{4444}][C_2COO]$-D_2O mixture, x_D 0.67, in ES^+ mode, representing deuteriated forms of the $[P_{4444}]^+$ cation, 260-264 m/z.*

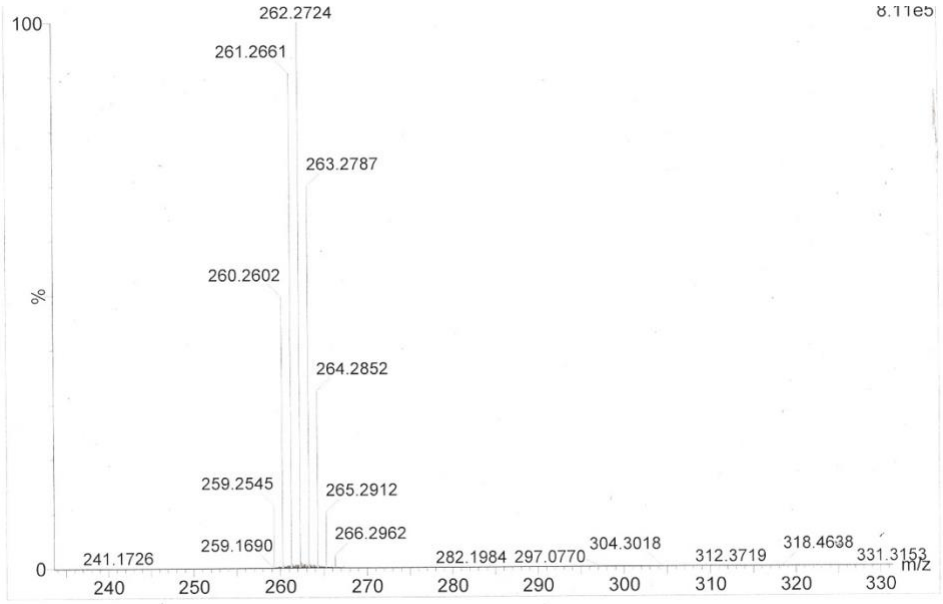

Figure S3.18 – *Mass spectrum of $[P_{4444}][C_7COO]$-D_2O mixture, x_D 0.67, in ES^+ mode, representing deuteriated forms of the $[P_{4444}]^+$ cation, 260-264 m/z.*

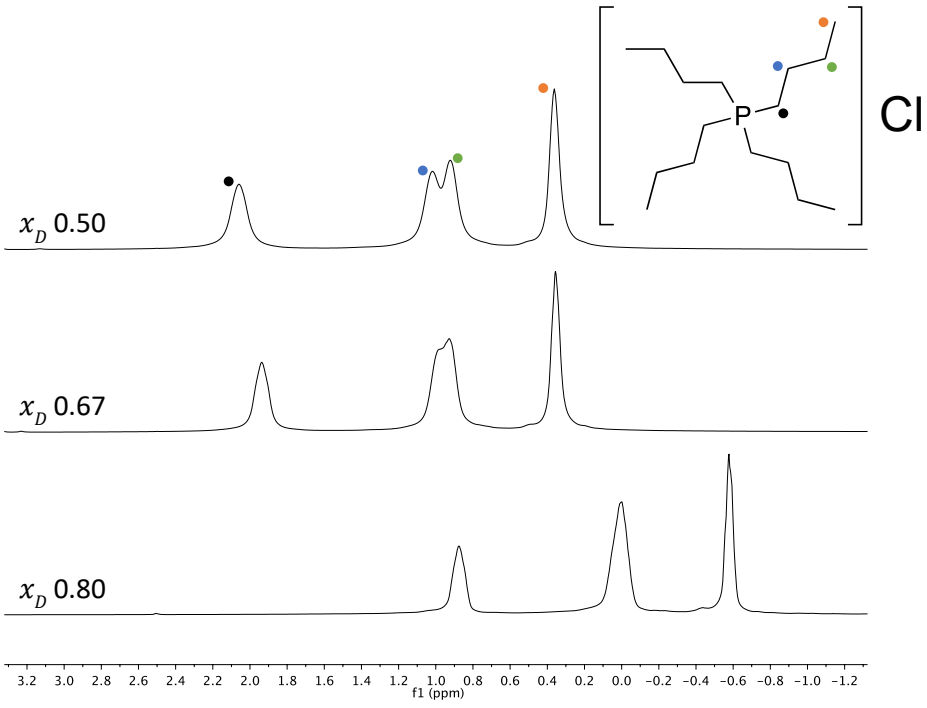

Figure S3.19 – *Stacked ^1H NMR spectra of $[P_{4444}]Cl$-D_2O mixtures (400 MHz; 27 ˚C; d_6-dmso internal capillary).*

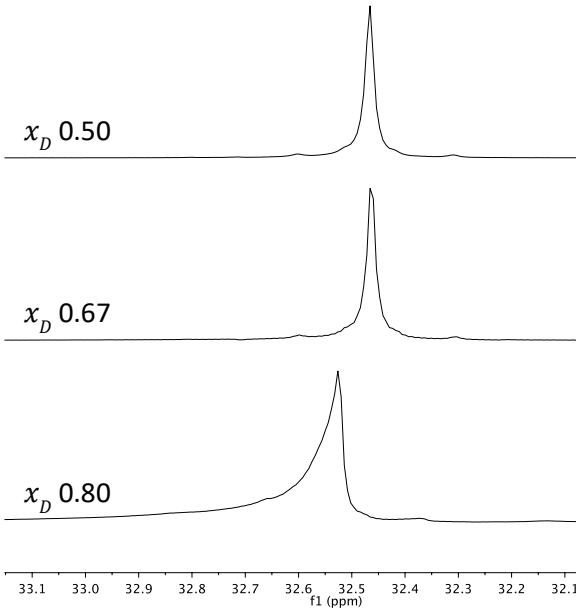

Figure S3.20 – *Stacked ^{31}P-NMR spectra of $[P_{4\,4\,4\,4}]$Cl-D_2O mixtures (161.9 MHz; 27 ˚C; d_6-dmso internal capillary).*

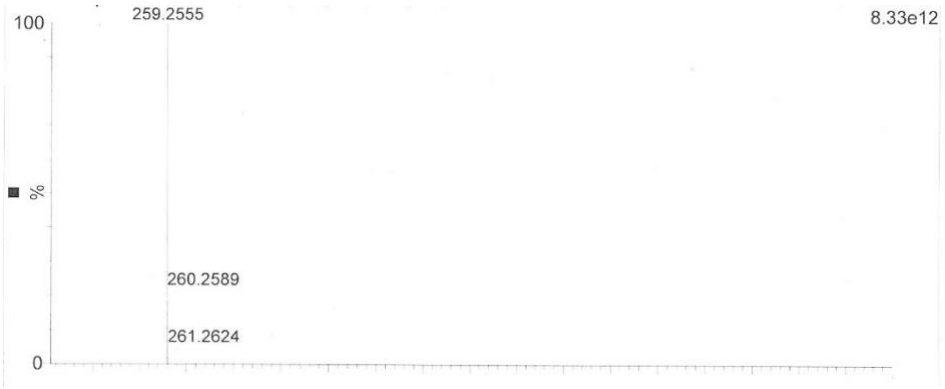

Figure S3.21 – *Mass spectrum of $[P_{4\,4\,4\,4}]$Cl-D_2O mixture, x_D 0.67, in ES$^+$ mode, representing no deuteration of the $[P_{4\,4\,4\,4}]^+$ cation, 259 m/z.*

4. Small- and Wide-Angle X-ray Scattering

Table S4.1 *SWAXS diffraction peak positions, q, and correlation distances, d, of $[P_{4444}][C_1COO]$-water mixtures.*

	Pre-peak		Shoulder peak		Principal Peak	
x_w	q / nm^{-1}	d / nm	q / nm^{-1}	d / nm	q / nm^{-1}	d / nm
0.3368	6.23	1.01	8.29	0.76	15.43	0.41
0.4051	6.18	1.02	8.13	0.77	15.49	0.41
0.5014	5.97	1.05	8.07	0.78	15.39	0.41
0.6017	5.90	1.06	8.00	0.79	15.46	0.41
0.6674	5.80	1.08	7.91	0.79	15.51	0.41
0.7531	4.50	1.40	7.92	0.79	15.24	0.41
0.8039	4.34	1.45	7.79	0.81	15.30	0.41
0.9007	3.68	1.71	7.62	0.82	15.93	0.39

Table S4.2 – *SWAXS diffraction peak positions, q, and correlation distances, d, of $[P_{4444}][C_2COO]$-water mixtures.*

	Pre-peak		Shoulder peak		Principal Peak	
x_w	q / nm^{-1}	d / nm	q / nm^{-1}	d / nm.	q / nm^{-1}	d / nm
0.3427	6.25	1.01			15.23	0.41
0.4031	6.18	1.02	8.16	0.77	15.49	0.41
0.5052	5.99	1.05	8.11	0.77	15.32	0.41
0.6046	5.88	1.07	8.03	0.78	15.40	0.41
0.6722	5.78	1.09	7.91	0.79	15.47	0.41
0.7512	5.73	1.10	7.69	0.82	15.78	0.40
0.8008	5.55	1.13	7.52	0.84	15.79	0.40
0.9006			7.17	0.88	16.61	0.38

Table S4.3 – *SWAXS diffraction peak positions, q, and correlation distances, d, of $[P_{4444}][C_7COO]$-water mixtures.*

	Pre-peak		Shoulder peak		Principal Peak	
x_w	q / nm^{-1}	d / nm	q / nm^{-1}	d / nm	q / nm^{-1}	d / nm
0	5.51	1.14			14.85	0.42
0.2042	5.4	1.16			14.86	0.42
0.4112	5.02	1.25	8.13	0.77	15.02	0.42
0.6734	5.97	1.05	7.98	0.79	15.54	0.40
0.7524	5.87	1.07	7.91	0.79	15.55	0.40
0.7990	5.73	1.10	7.69	0.82	15.77	0.40
0.9003			7.29	0.86	17.08	0.37

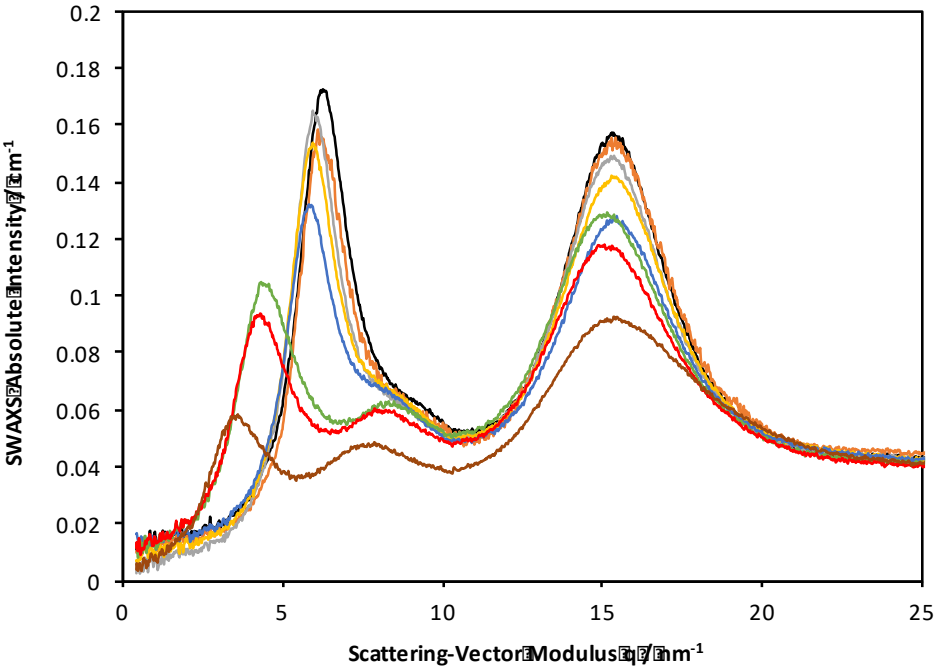

Figure S4.1 *– SWAXS patterns of [P_{4444}][C_1COO]-water mixtures, at: (–) x_w 0.34; (–) x_w 0.41; (–) x_w 0.51; (–) x_w 0.60.; (–) x_w 0.67; (–) x_w 0.75; (–) x_w 0.80; and (–) x_w 0.90.*

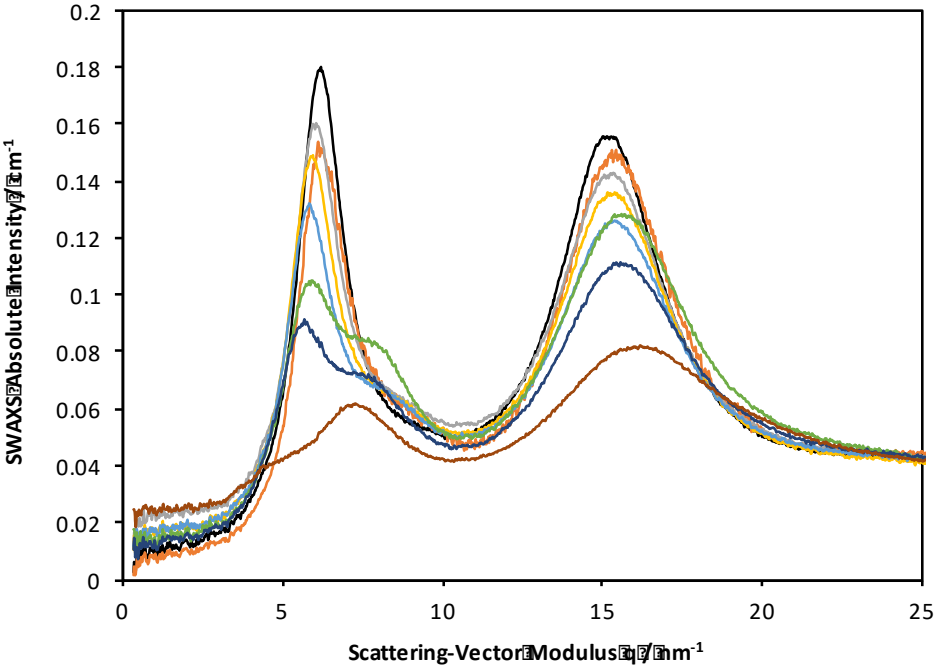

Figure S4.1 *– SWAXS patterns of [P_{4444}][C_2COO]-water mixtures, at: (–) x_w 0.34; (–) x_w 0.40; (–) x_w 0.50; (–) x_w 0.60; (–) x_w 0.67; (–) x_w 0.75; (–) x_w 0.80; and (–) x_w 0.90.*

5. Gas Absorption Work

Table S5.1 – *Absorption of CO_2 in dry $[P_{4\,4\,4\,4}][C_1COO]$ (1.8212 g) at 338.15 K, as a function of time, expressed as mole fraction, x_{CO_2}, and weight %.*

Time / min	Mass / g	x_{CO_2}	Weight % CO_2
0	0	0	0%
15	0.0325	0.11	1.75%
30	0.0358	0.12	1.93%
45	0.0396	0.14	2.13%
60	0.0447	0.15	2.40%
120	0.0501	0.17	2.68%
180	0.0525	0.17	2.80%
240	0.0562	0.18	2.99%
480	0.0603	0.19	3.20%

Table S5.2 – *Absorption of CO_2 in dry $[P_{4\,4\,4\,4}][C_7COO]$ (1.6585 g) at 338.15 K, as a function of time, expressed as mole fraction, x_{CO_2}, and weight %.*

Time / min	Mass / g	x_{CO_2}	Weight % CO_2
0	0	0	0%
15	0.0228	0.11	1.36%
30	0.0258	0.12	1.53%
45	0.0289	0.14	1.71%
60	0.0343	0.16	2.03%
120	0.0402	0.18	2.37%
180	0.0434	0.19	2.55%
240	0.0479	0.21	2.81%
506	0.0513	0.22	3.00%

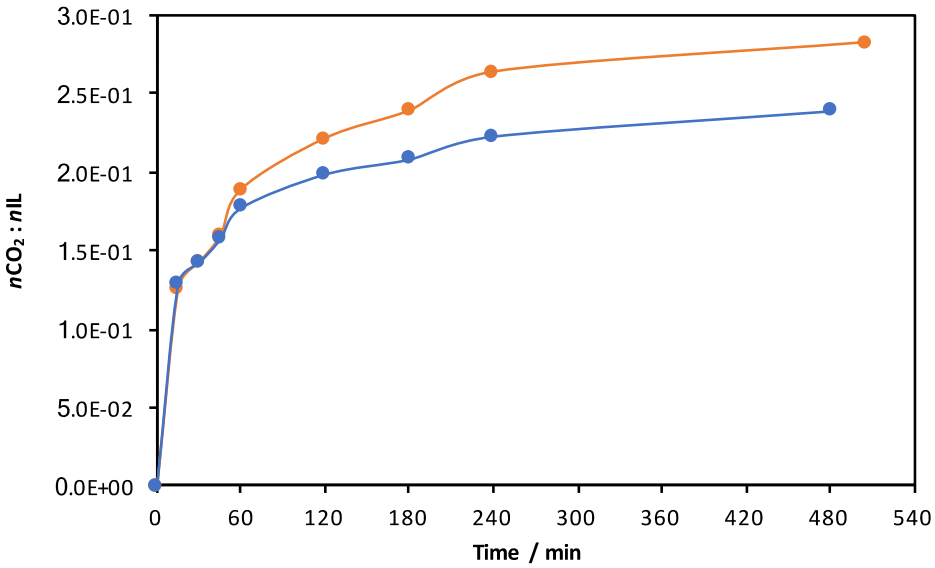

Figure S5.1 – *The uptake of CO_2 over time, minutes, in neat (–) $[P_{4444}][C_1COO]$ and (–) $[P_{4444}][C_7COO]$, at 338.15 K.*

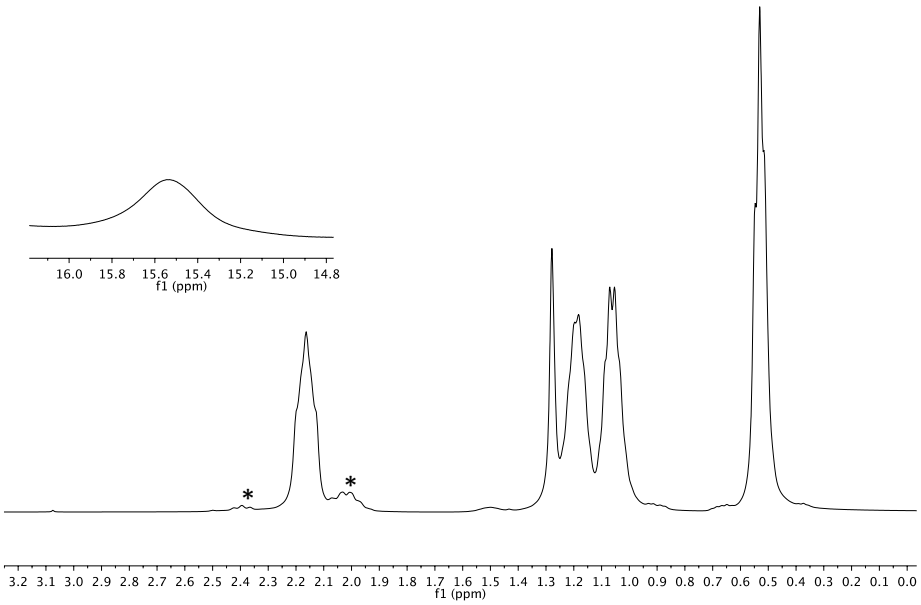

Figure S5.2 *– ^{1}H-NMR spectrum of the dry $[P_{4444}][C_1COO]$ indicating the formation of two new peaks marked with an asterisk after being bubbled with CO_2 for 8 h at 338.15 K (400 MHz; 80 ˚C; d_6-dmso internal capillary).*

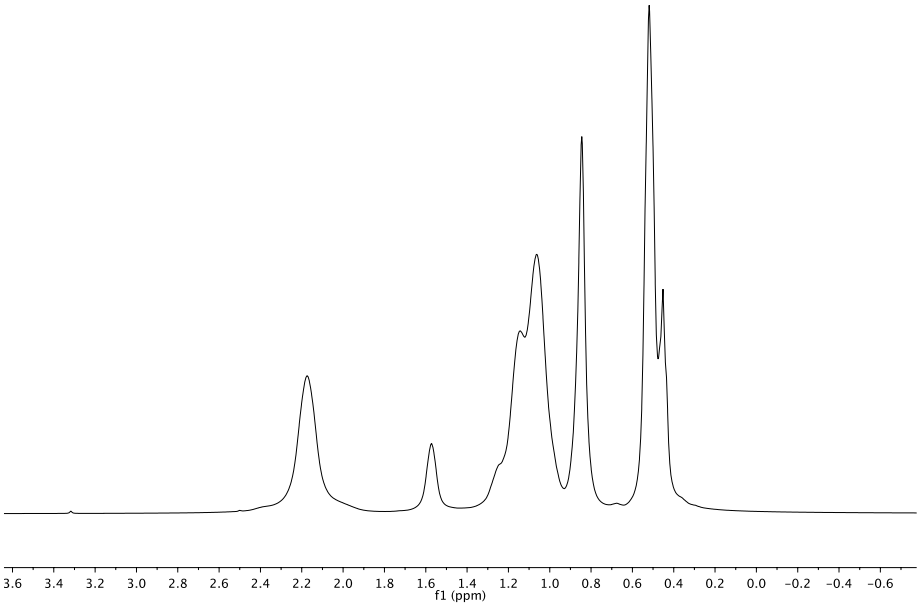

Figure S5.3 *– ^{1}H-NMR spectrum of the dry [$P_{4\,4\,4\,4}$][C_7COO] after being bubbled with CO_2 for 8.5 h at 338.15 K (400 MHz; 27 ˚C; d_6-dmso internal capillary).*

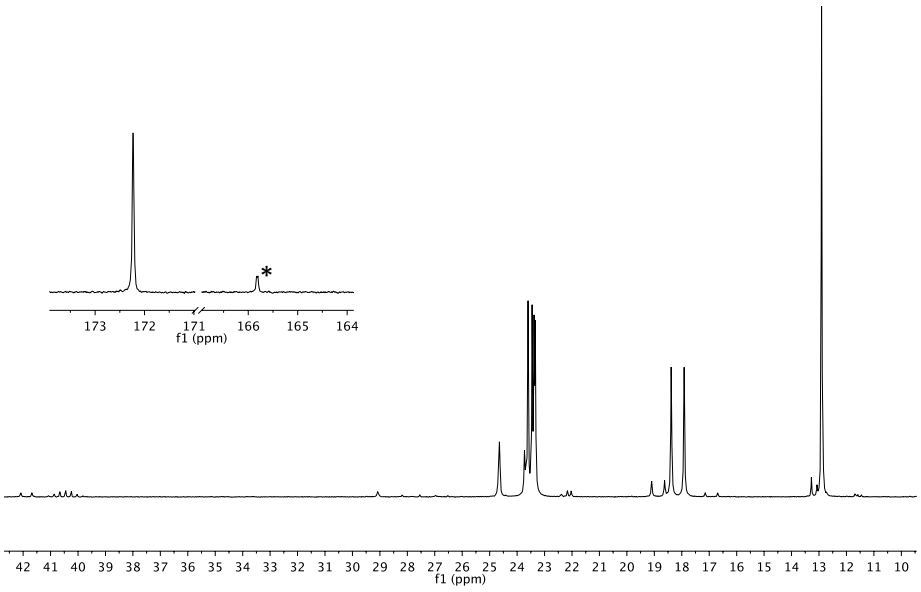

Figure S5.4 – *^{13}C-NMR spectrum of the dry [$P_{4\,4\,4\,4}$][C_1COO] indicating the formation of a new peak marked with an asterisk after being bubbled with CO_2 for 8 h at 338.15 K (400 MHz; 80 ˚C; d_6-dmso internal capillary).*

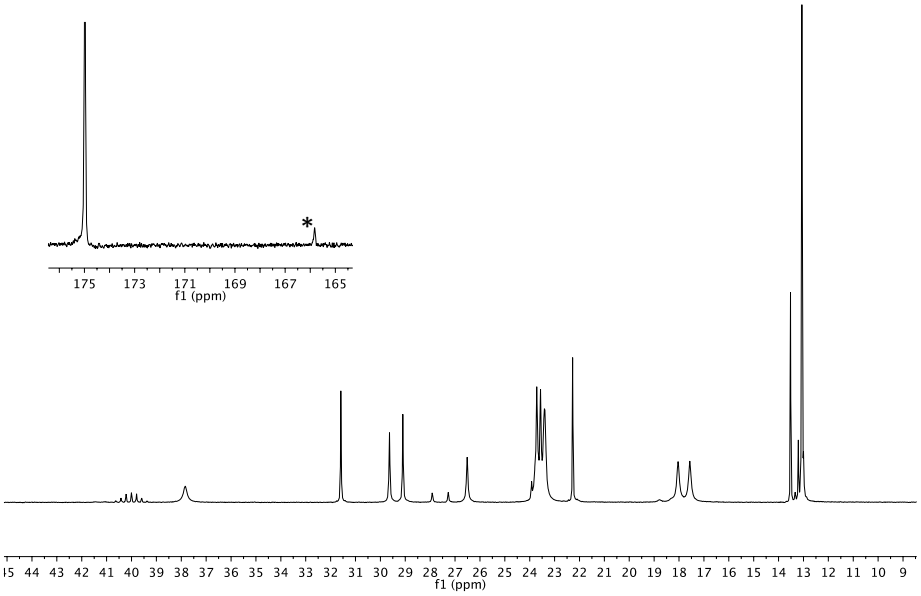

Figure S5.5 – *^{13}C-NMR spectrum of the dry [$P_{4\,4\,4\,4}$][C_7COO] indicating the formation of a new peak marked with an asterisk after being bubbled with CO_2 for 8.5 h at 338.15 K (400 MHz; 27 ˚C; d_6-dmso internal capillary).*

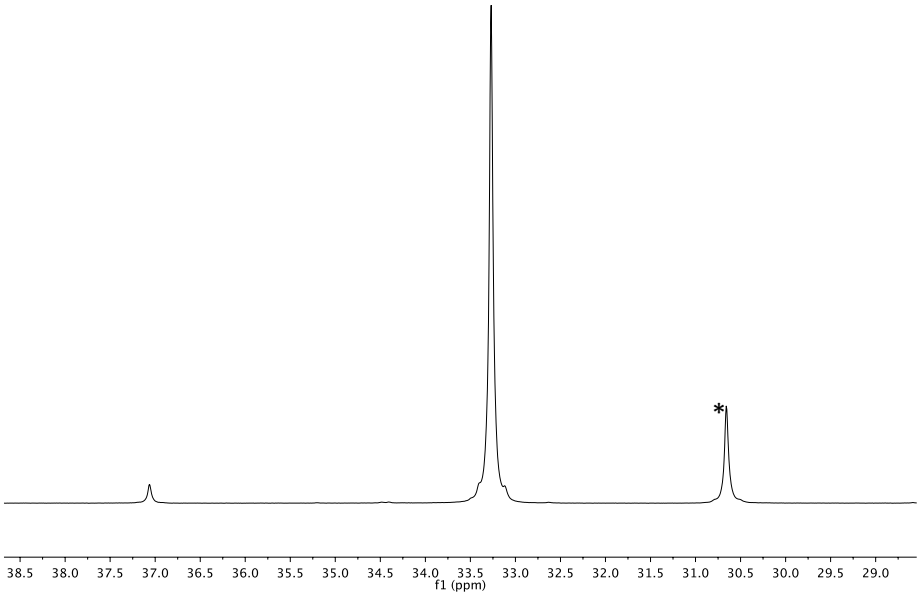

Figure S5.6 – *^{31}P-NMR spectrum of the dry [$P_{4\,4\,4\,4}$][C_1COO] indicating the formation of a new peak marked with an asterisk after being bubbled with CO_2 for 8 h at 338.15 K (400 MHz; 80 ˚C; d_6-dmso internal capillary).*

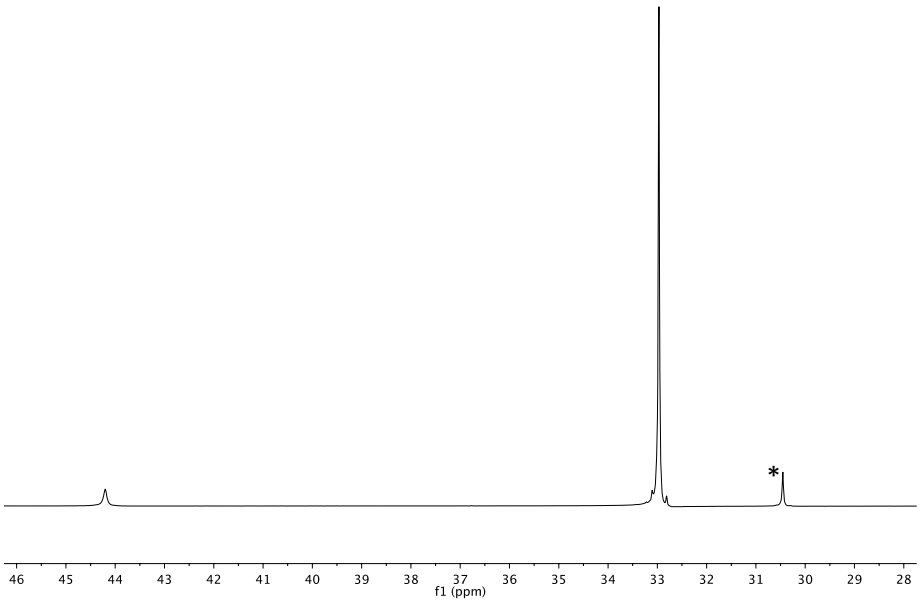

Figure S5.7 – *^{31}P-NMR spectrum of the dry [P_{4444}][C_7COO] indicating the formation of a new peak marked with an asterisk after being bubbled with CO_2 for 8.5 h at 338.15 K (400 MHz; 27 ˚C; d_6-dmso internal capillary).*

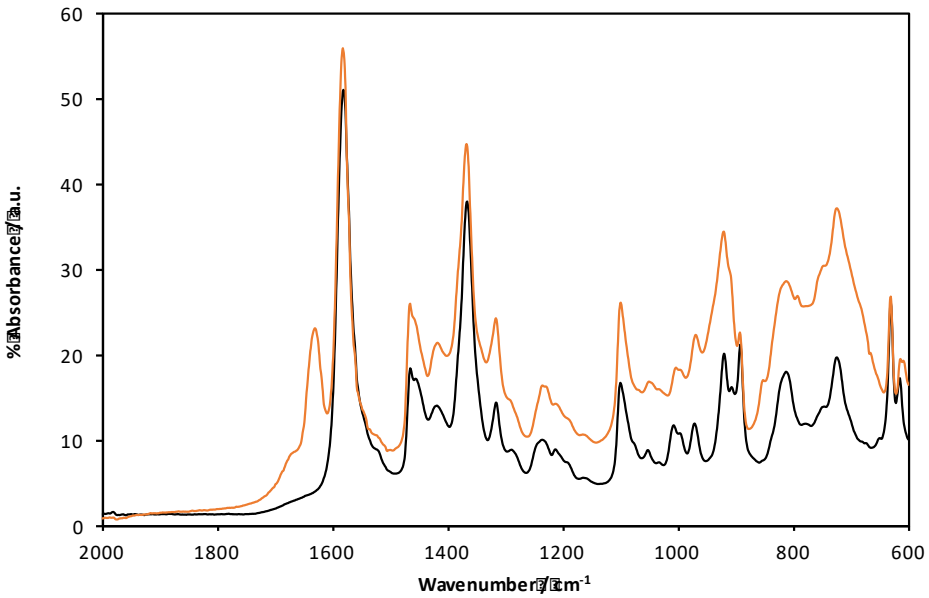

Figure S5.8 *– Expansion of infrared spectra (2000-600 cm^{-1}) of the dry (–) [P_{4444}][C_1COO] before exposure to CO_2 and after (–).*

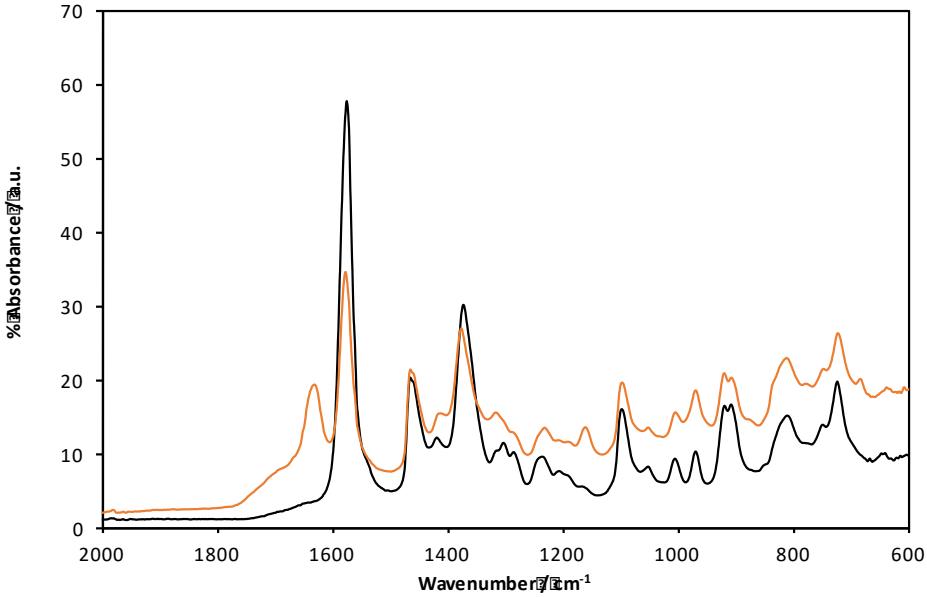

Figure S5.9 – *Expansion of infrared spectra (2000-600 cm^{-1}) of the dry (–) $[P_{4444}][C_7COO]$ before exposure to CO_2 and after (–).*

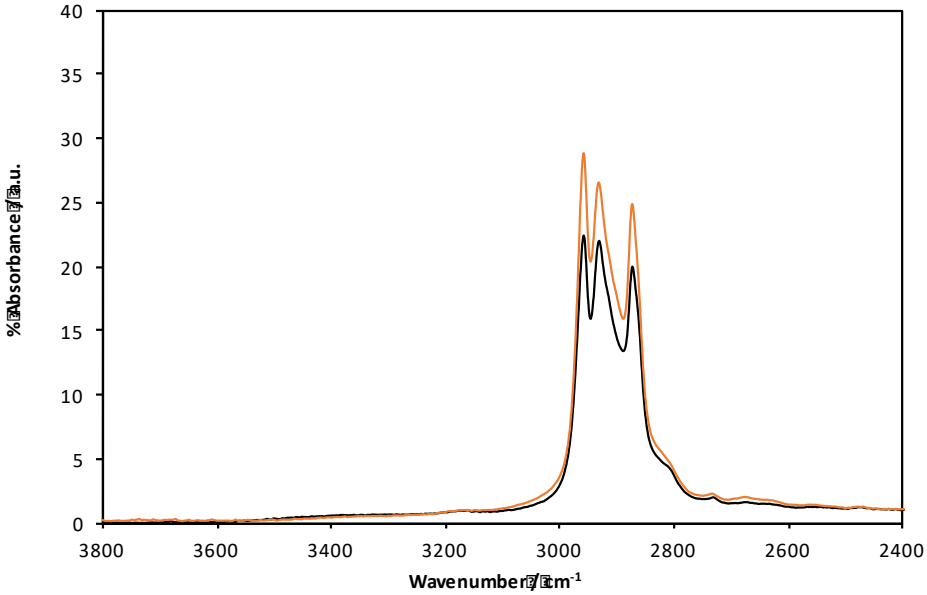

Figure S5.10 – *Expansion of infrared spectra (3800-2400 cm^{-1}) of the dry (–) $[P_{4444}][C_1COO]$ before exposure to CO_2 and after (–).*

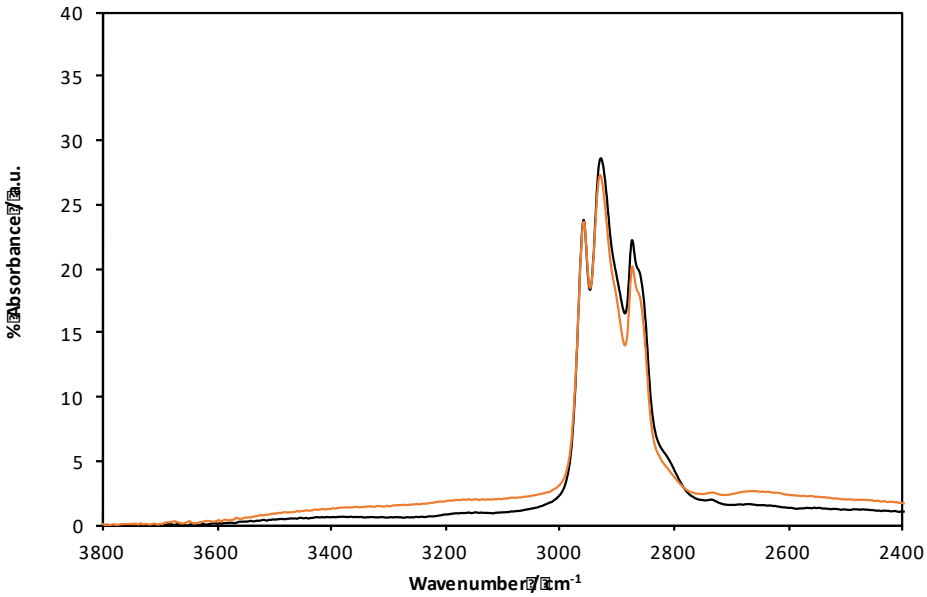

Figure S5.11 – *Expansion of infrared spectra (3800-2400 cm^{-1}) of the dry (–) $[P_{4\,4\,4\,4}][C_7COO]$ before exposure to CO_2 and after (–).*

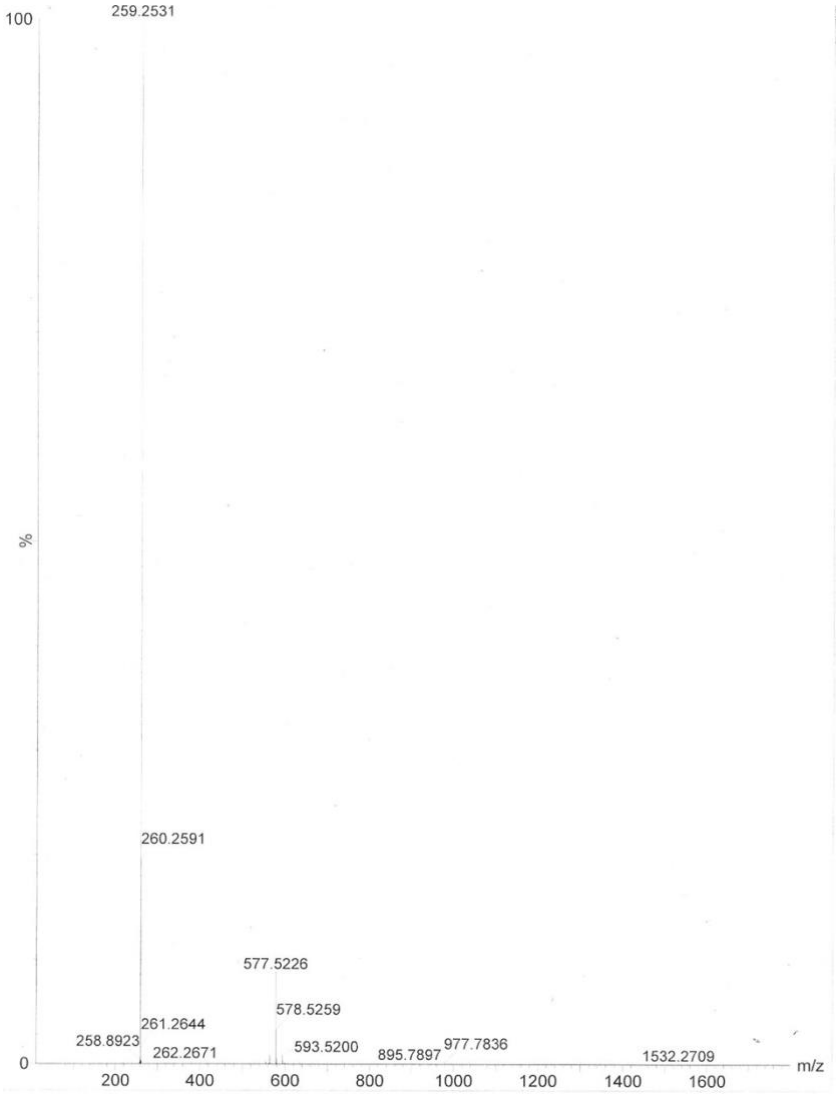

Figure S5.12 – *Mass spectrum of $[P_{4444}][C_1COO]$ in ES^+ mode.*

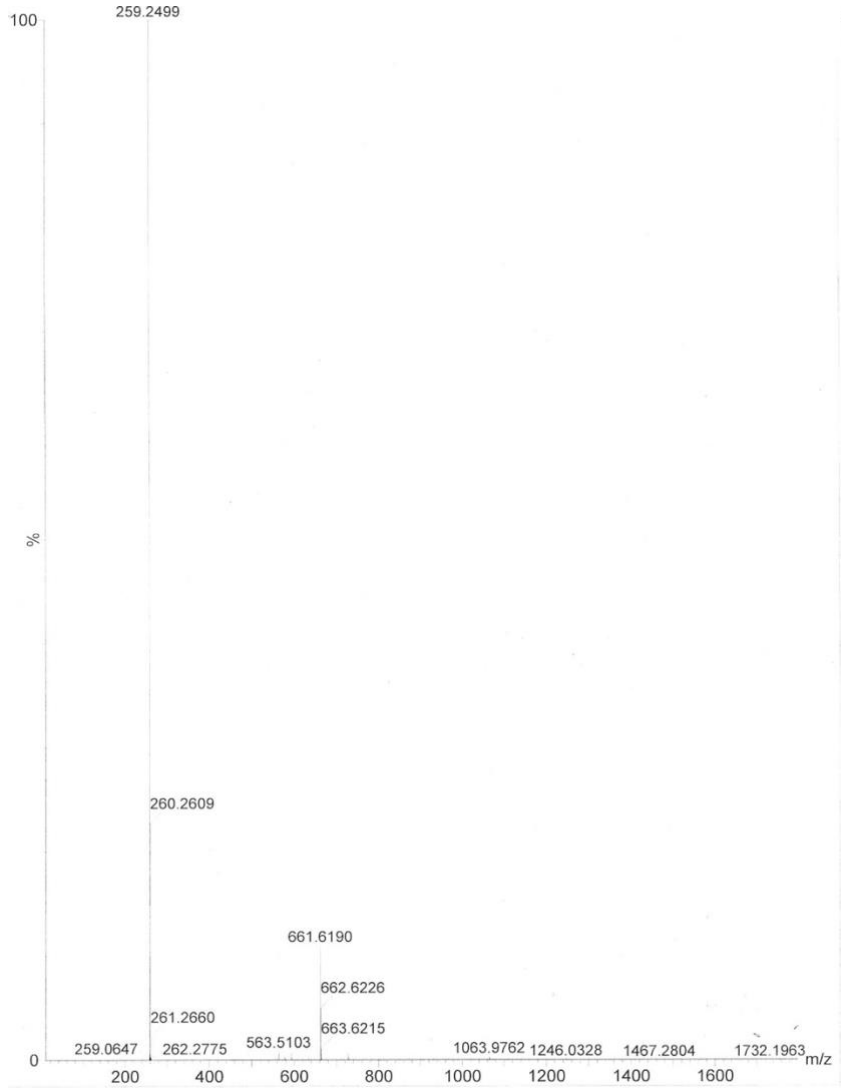

Figure S5.13 *– Mass spectrum of [P_{4444}][C_7COO] in ES⁺ mode.*

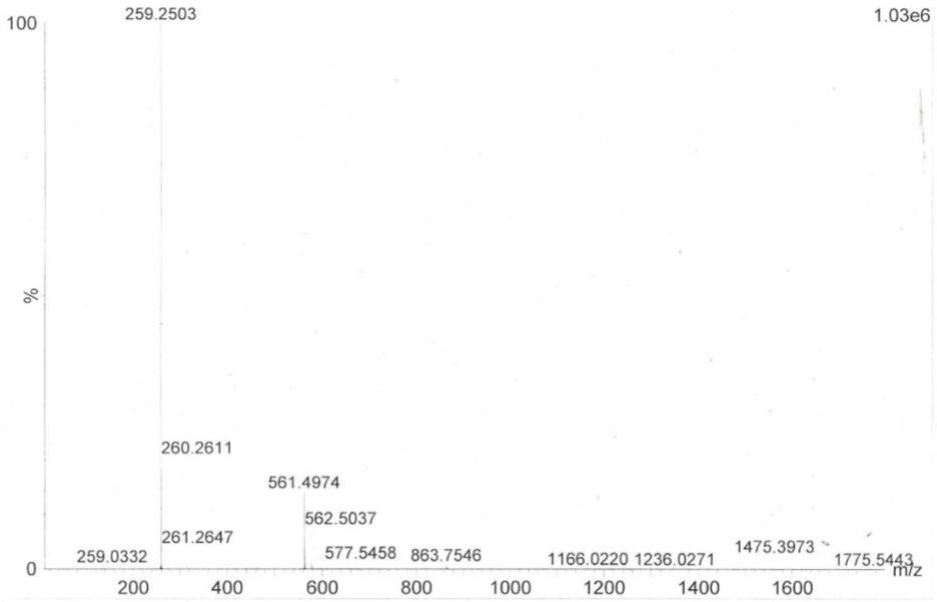

Figure S5.14 *– Mass spectrum of the dry [P_{4444}][C_1COO] in ES⁺ mode, after CO_2 absorption.*

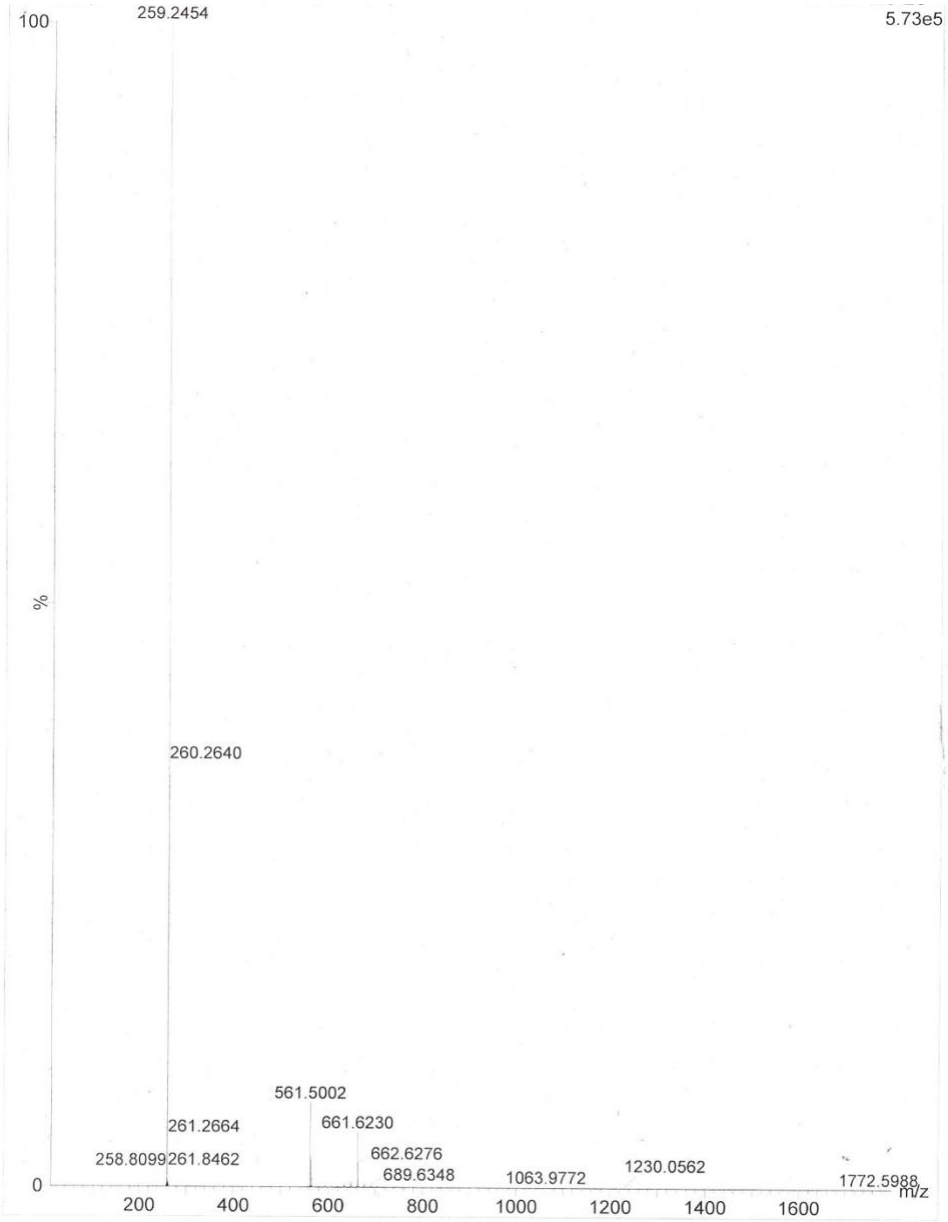

Figure S5.15 – *Mass spectrum of the dry $[P_{4\,4\,4\,4}][C_7COO]$ in ES^+ mode, after CO_2 absorption.*

Table S5.3 – *Absorption of CO_2 in equimolar mixture of $[P_{4\,4\,4\,4}][C_1COO]$ and water at 295.15 K, expressed as mole fraction, x_{CO_2}, and weight %.*

Time / min	Mass / g	x_{CO_2}	Weight % CO_2
0	0	0	0%
15	0.1762	0.40	8.47%
30	0.1761	0.40	8.46%
45	0.1768	0.40	8.49%
60	0.1770	0.40	8.50%
120	0.1758	0.40	8.45%

Table S5.4 – *Absorption of CO_2 in equimolar mixture of $[P_{4444}][C_7COO]$ and water at 295.15 K, expressed as mole fraction, x_{CO_2}, and weight %.*

Time / min	Mass / g	x_{CO_2}	Weight % CO_2
0	0	0	0%
15	0.1494	0.41	7.16%
30	0.1423	0.40	6.84%
45	0.1362	0.39	6.57%
60	0.1332	0.39	6.43%
120	0.1173	0.36	5.71%

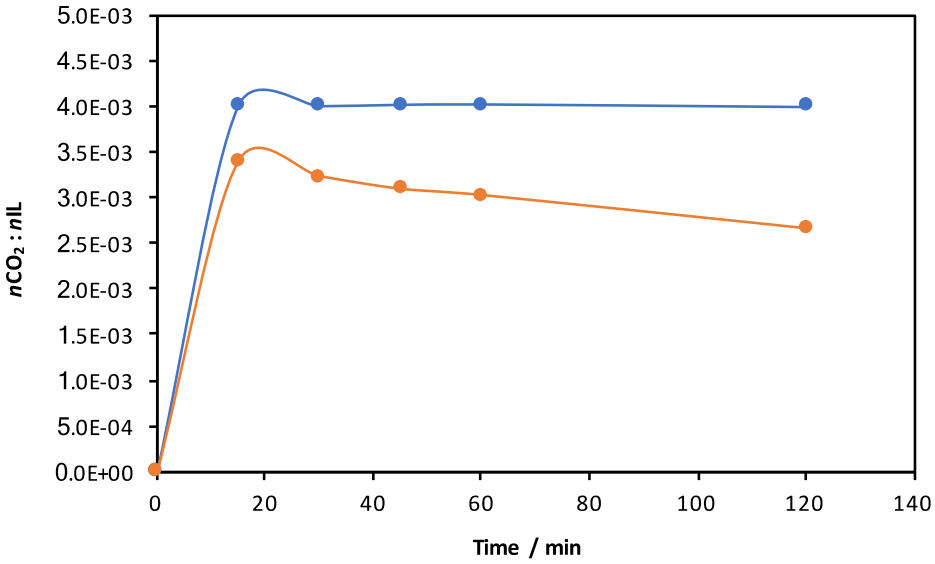

Figure S5.16 *– Uptake of CO_2 against time, minutes, in equimolar ionic liquid-water mixtures; (–) $[P_{4444}][C_1COO]$ and (–) $[P_{4444}][C_7COO]$, at 295.15 K.*

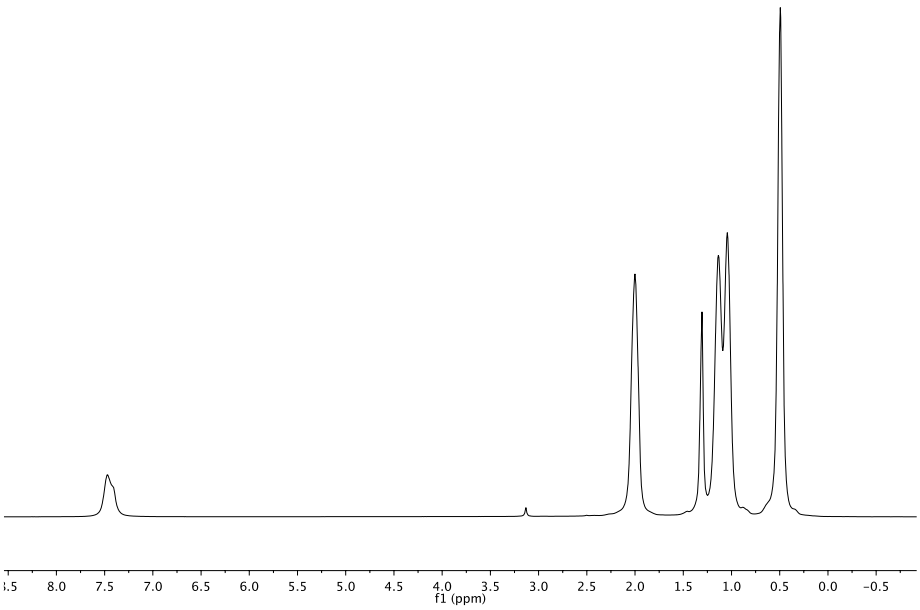

Figure S5.17 *– ^{1}H-NMR spectrum of the equimolar [P_{4444}][C_1COO]-water mixture after being bubbled with CO_2 for 2 h at 295.15 K, (400 MHz; 80 ˚C; d_6-dmso internal capillary).*

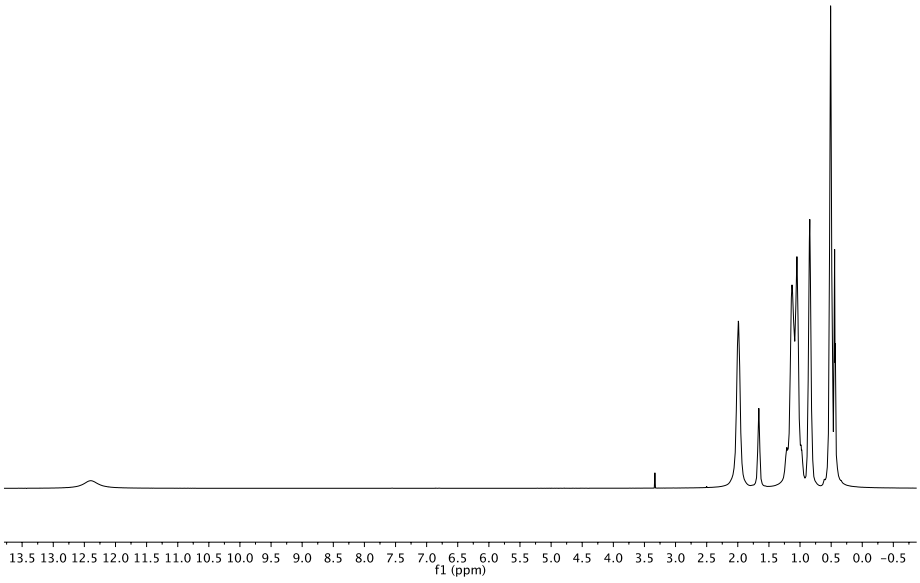

Figure S5.18 *– ^{1}H-NMR spectrum of the equimolar [P_{4444}][C_7COO]-water mixture after being bubbled with CO_2 for 2 h at 295.15 K, (400 MHz; 27 ˚C; d_6-dmso internal capillary).*

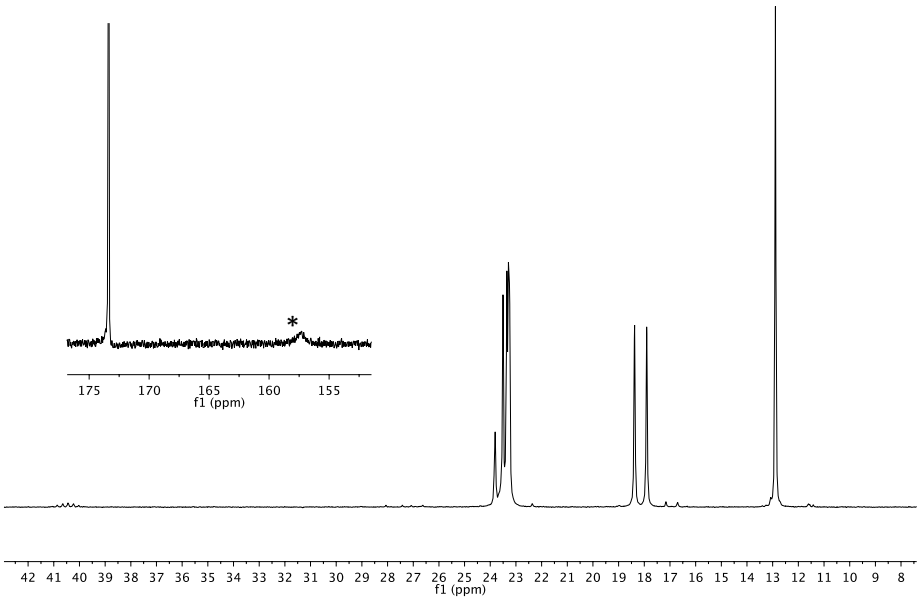

Figure S5.19 – *^{13}C-NMR spectrum of the equimolar [$P_{4\,4\,4\,4}$][C_1COO]-water mixture, indicating the formation of a new peak marked with an asterisk after being bubbled with CO_2 for 2 h at 295.15 K, (400 MHz; 80 ˚C; d_6-dmso internal capillary).*

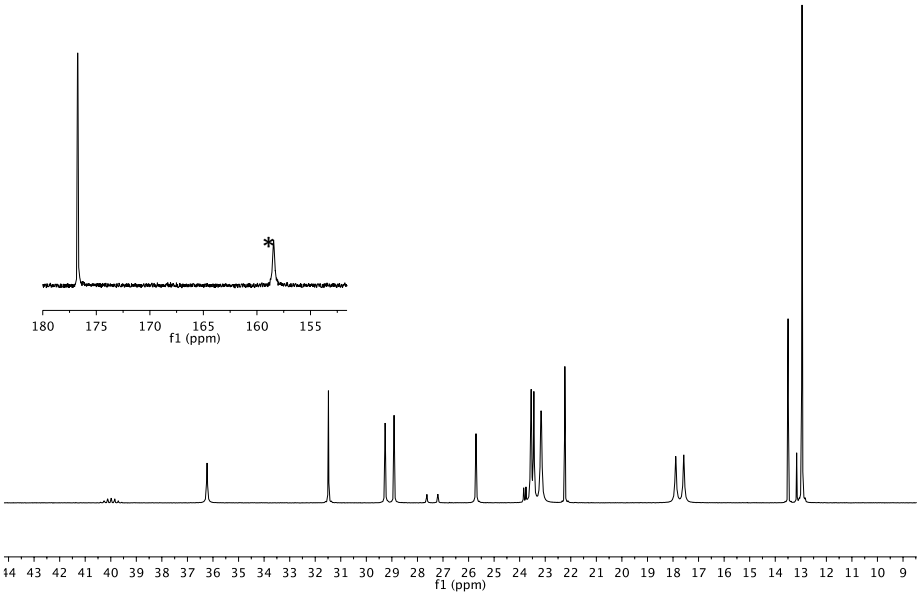

Figure S5.20 *– ^{13}C-NMR spectrum of the equimolar [$P_{4\,4\,4\,4}$][C_7COO]-water mixture, indicating the formation of a new peak marked with an asterisk after being bubbled with CO_2 for 2 h at 295.15 K, (400 MHz; 27 ˚C; d_6-dmso internal capillary).*

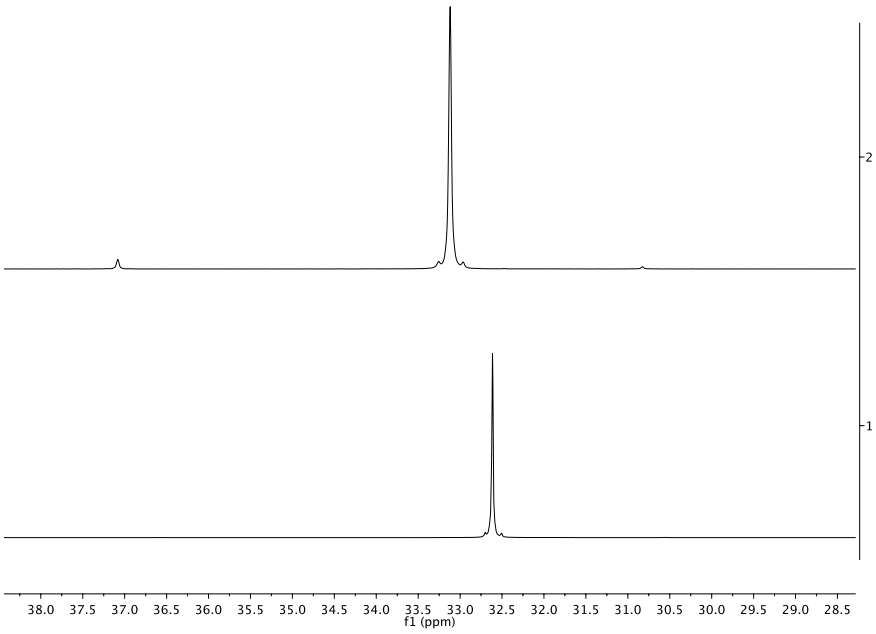

Figure S5.21 *– ^{31}P-NMR spectra of CO_2 absorption in binary equimolar ionic liquid-water mixtures of; $[P_{4\,4\,4\,4}][C_1COO]$ (top), and $[P_{4\,4\,4\,4}][C_7COO]$ (bottom) (161.9 MHz; d_6-dmso internal capillary.*

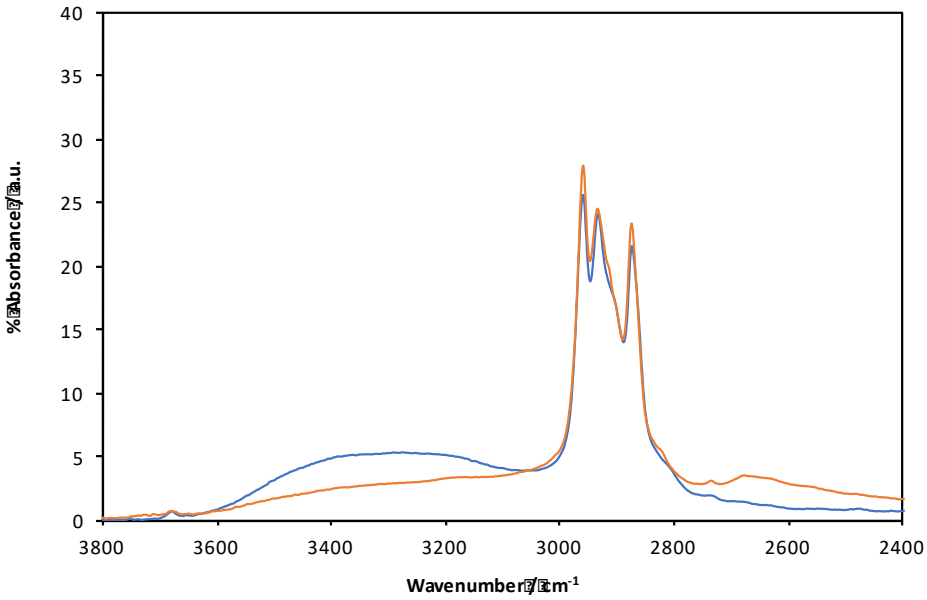

Figure S5.22 *– Expansion of (3800-2400 cm^{-1}) infrared spectra of the equimolar (–) $[P_{4\,4\,4\,4}][C_1COO]$-water mixture before exposure to CO_2 and after (–).*

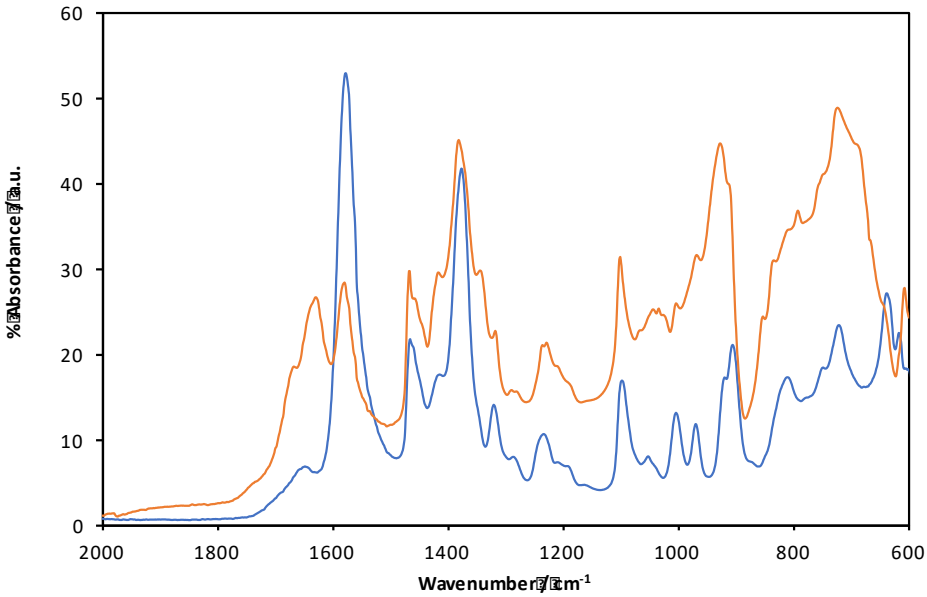

Figure S5.23 *– Expansion of (2000-600 cm^{-1}) infrared spectra of the equimolar (–) $[P_{4444}][C_1COO]$-water mixture before exposure to CO_2 and after (–).*

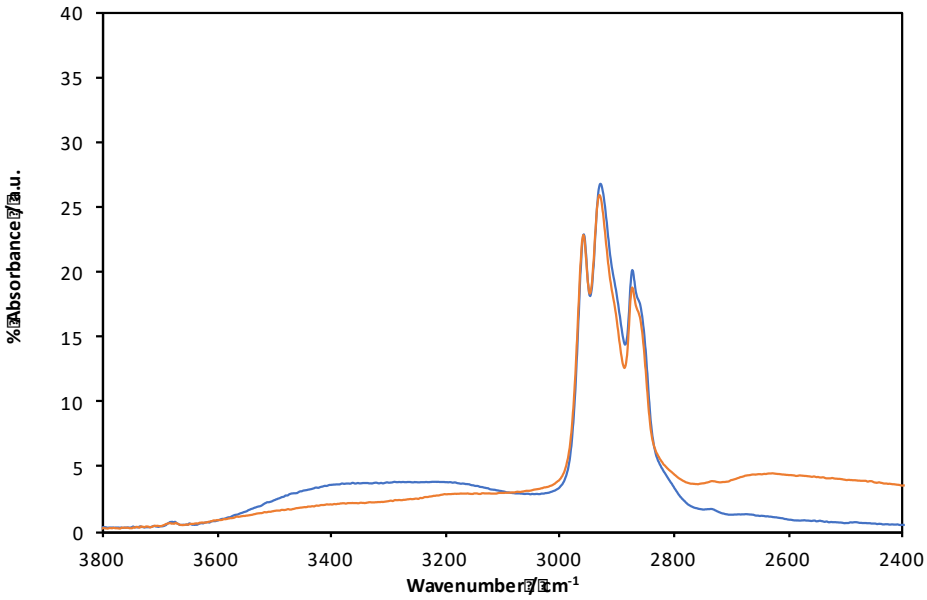

Figure S5.24 *– Expansion of (3800-2400 cm^{-1}) infrared spectra of the equimolar (–) $[P_{4444}][C_7COO]$-water mixture before exposure to CO_2 and after (–).*

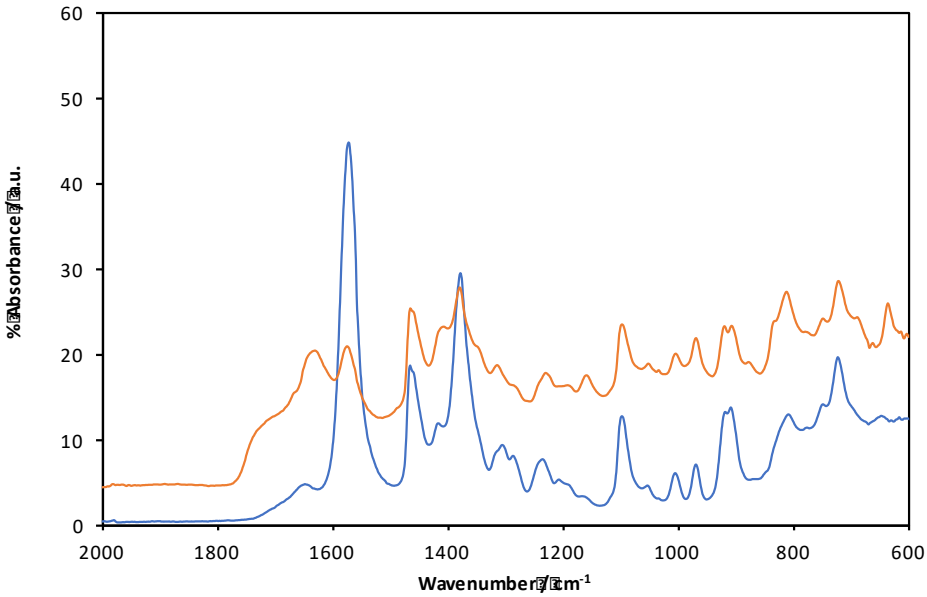

Figure S5.25 *– Expansion of (2000-600 cm^{-1}) infrared spectra of the equimolar (–) $[P_{4\,4\,4\,4}][C_7COO]$-water mixture before exposure to CO_2 and after (–).*

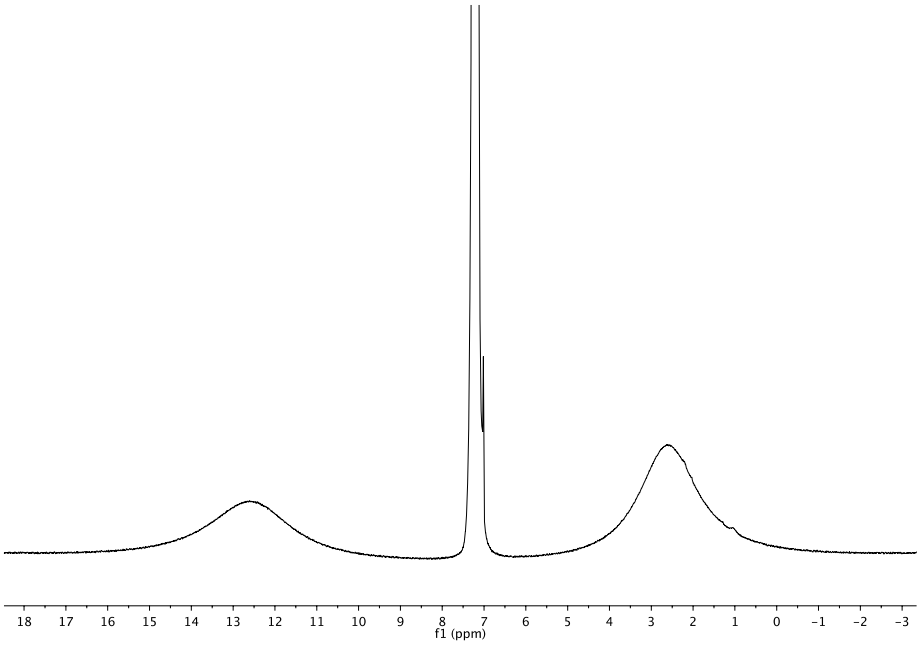

Figure S5.26 *– Deuterium, ^2H, NMR spectrum of $[P_{4\,4\,4\,4}][C_7COO]$-D_2O mixture at x_D 0.50 after being bubbled with CO_2 for 4 h at 295.15 K, representing a octanoic acid signal at 12.63 ppm and an exchanged ^2H on the α-H of the cation at 2.60 ppm (92.12 MHz; 27 ˚C; C_6D_6 internal capillary, 7.16 ppm).*

References

[1] D. J. Yeadon, J. Jacquemin, N. V. Plechkova, M. C. Gomes, K. R. Seddon, *Aust. J. Chem.* **2019**, *72*, 144.
[2] K. Ito, H. J. Bernstein, *Can. J. Chem.* **1956**, *34*, 170-178.
[3] E. Spinner, *J. Chem. Soc.* **1964**, 4217.
[4] M. Kakihana, T. Nagumo, *Z. Naturforsch. A* **1987**, *42*, 477-484.